Master Thesis, Department of Geosciences

The lithostratigraphy and history of the Caledonian mélange basin rocks below the Jotun Nappe in Bøverdalen, South Central Norway.

Manar Alsaif

UNIVERSITY OF OSLO

FACULTY OF MATHEMATICS AND NATURAL SCIENCES

The lithostratigraphy and history of the Caledonian mélange basin rocks below the Jotun Nappe in Bøverdalen, South Central Norway.

Manar Alsaif

Master Thesis in Geosciences

Discipline: Structural Geology and Tectonics

Department of Geosciences

Faculty of Mathematics and Natural Sciences

University of Oslo

09 March 2015

Supervisors: Prof. Torgeir B. Andersen and Prof. Fernando Corfu

This work is published digitally through DUO – Digitale Utgivelser ved UiO
http://www.duo.uio.no
It is also catalogued in BIBSYS (http://www.bibsys.no/english)

Acknowledgements

This Master thesis has been an educational experience in multiple ways and I am grateful to several people for making it possible. First and foremost, much gratitude is due to my field partner, Johannes Jakob. Many of the ideas in this thesis are the result of discussions with him in the field. I thank him for his scientific input and for making the work all the more enjoyable.

It goes without saying that my supervisors, Torgeir Andersen and Fernando Corfu, have been pivotal for this little production. Their guidance saved me from many a scientific ditch. A big thank you is due for their patience and availability.

My friends and family also deserve a salute for all their support and speeches of encouragement. Had they not been available to me on my time off, I'm not sure my mental state would have persevered.

I'd like to also send a general thank you to anyone who endured me during this work.

The work of science is never quite complete and in the case of this particular thesis, you will quickly see that we are only scratching the surface. I hope this work is part of a much longer line of studies, and I hope to look back at this in the future and laugh at how little we knew back then.

Contents

Abstract

The Scandinavian Caledonides have been long studied, yet their ever unfolding complexity renders them far from being fully understood. It has been recognized that the Caledonian Allochthons have neither a linear nor straightforward along-strike relationship. A mélange unit has been recently identified as a separate tectonic unit. This unit is structurally positioned below crystalline nappes previously assigned to the Middle Allochthon. The mélange comprises meta-sediments and minor meta-basalt/gabbro, but most intriguingly, numerous solitary meta-peridotites. These occur as 'Alpine type' meta-peridotites, serpentinites, soapstones and detrital serpentinites. This thesis presents results of a field study of the mélange in the Bøverdalen area structurally below the Jotun nappe, and suggests that this provides evidence that the regional mélange unit was formed in a hyperextended passive margin. The meta-peridotites represent exhumed serpentinized mantle and are intimately associated with meta-sediments. The sediments are garnetiferous chlorite-muscovite schists, graphitic schists, phyllites, amphibolites, meta-sandstones as well as quartzite-pebble dominated conglomerates. It is suggested that this highly heterogeneous mélange unit formed during the early stages of rifting and hyperextension along the Baltican passive margin. Characteristics of the detrital peridotites suggests that serpentinite-talc protrusions may have formed islands. The processes involved are observed in modern margins where the best-studied example is the Iberia-Newfoundland passive margin. Work in present-day margins (mostly seismic reflection data) elucidate the large-scale structure of hyperextended margins, while studies of ancient exposed examples in mountain belts provide insight into the lithology, geochemistry and details of these margins. The widespread distribution of hyperextended margins in modern margins and the increasing number of recognizable ancient margins in mountain-belts indicates the importance of hyperextension during the early stages of the Wilson cycle. Samples collected from the melange unit in the Samnanger area (Bergen) have been dated using U-Pb data from ID-TIMS (isotope-dilution thermal ionization mass spectrometry) analysis of zircon and rutile. These yielded two age groups, ~420 Ma and ~476.23 - 487 Ma, however, both of these bodies are thought to represent intrusive activity post-dating the development of the mélange. Tectonic reconstructions that account for such complexity may not only explain the origin of peridotite bearing mélange units, they may also aid the understanding of the exotic terranes identified in the Scandinavian Caledonides.

1. Introduction

1.1. Introduction to hyperextension

Hyperextension is s a process that has been recently recognized to thin continental crust in magma poor segments of passive margins until rupture. Better descriptions of hyperextension have been made possible by technological advancement in geophysical technologies. Much of what we know about hyperextension is inspired by the pioneering studies of the Iberian margin, where geophysical surveys have been combined with dredging and drilling across the margin (Boillot et al., 1980, Boillot et al., 1987). This gives us a well-studied type locality for a modern hyperextended margin. Subsurface data, however, do not provide detailed information on lithologies and contact relationships. For this, we turn to mountain belts that host ancient preserved hyperextended relics. The best studied example of this is in the Alps where we find 'solitary Alpine peridotites' and/or 'Alpine serpentinites', the first recognized characteristic of preserved hyperextended margins (e.g. Manatschal, 2004, Manatschal et al., 2006, Mohn et al., 2010). Since this reinterpretation of the variably serpentinized 'Alpine-type' peridotites, hyperextended remnants have been recognized in the Pyrenees (e.g. Lagabrielle et al., 2010), the Appalachians and the British-Irish Caledonides (Chew and van Staal, 2014, Van Staal et al., 2013) and in the Scandinavian Caledonides (Andersen et al., 2012). These have been combined with studies of modern margins to give a description of hyperextended margins (Manatschal, 2004, Mohn et al., 2010). Hyperextension is being increasingly recognized in other modern margins such as:

- South Atlantic (Moulin et al., 2005, Contrucci et al., 2004, Unternehr et al., 2010)
- South Australian margins (Direen et al., 2007)
  The Red Sea (Cochran and Karner, 2007)
- The Eastern gulf of Aden (D'Acremont et al., 2006)
- The South China Sea (Franke et al., 2011)
- North Atlantic basins (O'Reilly et al., 1996, Pérez-Gussinyé et al., 2003)
- The Norwegian Sea margin (Osmundsen and Ebbing, 2008)

This widespread occurrence of hyperextended margins points to the importance of this process in continental rifting. It likely plays a key role in the first stages of the Wilson cycle and ought to be better understood. Recognizing this process in an ancient margin such as the pre-Caledonian Baltican margin of Norway would be an important find. It would refine tectonic reconstructions but also provide possible explanations for some of the more poorly explained units presently found in the Caledonides, as will be discussed in this thesis.

1.1.1. Hyperextended margin structure

A hyperextended margin is characterized by continental crust of normal thickness thinned to <10km over a lateral distance of ~100km. This is facilitated by large detachment faults that appear to sole out in the mantle (Pérez-Gussinyé and Reston, 2001). As the extension is accommodated and the crust is thinned, the sub-lithospheric mantle is exhumed and serpentinized. Eventually, continental rupture is achieved and sea floor spreading may commence away from the continent. Prior to rupture, there are not necessarily significant amounts of magmatism (Péron-Pinvidic and Manatschal, 2009). It is, however, common that the actual break-up and start of sea-floor spreading is associated with a large influx of basaltic magmatism in the form of a large igneous province (LIP) and that the

passive margins comprise both magma-rich and magma-poor segments (e.g. Coffin and Eldholm, 1994, Coffin and Eldholm, 1992).

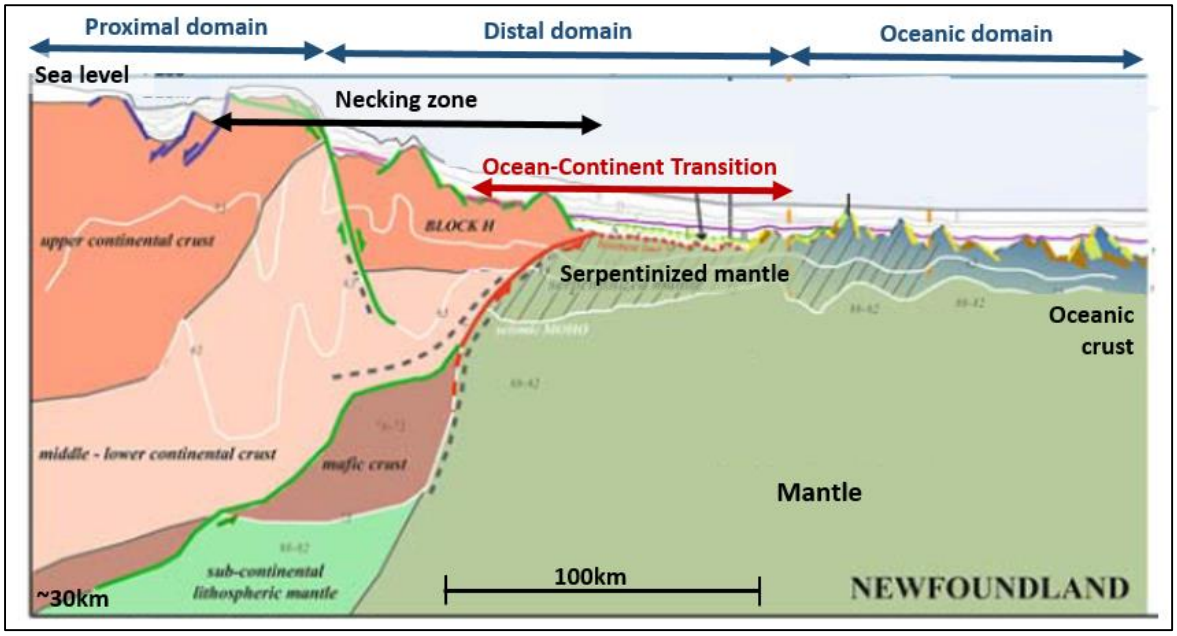

Figure 1: Observed structure of hyperextended margins as observed in Newfoundland. The margin consists of three primary domains, a necking zone where extreme thinning takes place and a gradual ocean-continent transition zone is formed. Modified after Péron-Pinvidic and Manatschal (2009).

In cross-section, margins can be viewed as having a proximal, distal and oceanic domain (Boillot et al., 1980). The proximal domain shows continental crust with classical half graben faulting, commonly with variable polarity, where the structure penetrates the upper crust and apparently dies out at the brittle-ductile transition in the mid-crust (Manatschal et al., 2006). In the distal domain, the extensional faults are lower angle, larger detachment faults that reach the mantle. This enables necking of the crust, thinning the continental crust from >30km to <10km (Manatschal et al., 2006). This zone is made of attenuated crust that is neither properly continental nor oceanic (Unternehr et al., 2010). This is the ocean-continent transition (OCT from here on). The OCT grades into proper oceanic crust in the oceanic domain when sea floor spreading is achieved, whereas transitonal crust may be preserved within aborted extensional basins such as those in the wide margin of the north Atlantic, illustrated in Figure 1 and Figure 2**Error! eference source not found.** (Manatschal, 2004, Péron-Pinvidic and Manatschal, 2009, Andersen et al., 2012).

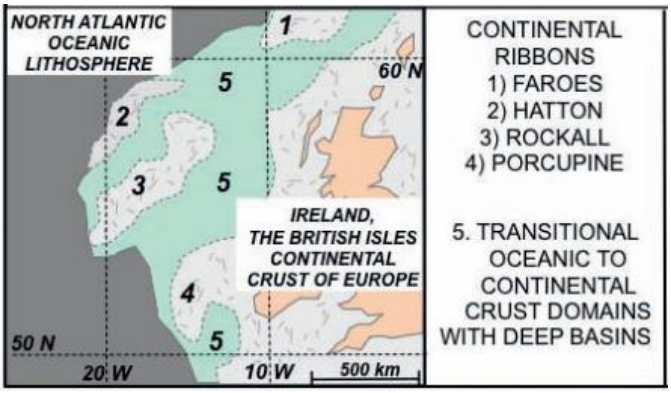

Figure 2: Sketch map showing distribution of oceanic, continental and transitional crust domains along the European North Atlantic margin between ~50° and 60° N (Andersen et al., 2012).

The OCT has been dredged and drilled in several places in the Iberian margin and is found to be made up of serpentinized mantle. Thus, the OCT seems to be made up of exhumed mantle rock (Péron-Pinvidic et al., 2007). The detachment faults soling in the mantle would enable fluids, in particular water, to infiltrate the mantle peridotite, causing serpentinisation and talcification as well as carbonatisation (the basic mineral reactions of these processes are shown in Box 1).

Box 1: The serpentinisation process.

The serpentinisation process:

Olivine, which together with pyroxenes makes up most peridotites, commonly alters to serpentine in low-grade, water-rich metamorphic environments. Serpentinisation often takes place during ocean floor metamorphism, ophiolite obduction, contact metamorphism where abundant aqueous fluids are involved and in shear zones developed during orogenesis. Serpentinisation requires the addition of water and generally takes place below 500°C, and commonly below 350°C. Serpentinising a peridotite will generally increase its volume by 35-45%. The basic serpentinisation equations are shown below:

$$2Mg_2SiO_4 + 3H_2O = Mg_3Si_2O_5(OH)_4 + Mg(OH)_2$$
forsterite — serpentine — brucite

and

$$3MgSiO_3 + 2H_2O = Mg_3Si_2O_5(OH)_4 + SiO_2$$
enstatite — serpentine — silica

If there is an iron component in the original olivine or pyroxene, this will produce an additional product of magnetite. The reaction rate increases with increasing water pressure.

(Barker, 1998)

1.1.2. The process of hyperextension

It is still unclear exactly how hyperextension takes place in a magma poor passive margin. Seismic reflection images of modern margins show lithosphere-scale detachment faults reaching the mantle (Osmundsen and Ebbing, 2008, Péron-Pinvidic and Manatschal, 2009). High-angle faults are only observed in the upper crust and in the distal domain. This may, however, be due to the technological difficulty in imaging high-angle faults seismically (Reston, 2005). The data currently available suggest that the detachment faults accommodate most of the extension and lead to mantle exhumation. This would be analogous to detachment faults in continental crust exhuming metamorphic core complexes (e.g. Wernicke, 1985). Most authors are apparently of the opinion that the detachments faults may be active at low-angles and a polyphase model of extension has been proposed (e.g. Manatschal et al., 2001, Péron-Pinvidic and Manatschal, 2009, Péron-Pinvidic et al., 2007, Reston, 2005). The model is illustrated in Figure 3. Here, the crust is first stretched by high angle brittle faults. This is followed by detachment faults forming across the lithosphere and thinning the crust, which eventually may lead to mantle exhumation and to continental rupture if mantle lithosphere reaches the syn-extensional sea-floor surface. This mode of extension is dominated by simple shear (Wernicke, 1985, Wernicke and Burchfiel, 1982), particularly in the later stages. Once the faults penetrate into the mantle lithosphere, water can migrate down causing mantle serpentinisation. Since the serpentinisation process leads to a volume increase of ~35%, the mantle may rise under its own buoyancy and aid rifting (Pérez-Gussinyé, 2013).

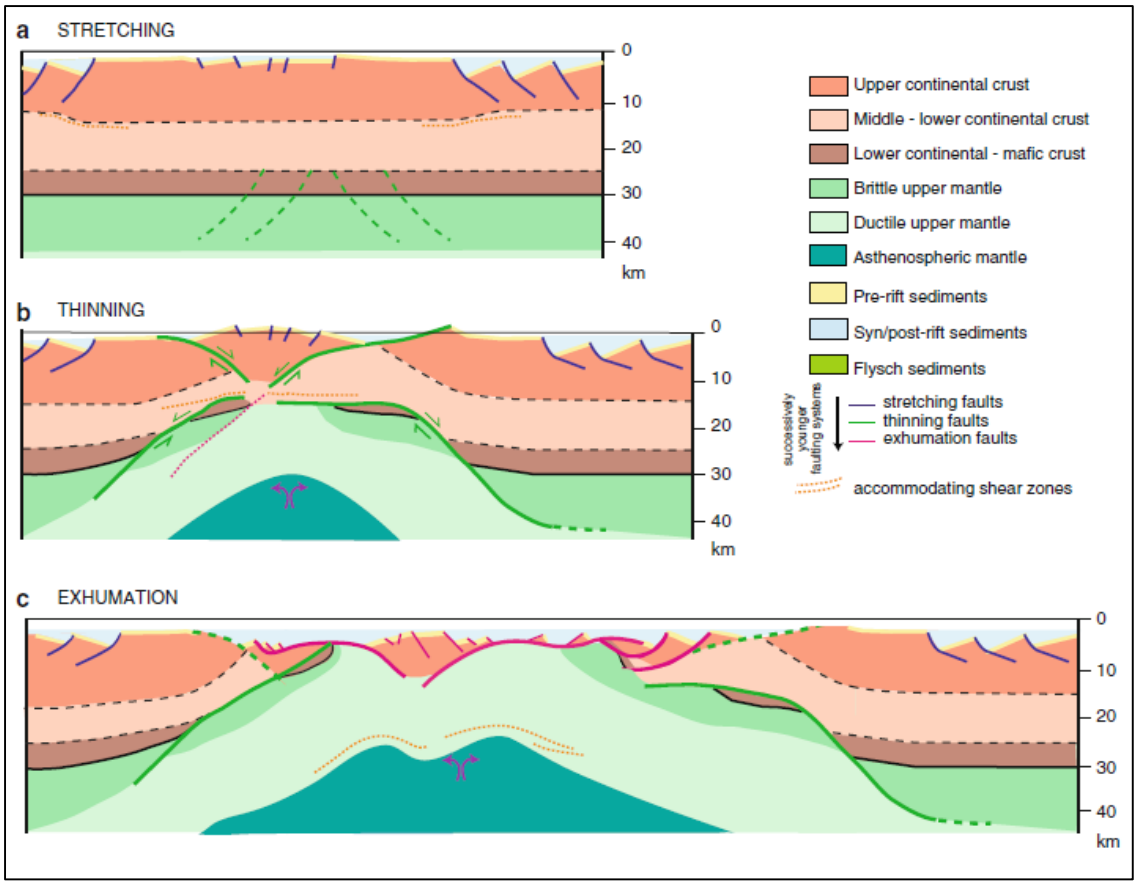

Figure 3: Conceptual 2D model of polyphase evolution of magma poor rift margins in three stages off differing extensional modes (Mohn et al., 2010).

It is worth noting that an alternative model for extension is presented by Pérez-Gussinyé (2013), where the faults are not active at low angles. Instead, active faulting takes place at high angles, but extension results in block rotation leading to an apparent low angle of older faults. This model is suggested as a solution to the mechanical problem of activating low angle faults. The 'Andersonian' framework (normal faulting occurs at 60° and reverse faulting at 30°, Anderson, 1951) in which this model is presented, however, is intended for the brittle crust. As the observed faults cross the brittle ductile transition extending through the lithosphere, they are expected to have different geometries to those limited to the crust. Additionally, low angle faulting can take place if the faults have been weakened, e.g. by elevated fluid pressure (Monigle et al., 2012) or by a lower coefficient of friction in the fault fill (Collettini and Sibson, 2001). We do not yet have information on fault lining from modern margins. Exposed ancient detachments from the Alps, however, show cataclasites and gouge (e.g. Bernoulli and Weissert 1985, Müntener and Manatschal, 2006).

The ancient exposed examples also show ophicarbonates in the exhumed ultramafic units. These are fractured, brecciated and veined peridotites/serpentinites with variable degrees of carbonate mineralization (often calcite) in the matrix and/or in veins (e.g. Spooner and Fyfe, 1973, Lagabrielle and Cannat, 1990, Clerc et al., 2014). Ophicarbonates and are also observed at the axes of slow spreading ridges in association with detachment faults (Picazo et al., 2012). Ophicarbonates can occur in various types that can form by different processes. A detailed description of this is outside the scope of this thesis, it is important to note that ophicarbonates can occur as massive serpentinites replaced by carbonate as well as sedimentary breccias of an ultramafic protolith. This

is observed both in the Pyrenees (Lagabrielle et al., 2010) as well as in the Alps (Manatschal et al., 2006).

While characterisation of the lithological association of rocks formed by hyperextension in magma poor rifted margins is the primary topic of this thesis, it is important to note that magmatism in hyperextended margins varies in volume and nature (Müntener and Manatschal, 2006). Additionally, hyperextension has been identified in volcanic margins, which are characterized by seaward-dipping reflectors (SDR) thought to be lavas. For example, the northeast Atlantic and the Norwegian-Greenland Sea. Additionally, Jan Mayen micro-continent margins commonly have SDRs and are thought to have been affected by hyperextension in the Late-Jurassic – Early Cretaceous prior to the the break-up and sea-floor spreading (Osmundsen and Ebbing, 2008, Lundin and Doré, 2011, Peron-Pinvidic et al., 2012a, Peron-Pinvidic et al., 2012b).

1.2. Regional geology

1.2.1. Regional geology of mainland Norway

The geology of mainland Norway (Figure 4) is dominated by three geological domains:

- Precambrian basement in the south and east
- Precambrian basement variably affected by Caledonian overprint in the west
- Caledonian thrust sheets and Upper Proterozoic- to Lower Palaeozoic cover

The Caledonian cover and nappes extend from the Stavanger area in the south west to the Varanger peninsula in the north. This is shown on the simplified geological map in Figure 4 where it is immediately apparent that most of the country's geology has been affected by the Caledonian orogeny. During this event, large allochthon complexes were emplaced along the length of Scandinavian (see recent review in Corfu et al., 2014a). The south east and north east, however, have preserved Fennoscandian Middle Proterozoic to Archean basement. With the exception of local dolerite dykes in the Egersund area (Bingen et al., 1998) and the Fen and Alnø alkaline/carbonatite complexes (e.g. Meert et al., 1998, Meert et al., 2007) there are no known

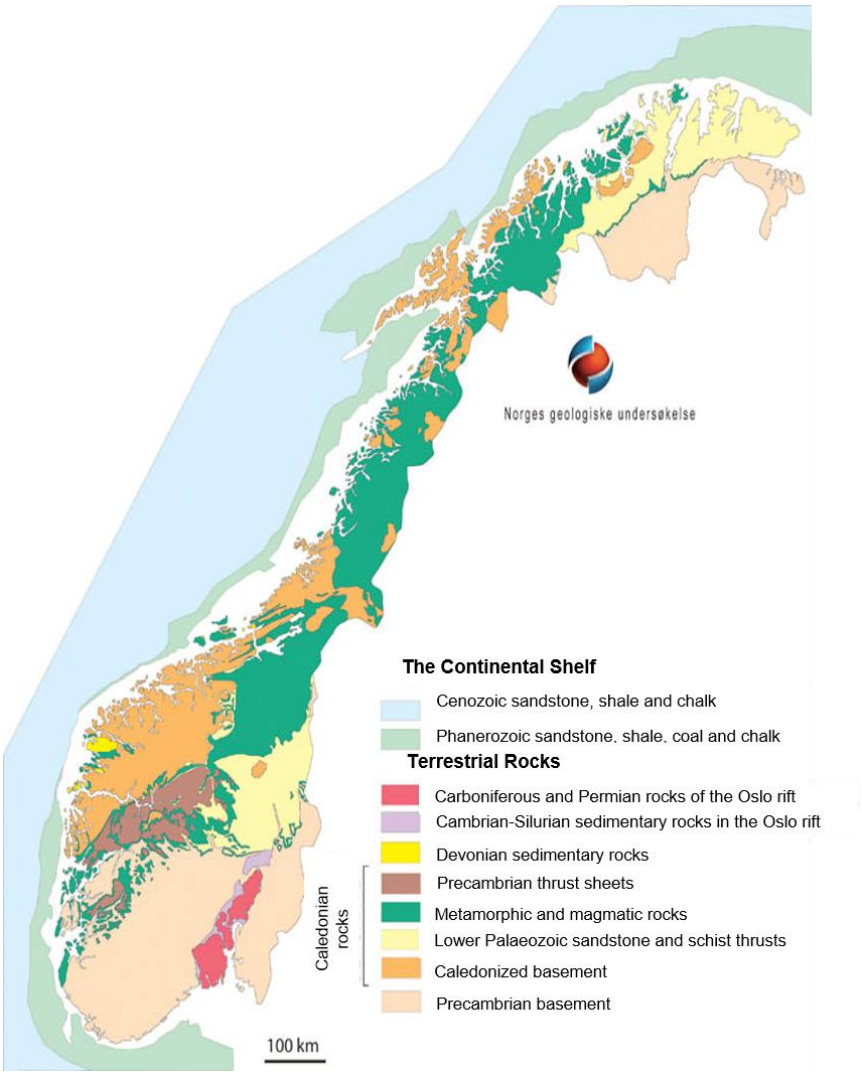

Figure 4: Simplified geological map of Norway (Norges Geologiske Undersøkelse, 2011)

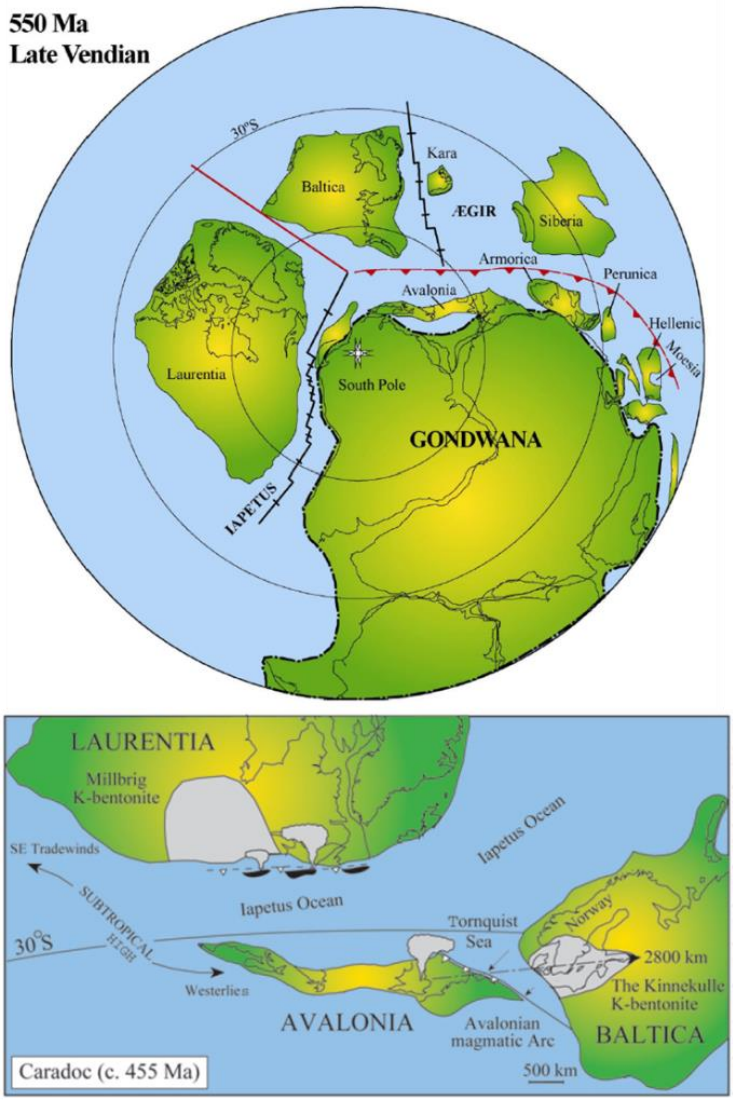

Figure 5: Tectonic reconstructions showing the break-up of Rodinia by 550 Ma and the closing of the Iapetus around 455Ma. After Torsvik and Cocks (2005).

late Precambrian rift-related magmatic rocks cutting the autochthonous Fennoscandian basement, hence the pre-Caledonian rifting and extension left little trace in the autochthon. Remnants of the rifted to hyperextended margin of Baltica are only found in the Caledonian nappes, and have therefore been subjects to structural and metamorphic modification (Nystuen et al., 2008, Andersen et al., 2012). The emplacement of the nappe complexes created an overall E-SE dipping regional structure structure which was later overprinted W-SW extensional collapse and open bending (Corfu et al., 2014a).

1.2.2. Tectonic history

In order to understand the current make up of Norway's geology, the tectonic history must first be considered. A brief account of our current knowledge of this is recounted below, as presented in Torsvik and Cocks (2005) except where otherwise cited:

The Norwegian basement rocks formed in the Precambrian by several tectonic events between 1900- 900 Ma. By 1000 Ma, most of the Norwegian basement rocks were part of the supercontinent Rodinia, which broke up by 750 Ma creating Gondwana and some smaller terranes including Baltica (which included Norway) and Siberia. The Ægir Sea separated Baltica and Siberia by ~550 Ma. The final stage of Rodinia's break up opened the Iapetus and is marked by the emplacement of dolerite-dyke swarms, now found in nappes interpreted to have been formed along the Baltoscandian margin at ~600 Ma (Nystuen et al., 2008).

Traditionally, reconstructions have placed Norway on the Iapetan (Laurentian facing) margin of Baltica. Recent reconstructions, however, invert Baltica (Torsvik et al., 1991), placing Norway on the Ægirian (Siberian facing) margin (Hartz and Torsvik, 2002, Torsvik, 2003).The Iapetus probably reached its widest size around 480 Ma (Cocks and Fortey, 1982, Cocks and Torsvik, 2002). At this time, Baltica was upside down at mid-southerly latitudes (according to the reconstructions with Baltica inverted). The Tornquist Sea separated Baltica from northwest Gondwana, while the Iapetus separated it from Laurentia. Avalonia also rifted off Gondwana at this time and started drifting towards Baltica, opening the Rheic Sea and commencing the closure of the Tornquist Sea. Baltica

then rotated counter clockwise towards its current orientation. Norway, thus, faced Laurentia by the Late Ordovician (Figure 5). By this time, Avalonia and Baltica collided (~441Ma) and the amalgamated Avalonia-Baltica started drifting towards Laurentia, closing the Iapetus. The Iapetus closed around 430 Ma (Labrousse et al., 2010) as shown by fauna provinciality (Cocks and Fortey, 1982) and subduction related magmatism (Torsvik et al., 1996). Subduction of the Iapetus had a westward polarity under Laurentia and ended in continental collision between Baltica and Laurentia in the form of the Caledonian orogeny.

The final stages of the Caledonian orogeny in Scandinavia and East Greenland are known as the Scandian orogeny (Gee, 1975). The Scandian orogeny is dated at ~430-410 Ma (Corfu et al., 2006), although some authors suggest that more distal parts of Baltica were undergoing metamorphism already at ~440 Ma (Hacker et al., 2003). The continental collision is thought to have lasted for approximately 20 to 25 myr (~430-405 Ma). Its initiation is dated by the obduction of marginal basin ophiolites in the mid-Silurian (Andersen et al., 1990) as well as by the cessation of subduction-related island arc magmatism (Corfu et al., 2006, Torsvik and Cocks, 2005). The end of the collision in the early Devonian is marked by the maximum burial of the high pressure and ultra-high pressure rocks of the Western Gneiss Region (WGR) at approximately 410-400 Ma (Hacker et al., 2010). The Scandian continental collision created the continent known as 'Laurussia' (Torsvik and Cocks, 2005).

The nature of the Caledonian orogeny has been the topic of some debate. Traditionally, it has been considered as one orogenic event (Størmer, 1967, Gee, 1975), however, questions have arisen as to whether it was an orogeny of multiple phases (e.g. Roberts et al., 2003). The Scandian orogeny emplaced the allochthons that now cover most of Norway. A review of the evolution of the Scandinavian Caledonides was recently published by Corfu et al. (2014a). The orogeny was accompanied and followed by extensional gravitational collapse (Andersen, 1998a, Fossen, 2010).

1.2.3. Present tectono-stratigraphy

Considering the dominant role of the Caledonian orogeny on the geology of mainland Norway, Norwegian geology has been traditionally described in reference to this orogeny, such that the Precambrian basement is described as the autochthon; while the thrust sheets are described as the allochthons. These have been traditionally split into the Lower, Middle, Upper and Uppermost allochthons (e.g. Gee et al., 1985, Roberts and Gee, 1985), where the Upper and Uppermost allochthons (with the exception of the Seve units) are outboard terranes of non-Baltican origin. The Uppermost allochthon seems to be Laurentian (from the overriding plate) whereas the Upper allochthon appears to be mostly made up of outboard oceanic terranes (e.g. Roberts et al., 2002, McArthur et al., 2014, Augland et al., 2014).The Middle and Lower allochthons have been traditionally thought to be of Baltican origin. The Middle allochthon in southern Norway consists of large Proterozoic crystalline nappe complexes (Dalsfjord, Lindås, Jotun, Bergsdalen and Hardanger-Ryfylke nappe complexes). These mostly have a metasedimentary cover of quartzites, meta-arkoses and schists. The nappe complexes and their metasedimentary covers seem to have an affinity to the autochthonous basement and originate on the Caledonian margin of Baltica before collision (Lundmark et al., 2007).

The traditional interpretation of the tectono-stratigraphy has been recently questioned. While a four-allochthon model suffices for a linear top-bottom reconstruction, the Caledonian thrusts show a larger degree of complexity. Several studies, particularly in the northern parts of the orogen from

Nordbotn to Finnmark, may be used to suggest that the Seve and Kalak nappe complexes have a possible exotic (outboard) origin (e.g. Corfu et al., 2011, Corfu et al., 2007, Kirkland et al., 2008). These complexes have traditionally been assigned to the Middle Allochthon, implying Baltic affinity. The Kalak nappe complex, however, shows a Neoproterozoic tectono-thermal history atypical for both the Baltican margin (Middle allochthon) as well as the Iapetan realm (Upper allochthon), making it difficult to fit it into the traditional scheme (Corfu et al., 2007, Kirkland et al., 2007).

Additionally, the transition between the Iapetus-derived Upper Allochthon and Laurentian margin-derived Uppermost Allochthon is unclear as elements of both occur in complex associations (Corfu et al., 2014a). This is seen, for example, in the Leka ophiolite which is of oceanic affinity (Upper allochthon) but both overlain and underlain by sediments of continental affinity (Barnes et al., 2007, Corfu et al., 2014b).

The traditional scheme also fails to include or explain the occurrence of a regionally extensive thin mélange unit and its pre-Caledonian sedimentary cover (local occurrences). The mélange unit occurs structurally below the crystalline nappes of the Middle Allochthon but has traditionally been assigned to the Upper Allochthon, which is inconsistent with the tectonic scheme of the traditional designations. Corfu et al. (2014a) thus propose a new nomenclature for naming the tectonics units relating their geography but with no genetic connotations. This allows the units to be interpreted in a modern tectonic framework which accommodates the complexity of passive margins, the oceanic realm and polyphase deformation. The new scheme also allows for tectonic sources other than Baltica and Laurentia (the Baltican margin may have faced different seaways and terranes before it collided with Laurentia, see tectonic history above). The proposed terminology and the corresponding traditional designations are shown in Table 1.

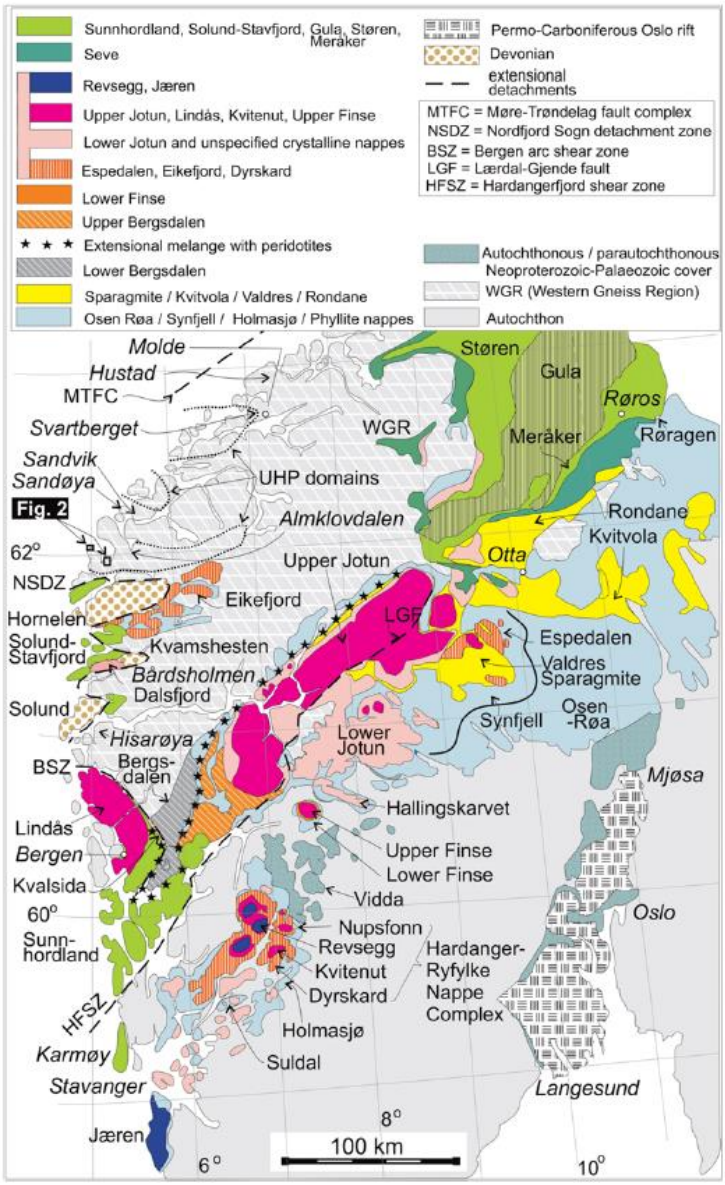

Figure 6: Tectonic map of southern Norway as it appears in Corfu et al. (2014b) (adapted from Gee et al., 1985). Note the position of the mélange unit marked with black stars.

Using this new terminology, the mélange unit mentioned above is found in the southern segment (Andersen et al., 2012). This unit consists of metamorphosed sedimentary rocks of marine affinity with lenses (m to km- scale) of ultramafic bodies. It was previously considered ophiolitic; however the dominance of mantle peridotite and the absence of a typical "Penrose-type" ophiolite pseudo-stratigraphy (particularly the sheeted dyke complex) does not support this interpretation (Andersen et al., 2012). Additionally, the metamorphosed peridotites in the mélange are closely associated with coarse-grained meta-sediments that seem to have been deposited prior to and during (?) the Caledonian orogeny (see also Qvale and Stigh, 1985). The mélange unit is the subject of this thesis and is described and discussed in more detail below:

Table 1: New names of tectonic units in the Scandinavian caledonides proposed by Corfu et al. (2014a) with reference to the traditional designation of Gee et al. (1985).

Main units of the Scandinavian Caledonides distinguished in this paper	Classification used in Gee *et al.* (1985)
Northern segment	
Lyngen ophiolite	UMA
Hellefjord	MA
Magerøy, Reisa (Vaddas)	UA
Kalak Nappe Complex	MA
Laksefjord, Gaissa	LA
Autochthonous cover	A
Reworked basement	PA
Barents Sea Region	A
Autochthon	A
Central segment	
Devonian	Devonian
Beiarn, Niingen, Nakkedal, Tromsø	UMA
Helgeland, Ofoten, Lyngen	UMA/UA
Rödingsfjället, Heggmo	UMA
Fauske	UMA
Narvik, Lyngen ophiolite	UMA
Köli, Støren, Meråker, Leka, Reisa	UA
Gula	UA
Seve	UA (MA)
Särv	MA
Kvitvola, Rondane, Tännäs, Veman, Offerdal, Akkajaure	MA
Osen–Røa, Jämtland	LA
Autochthonous to allochthonous cover	A-PA-LA
Reworked basement	PA-LA
Autochthon	A
Southern segment	
Devonian	Devonian
Sunnhordland, Solund–Stavfjord, Gula, Støren, Meråker	UA
Seve	UA (MA)
Revsegg, Jæren	MA
Upper Jotun, Lindås, Kvitenut, Upper Finse	MA
Lower Jotun and unspecified crystalline nappes	MA
Espedalen, Eikefjord, Dyrskard	MA
Lower Finse	MA
Upper Bergsdalen	MA
Sparagmite, Kvitvola, Valdres, Rondane	MA
Extensional mélange	–
Lower Bergsdalen	LA
Osen–Røa, Synfjell, Holmasjø, Phyllite nappes	LA
Autochthonous to allochthonous cover	A-PA-LA
Reworked basement	PA-LA
Autochthon	A

Note: A, Autochthon; PA, parautochthon; LA, Lower Allochthon; MA, Middle Allochthon; UA, Upper Allochthon; UMA, Uppermost Allochthon.

1.2.4. Mélange unit

The mélange unit can be identified almost continuously between the upper and lower Bergsdalen nappes in western Norway. It occurs structurally below the Jotun and the Lindås nappe as well as the Sunnhordland nappe which comprises ophiolites and Island-arc complexes (Corfu et al., 2014a). It extends for more than 400km from the Bergen Arcs north-eastwards to Røros as seen in Figure 6. First described as a tectono-stratigraphic entity by Andersen et al. (2012), it consists mostly of schistose siliciclastic meta-sediments, local amphibolites, thin sheets of mylonitic felsic gneisses and ultramafic lenses. It is locally intruded by younger granitoids (Jakob et al. work in progress, and below Chapter 6). Of particular interest here are the solitary, 'Alpine-type' ultramafic lenses and their sedimentary derivatives. These occur as solitary ultramafic lenses (variably serpentinized peridotites), detrital serpentinites, soapstones, and talc schists.

The solitary ultramafic lenses are conspicuous, massive and largely serpentinized bodies of peridotite. These are mostly less than 1 km in size, however, some of the larger lenses may be up to 5 km across, for example near Røros. Primary minerals are preserved in some of the larger, better

preserved lenses (Andersen et al., 2012). Some of these have been studied over the last century, however, their genesis has been unclear. Peridotite lenses are also observed in the Western Gneiss Region (e.g. the Almklovdalen peridotite massif) where they were suspected to have originated as Archean sub-Laurentian mantle that was thrust up (?) or introduced during Caledonian subduction-eduction of the Baltican margin (Kostenko et al., 2002, Beyer et al., 2012, Andersen et al., 1991).

Figure 7: Serpentine conglomerate with 100% ultramafic pebbles and matrix in the mélange unit, at Reiggehaugen, (for details and location see Chapter 5).

The detrital serpentinites occur both as sandstones and conglomerates (Qvale and Stigh, 1985), but the Caledonian overprint commonly conceals primary structures (Andersen et al., 2012). One of these occurrences is found in association with Mid Ordovician fauna near Otta (Strand, 1951, Bruton and Harper, 1981). This fauna occurs in serpentinite conglomerate overlying ultramafic rocks assigned to the Vågåmo ophiolite. This was described by Sturt and Ramsay (1999) who suggested that the serpentinite conglomerates represent an unconformable sequence deposited on the Vågåmo ophiolite after obduction onto Baltica. The fossils, however, are Celtic and show mixed Baltic and Laurentian affinity and are therefore unlikely to have been deposited after obduction onto Baltica (Andersen et al., 2012, Bruton and Harper, 1981). Sedimentary structures in soapstone are also seen in various deposits, particularly in the Gudbrandsdalen area, eastern Norway (Storemyr and Heldal, 2002, Bøe et al., 1993). Detrital serpentinites have also been observed at Hana near Trengereidfjorden, close to Bergen, and near Raudberget in Stølsheimen in Western Norway (fig. 2 in Andersen et al., 2012 and work in progress). The detrital serpentinites consist only of ultramafic material with mostly well rounded clasts.

All of the reported ultramafic rocks in the mélange have been heavily altered. While some of the larger bodies contain preserved peridotite in their centres, many seem to be completely serpentinized. The peridotites are most commonly altered to serpentinite and talc-carbonate spinel rocks, often containing magnesite, chlorite, chromite and magnetite (Andersen et al., 2012). Serpentinisation and talc crystallization result from hydration and metasomatism (see Box 1 for mineral reactions). In addition to bulk recrystallization of the rock, serpentine and talc veins are present. The contact between the ultramafic bodies and the surrounding felsic rocks often shows “black wall” alteration (Andersen et al., 2012, Harlov and Austrheim, 2012). This is where a soft chlorite-amphibole rich contact is created between felsic rocks and chemically contrasting Mg-rich ultramafics via hydrothermal alteration. Local alteration to listwanite (quartz-carbonate rock) is also common, as is ophicarbonate alteration (Andersen et al., 2012).

The ultramafic bodies in the mélange are dispersed in a matrix of metasedimentary rocks. These are mostly garnet-micaschists, phyllites and graphitic schists which underwent greenschist-lower amphibolite facies metamorphism during the Caledonian orogeny (Andersen et al., 2012). There are also quartz schists and amphibolite bearing schists (garben schists) indicating further metasomatism.

Similar assemblages have been described from various locations in the mélange including the Samnanger Complex in the Major Bergen Arc (local name 'Samnanger Complex') (Færseth et al., 1977, Ingdahl, 1985), Stølsheimen, Sogn and near Lom (Andersen et al., 2012).

There has not been a satisfactory explanation for the occurrence of this mélange unit. It has traditionally been considered ophiolitic; however, the solitary occurrences of peridotites coupled with the absence of the sheeted dyke complex challenges the validity of the ophiolite interpretation. Andersen et al. (2012) suggest that these instead originate in a hyperextended margin as an alternative interpretation that would better explain the petrology and the lithological association. This thesis explores this idea by studying an ultramafic lens and its immediate vicinity in Bøverdalen, Jotunheimen close to Lom.

1.3. Project scope

Few studies have been carried out to characterize the hyperextended margin preserved in the Caledonides. This thesis presents evidence that hyperextension took place on the Baltican passive margin before the Caledonian orogeny. The primary method used was to examine lithological associations and compare them to those found in modern and fossil hyperextended margins. This was done by detailed field mapping of 1 km^2 of the mélange unit in Norway, which contains Alpine peridotites and detrital serpentinites (described above). Two additional metamorphosed conglomerate occurrences in the mélange unit were studied: The Høyvatnet quartz meta-conglomerate and the Reiggehaugen serpentinite conglomerate. The studied units were sampled and examined petrographically. Selected magmatic occurrences in the mélange from the Bergen area were dated using U-Pb geochronology in an attempt to constrain the age of the mélange. Each studied locality is presented in an individual chapter and followed by a discussion of the mode of formation of the mélange unit.

2. Analytical methods

2.1.Petrographic analysis

A standard petrographic microscope was used for the examination and description of the thin sections. In order to investigate specific chemical compositions of the main rock forming minerals, an electron microprobe (EMP) was used. The EMP performs precise chemical analyses of minerals in situ.

The microprobe used is a CAMECA SX 100 fitted with five wavelength dispersive system spectrometers (WDS from here on) and an energy dispersive system (EDS from here on). Quantitative analyses were done in WDS mode, while EDS was used to qualitatively aid mineral identification.

The following analytical conditions were used:

- Accelerating voltage: 15 kV.
- Beam current: 10-15 nA (mostly 10 nA).
- Beam size: Focused, or 5-10 µm on beam sensitive minerals such as carbonate.
- Counting time on peak: 10 s.

Na and K were analyzed first and the analyses were corrected using the PAP (Pouchou and Pichoir) procedure (Pouchou and Pichoir, 1991).

The following minerals were used for calibration:

- Wollastonite for Si and Ca.
- Synthetic Al_2O_3 for Al.
- Synthetic MgO for Mg.
- Fe-metal for Fe.
- Pyrophanite for Mn and Ti.
- Synthetic Cr_2O_3 for Cr.
- Orthoclase for K.
- Albite for Na.
- Synthetic NiO for Ni.
- Synthetic Sr_2O_3 for Sr.

Electron back scatter images (BSE) were used to locate the points to analyze and saved for later reference.

The formulae of the main minerals were then calculated from the oxide weight % analyses using the following steps:

1- Calculate mole units (atoms per formula unit) by dividing the oxide weight % (from the analysis) by the atomic weight.
2- Multiply the mole units by the number of oxygens in the oxide formula. This gives the 'oxygen units'.
3- To calculate the normalized oxygen units, multiply the oxygen number by a normalization constant. The normalization constant is the desired number of oxygens (from the mineral formulae) divided by the sum of the actual oxygen numbers.
   The oxygen normalisation constants used for each mineral were:
   - Amphibole: 23
   - Feldspar: 8
   - Garnet: 12
   - Muscovite, biotite: 11
   - Epidote: 12.5
4- Multiply the normalized oxygen numbers by the number of cations per oxygen in the oxide formula to get the atom units (which are used in standard expressions of mineral formulae).

The spreadsheets built for these calculations can be found in Appendix II. Note that measured elements of an atomic proportion smaller than 0.01 are considered insignificant amounts and are omitted from the mineral formulae.

2.2. Geochronology

U-Pb ages of zircons from magmatic rocks were calculated using ID-TIMS (Isotope dilution thermal ionization mass spectrometry). The samples were first crushed and the heavy fractions were isolated using a Wilfley table, magnetic separation and heavy liquid separation. Zircon grains were then manually selected from the light fractions and subjected to mechanical abrasion using compressed air (Krogh, 1982). A spike of ^{202}Pb, ^{205}Pb and ^{235}U was added to the abraded grains which were then dissolved using hydrofluoric acid in Teflon bombs at 195°. A detailed account of sample preparation is given in Appendix I.

The U and Pb ratios were measured using ID-TIMS from which the ages were calculated.

The U-Pb dating system relies on two isotopic clocks with identical chemical characteristics but different decay constants, where:

$^{238}U \rightarrow {}^{206}Pb$, half-life of 4.47Ga.

$^{235}U \rightarrow {}^{207}Pb$, half-life of 0.7Ga.

A single isotopic clock can be solved for time using the age equation:

$$^{206}Pb = {}^{238}U\,(e^{\lambda t} - 1)$$

Where t=time and λ= decay constant of ^{238}U (known empirically).

It is instrumentally difficult to measure an absolute isotopic quantity, so ratios of the same element are measured. Since ^{235}U has a much shorter half-life than ^{238}U, the $^{238}U/^{235}U$ ratio varies with geological time and is currently 137.88. The two isotope clocks can be linked and solved for time using the following equation:

$$\frac{^{207}Pb}{^{206}Pb} = \frac{^{235}U\,(e^{\lambda_{235}t} - 1)}{^{238}U\,(e^{\lambda_{238}t} - 1)} = (1/137.88)\ \frac{(e^{\lambda_{235}t} - 1)}{(e^{\lambda_{238}t} - 1)}$$

The Pb and U ratios are measured, the decay constant λ is known empirically, leaving time t as the only unknown variable which can be solved for. An intermediate step often involves dividing each age equation by ^{204}Pb to work with a ratio throughout. ^{204}Pb is used since it is the primordial Pb isotope, i.e. it is non-radiogenic and constant through time (adapted from Dickin, 2005). The calculated ages are presented in Chapter 6.

3. Bøverdalen

3.1.Field mapping in Bøverdalen

The mélange unit referred to above is found in Bøverdalen close to Lom in Jotunheimen. The location and geological position of the mapped area is shown in Figure 8.

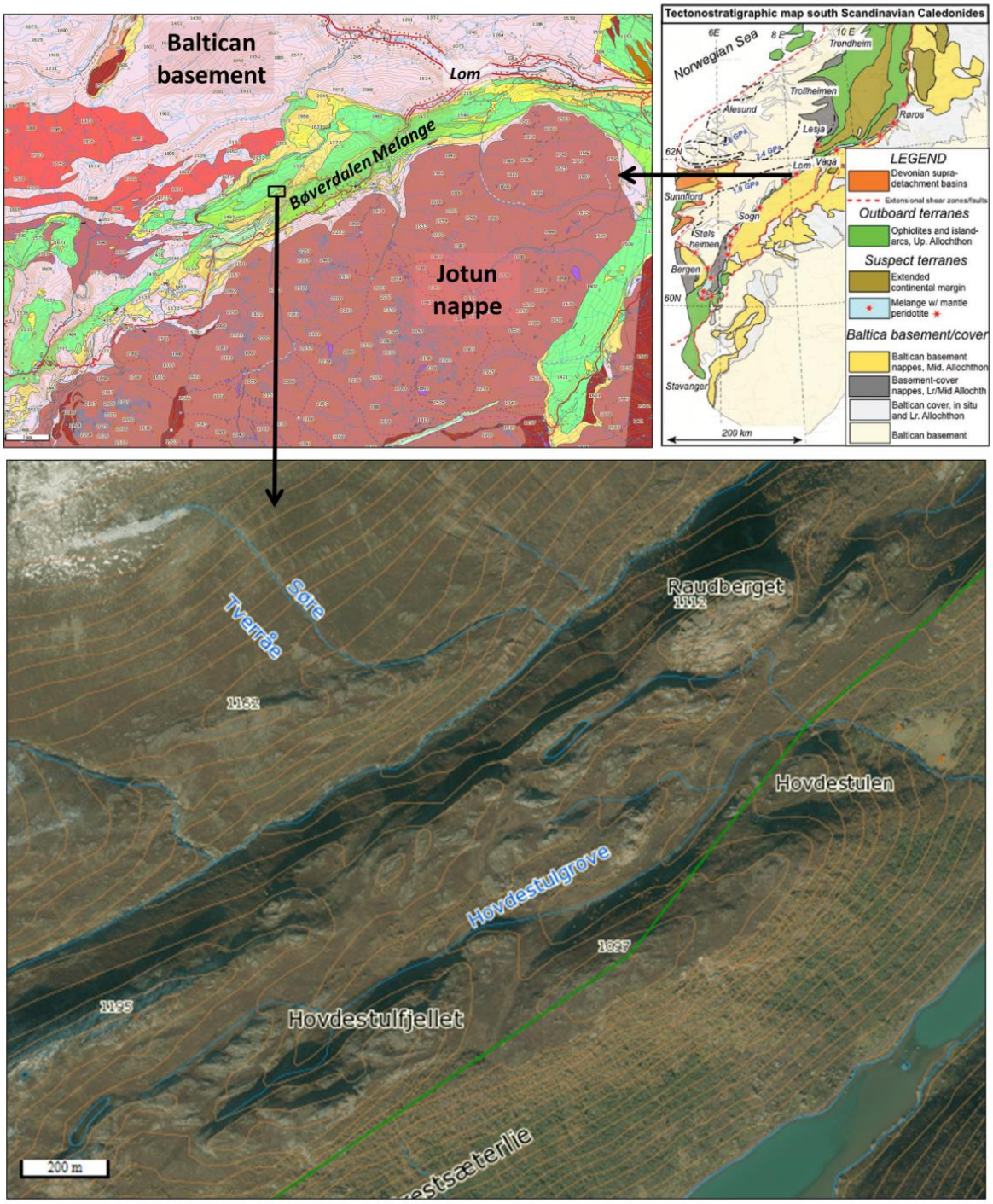

Figure 8: Aerial photograph of the mapped area in Bøverdalen and its tectonostratigraphic position. The aerial photograph and the geological overview map are from "Norge i Bilder" and the NGU, respectively. Here we find solitary serpentinite bodies that contrast to their surroundings both geologically and topographically. They lie structurally below the Jotun nappe, as is seen in the tectonostratigraphic map of the southern Norwegian Caledonides (taken from (Andersen et al., 2012)).

Two serpentinite bodies are discernible on the aerial photograph in Figure 8 (Raudberget and Hovdestulfjellet). These occur structurally below the Jotun nappe, as can be seen in the tectonostratigraphic overview in Figure 8. Detailed field mapping was carried out around and between the two serpentinite bodies shown above to elucidate their lithological association. The north eastern serpentinite body, Raudberget, is the topographically more prominent body. Hovdestulgrove (the area south west of Raudberget) is the main mapped area in this thesis.

The lithological map produced is presented in Figure 9 below. Eight units were distinguished, one of which (garnet schist) is seen twice in the mapped area. A simplified cross section through the succession is shown in Figure 10, while an extended cross section of the region is shown in Figure 11.

The field map in this thesis primarily differs from the NGU (Norwegian Geological Survey) map in the level of detail. The garnet schist, quartz schist, graphitic schist and actinolite schist mapped in this thesis are grouped into one unit in the NGU map. Additionally, the Hovdestulfjellet serpentinite body was found to be larger and extends farther north than originally mapped.

Apart from the serpentinites, the lithologies found are metamorphosed, originally marine sediments. An overview of the units is presented in Table 2 below, followed by a detailed description of each unit and an interpretation of the lithological association.

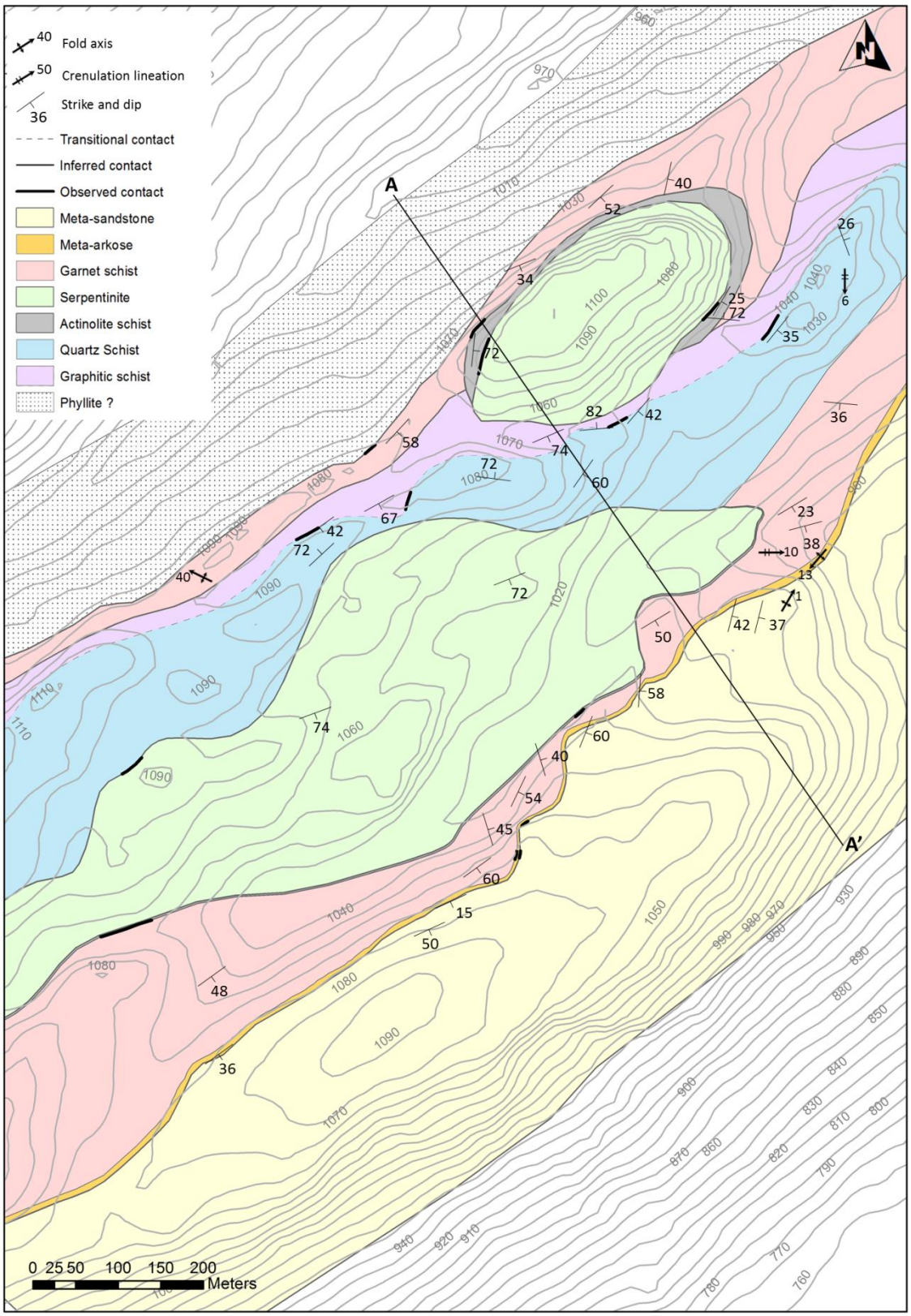

Figure 9: Lithological map of Hovdestulgrove in Bøverdalen, Jotunheimen. Produced by field mapping and analysis of the mapped units.

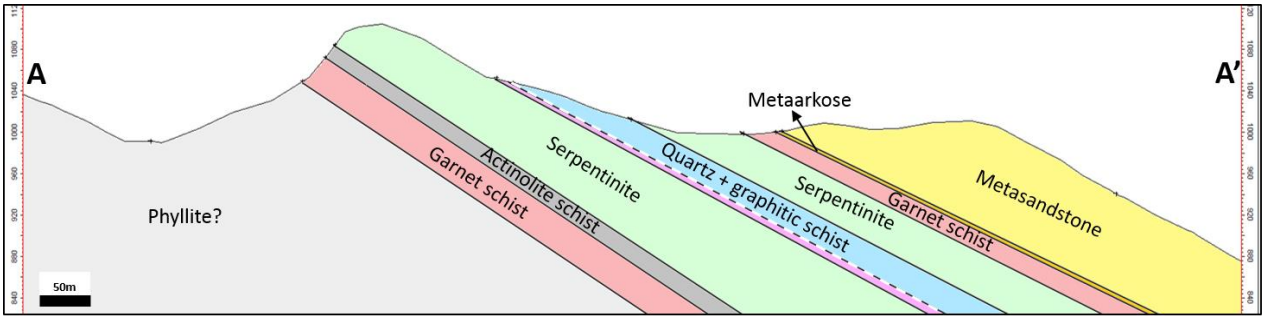

Figure 10: Simplified cross section through the mapped mélange in Bøverdalen showing the structure and stratigraphy. An extended cross section is shown in Figure 11 below.

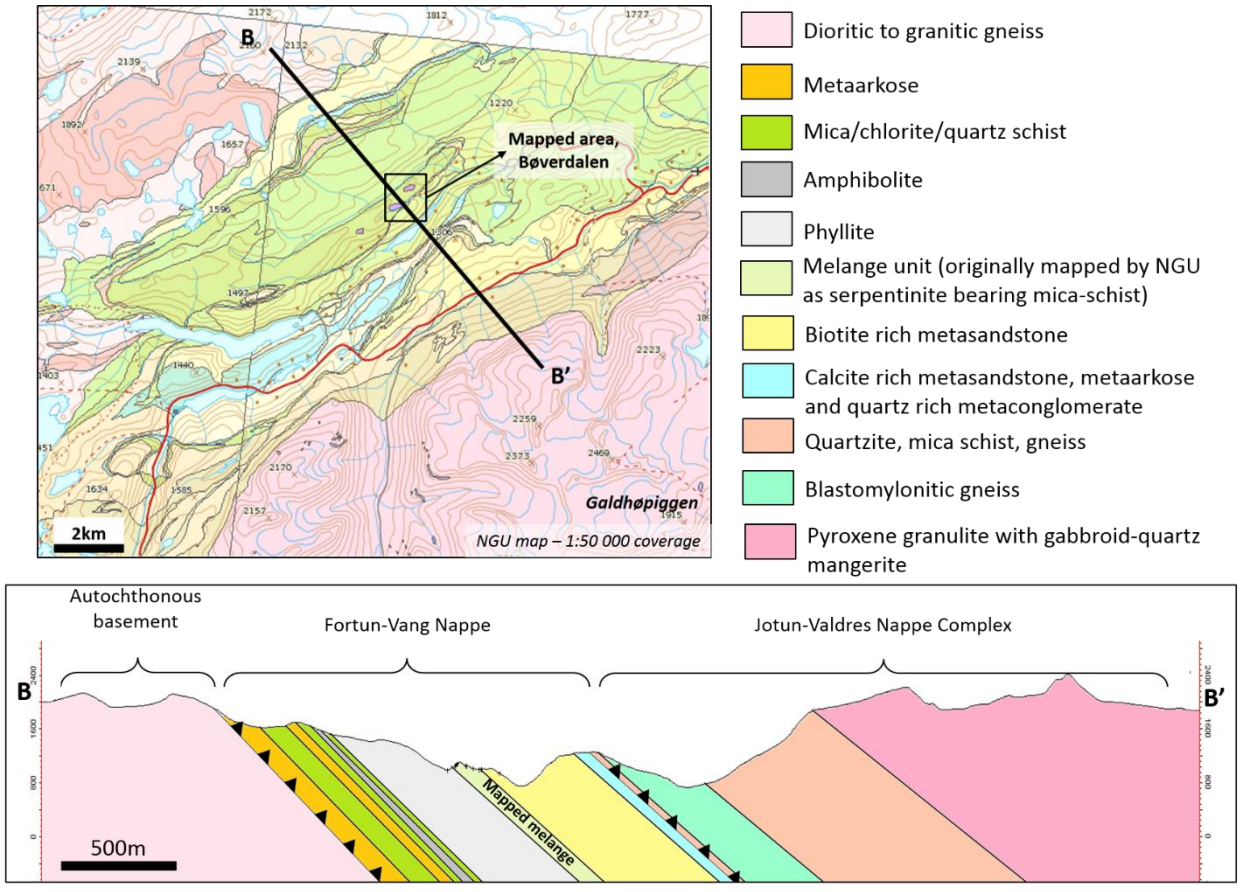

Figure 11: A simplified cross section through the mapped mélange in Bøverdalen and its neighbouring tectonic units. The mélange here was previously grouped in the Fortun-Vang Nappe and sits structurally below the Jotun-Valdres Nappe Complex.

Unit	Lithology	Mineralogy	Short description
Meta-sandstone	Semi-pelite	Alkali feldspar (20-30%) Biotite (ca. 25%) Quartz (ca. 20%) Muscovite (ca. 10%) Chlorite (ca. 5%) Plagioclase (<5%) Acc: Epidote, zircon, magnetite.	Altered, plagioclase rich semi-pelite. Probably sedimentary protolith.
Meta-arkose	Semi-pelite	Albite (50-60%) Quartz (10-20%) K-feldspar (5-10%) Epidote (5-10%) Chlorite (ca. 5%) Biotite (<5%) Muscovite (<5%) Phlogopite (<5%) Acc: Titanite + magnetite (ca. 5%), ilmenite.	Fine grained semi-pelite with K-feldspar porphyroclasts. Some alteration; large grains of epidote and titanite.
Garnet schist	Garnet muscovite schist	Muscovite (ca. 50%) Albite (20-30%) Quartz (10-20%) Chlorite (ca. 10%) Acc : Magnetite, tourmaline, garnet, apatite.	Garnet muscovite schist showing a chloritization. Strongly foliated. Probably sedimentary protolith.
Quartz schist	Psammite	Quartz (ca. 35%) Feldspar (ca. 25%) Calcite (ca. 15%) Biotite (ca. 8%) Chlorite (ca. 8%) Muscovite (ca. 8%) Acc: Ilmenite	Carbonaceous quartz-feldspar rich, foliated schist. Probably sedimentary protolith.
Graphitic schist	Graphitic schist	Graphite (ca. 50%) Quartz (ca. 30%) Muscovite (ca. 20%) Acc: Fe-oxide (non-crystalline), sulphides.	Graphitic schist with quartz and sulphides.
Serpentinite	- Serpentinite - Talc schist	Serpentine (ca. 80%) Magnetite (ca. 10%) Carbonate (ca. 10%) Talc (50%) Carbonate (50%)	Mostly serpentinites. Carbonate rich talc schists also occur in places.
Actinolite schist	Actinolite schist	Actinolite (ca. 60%) Albite (ca. 30%) Epidote (0-10%) Chlorite (<5%) Biotite (<5%) Calcite (<5%) Acc: Titanite	Actinolite schist of varying grain size found at contact with serpentinite bodies.

Table 2: Overview of the mapped rock units in the Bøverdalen mélange.

3.2.Description of the mapped units:

3.2.1. Meta-sandstone unit:

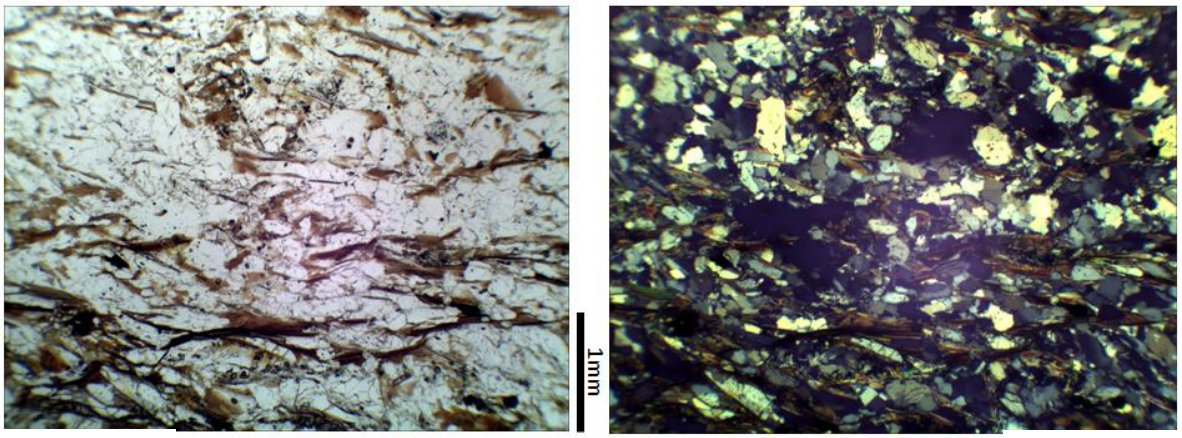

Figure 12: Thin section micrograph of the meta-sandstone unit in (a) plane and (b) cross polarized light, showing the distribution of the main minerals; feldspar, biotite, quartz and opaque magnetite grains. Foliation can be seen in (a) where the biotite grains are elongated in a left-right orientation.

This unit is mostly made up of alkali feldspar, biotite, chlorite, quartz, muscovite and lastly, plagioclase. There are also small amounts of Fe-oxide which is probably magnetite and very small amounts of epidote and zircon. Many of the feldspars show sericitisation which affects the K-feldspars more than the plagioclase grains (sericite growing on the grains). This suggests that more of the plagioclase grew later than the K-feldspar as a metamorphic mineral since it shows less alteration. The biotite grains are partially altered to chlorite. The rock shows a vague foliation in thin section (see Figure 12 above) which is clearer in the field (e.g. Figure 13).

Figure 13: Meta-sandstone unit showing foliation fish with a top to the west shear sense.

This unit also shows quartz veins of varying sizes. These are folded and follow the unit's main foliation.

Lithologically, this unit has been classified as a semi-pelite because of a relatively high content of phyllosilicates (ca. 40%). It most likely originated as a relatively fine-grained, immature (feldspar-rich) sandstone. The unit has been called a 'meta-sandstone' in keeping with the NGU's classification, as we have not found anything to contradict this.

3.2.2. Meta-arkose unit:

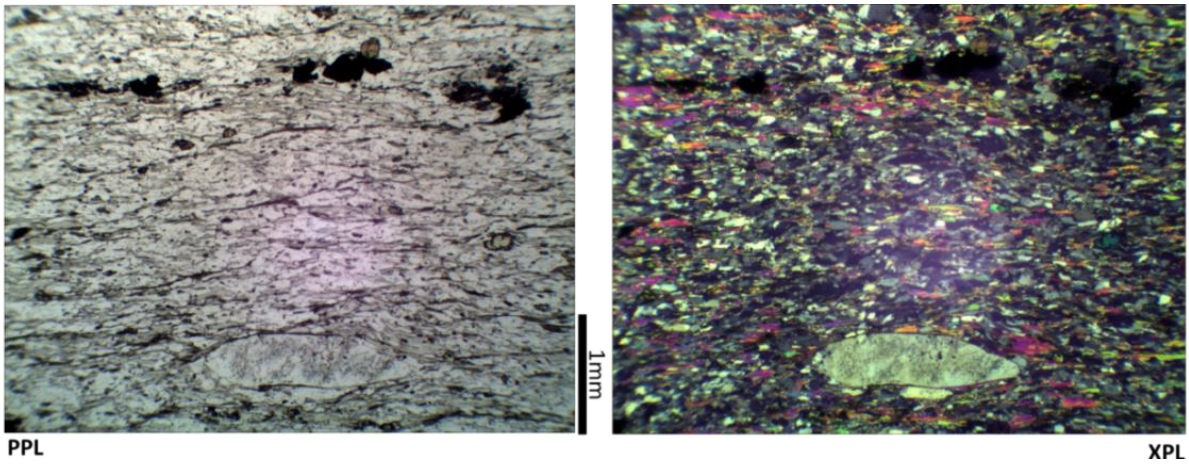

Figure 14: Thin section micrograph of the meta-arkose unit showing a K-feldspar porphyroclast in an albite, quartz and muscovite matrix. Magnetite and titanite can also be seen towards the top of the image.

Much like the meta-sandstone described above, this unit is semi-pelitic, however, with less mica/chlorite and a larger proportion of feldspar. This is consistent with the NGU's classification of this unit as a meta-arkose, thus the same name is used here for consistency.

Feldspar is present in two forms; large K-feldspar porphyroclasts and fine grained albite. The K-feldspar porphyroclasts are probably clasts from the eroded protolith. The albite is mostly secondary and is seen replacing the K-feldspar in places. An example of this is shown in Figure 15 below.

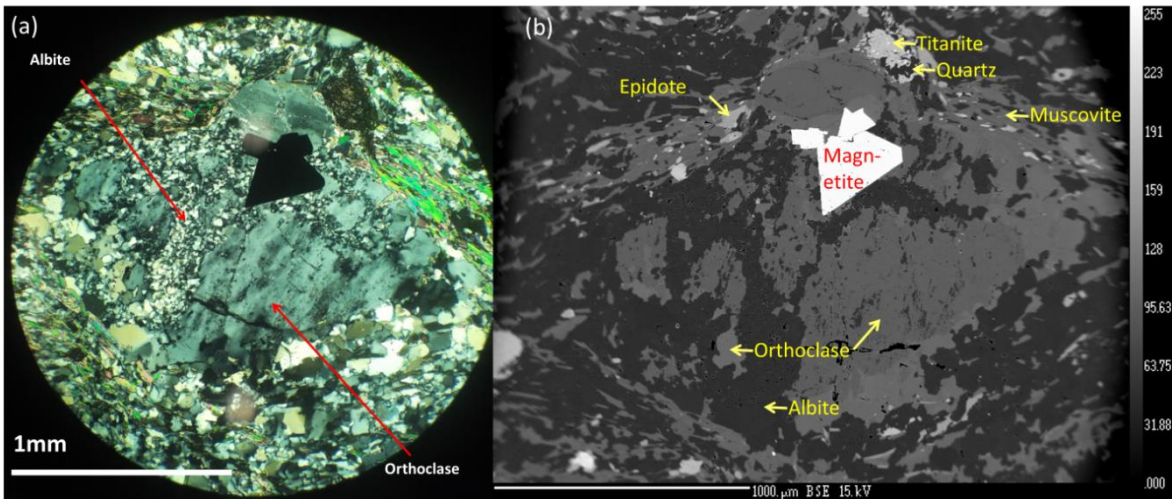

Figure 15: (a) Thin section micrograph in XPL and (b) electron backscatter image of the Meta-arkose unit: Orthoclase porphyroclast partially replaced by albite with additional growth of magnetite. Titanite, quartz, muscovite and epidote have also grown around the grain. The large feldspar porphyroclast is probably a remnant detrital grain of the clastic sedimentary protolith.

Quartz is also present in the fine grained matrix. It appears to make up no more than 20% of the rock, however, its proportion is difficult to estimate optically due to its similarity to albite which is abundant in the matrix. The unit also contains ca. 10% mica in the form of muscovite, biotite and phlogopite, while chlorite makes up about 5% of the rock. Epidote is slightly more abundant and makes up 5-10% of the rock in grains that reach up to 1 mm in size. Titanite and magnetite are also present, both of which form grains in the order of 1 mm in size and together make up about 5% of the rock. Ilmenite is also present, albeit much more sparsely, and is seen replaced by titanite.

The unit shows one main foliation and the porphyroclasts have been rotated along the foliation planes. The higher content of quartzo-feldspathic material in this unit may suggest that it originally formed as a less clay-rich sedimentary deposit, but the relatively high content of feldspars suggests that it was relatively immature and probably best classified as arkosic. Some relatively coarse (ca. 2 mm-sized) grains described as porphyroclast may represent original sand grains.

3.2.3. Garnet schist unit:

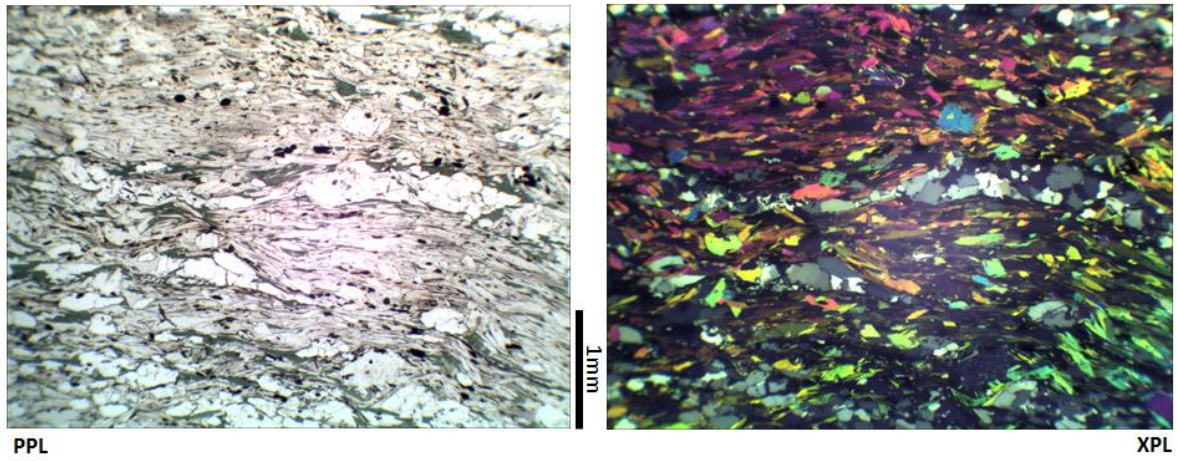

Figure 16: Thin section micrograph of the Garnet schist unit in plane and cross polarized light, showing the texture and distribution of the main minerals: muscovite, albite, quartz and chlorite. A left-right foliation is visible, while the quartz occurs in veins which are seen in the middle of the micrographs.

This is a well foliated mica schist dominated by muscovite. Feldspar is present as albite and is accompanied to a lesser degree by quartz (confirmed by electron microprobe analysis). Chlorite gives the rock its greenish tint with a modal percentage of about 10%. The accessory minerals include tourmaline (zoned), apatite and magnetite. All of the accessory minerals except for the apatite are present in relatively large amounts. Garnets are found with variable sizes and distribution, where they are concentrated in places and sparse in others. This heterogeneity probably reflects primary differences in sedimentation in the original protolith. An example of smaller garnets (ca. 0.1 mm large) concentrated along a band is shown in Figure 17 in contrast to larger garnets (ca. 3mm large) observed in the field in as shown in Figure 18.

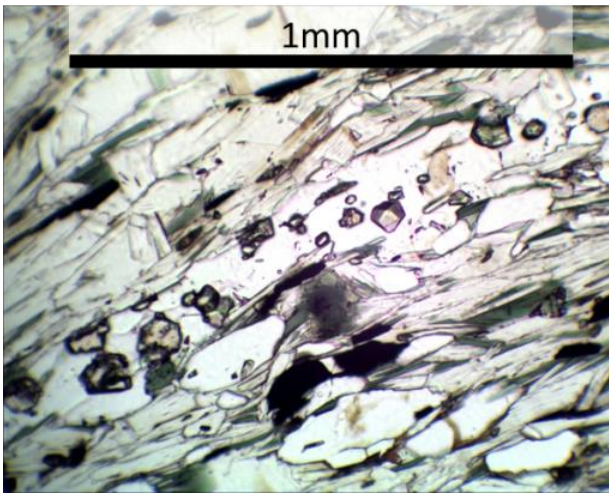

Figure 17: Band of small garnets seen in thin section (PPL).

Figure 18: Field picture of a large garnet porphyroblast in the crenulated garnet schist unit. The crenulation shows a dominant top to the west shear sense, with alternating chlorite-muscovite and quartz layers making up the foliation.

Several garnet grains have been analysed using the electron microprobe, all of which show a pyrope ($Mg_3Al_2Si_3O_{12}$), almandine ($Fe^{2+}{}_3Al_2Si_3O_{12}$), spessartine ($Mn_3Al_2Si_3O_{12}$), andradite ($Ca_3Fe^{3+}{}_2Si_3O_{12}$) and grossular ($Ca_3Al_2Si_3O_{12}$) component (see Figure 19 for calculated formulae). The garnets analysed are quite small and do not show any significant zoning. This is shown in Figure 20, where the analyses of four points from one garnet grain are presented. There are no significant differences between the analyses in the different parts of the grain.

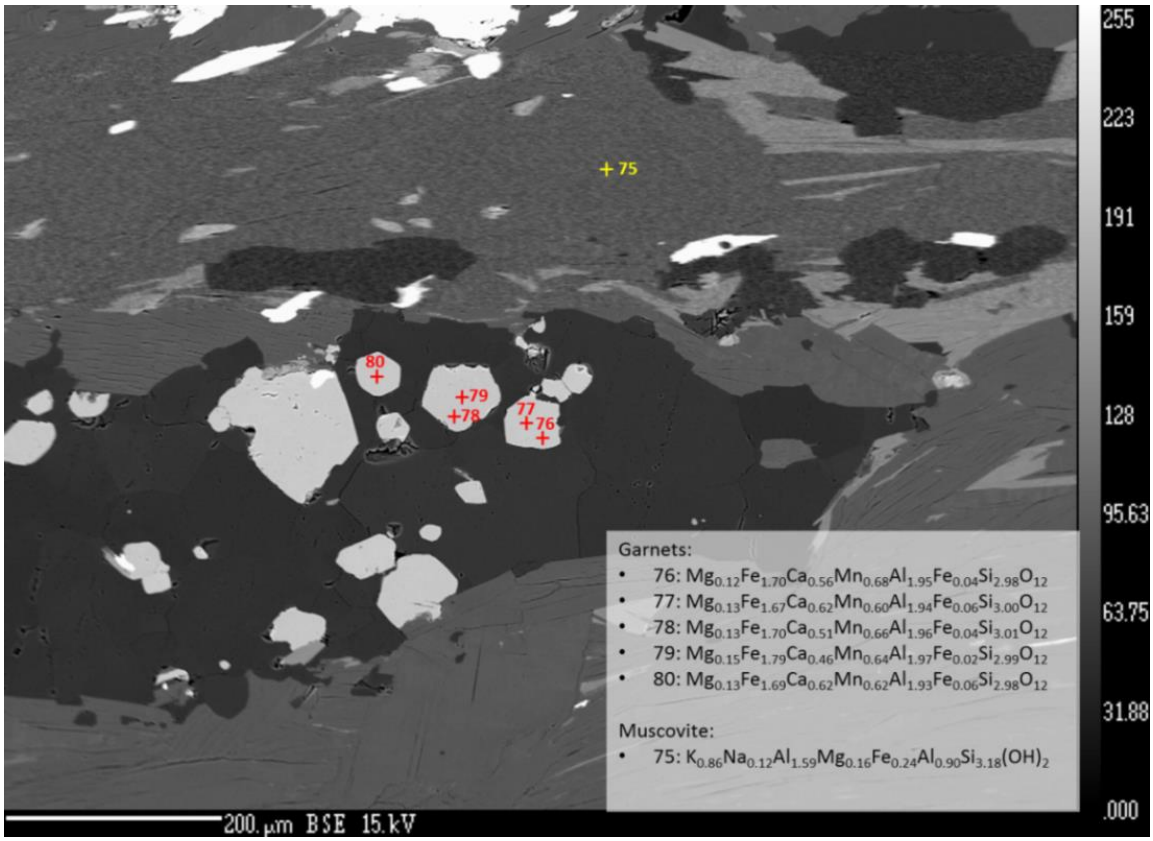

Figure 19: Electron back scatter image showing garnet and muscovite mineral chemistry calculated from electron microprobe analysis. From the garnet schist unit.

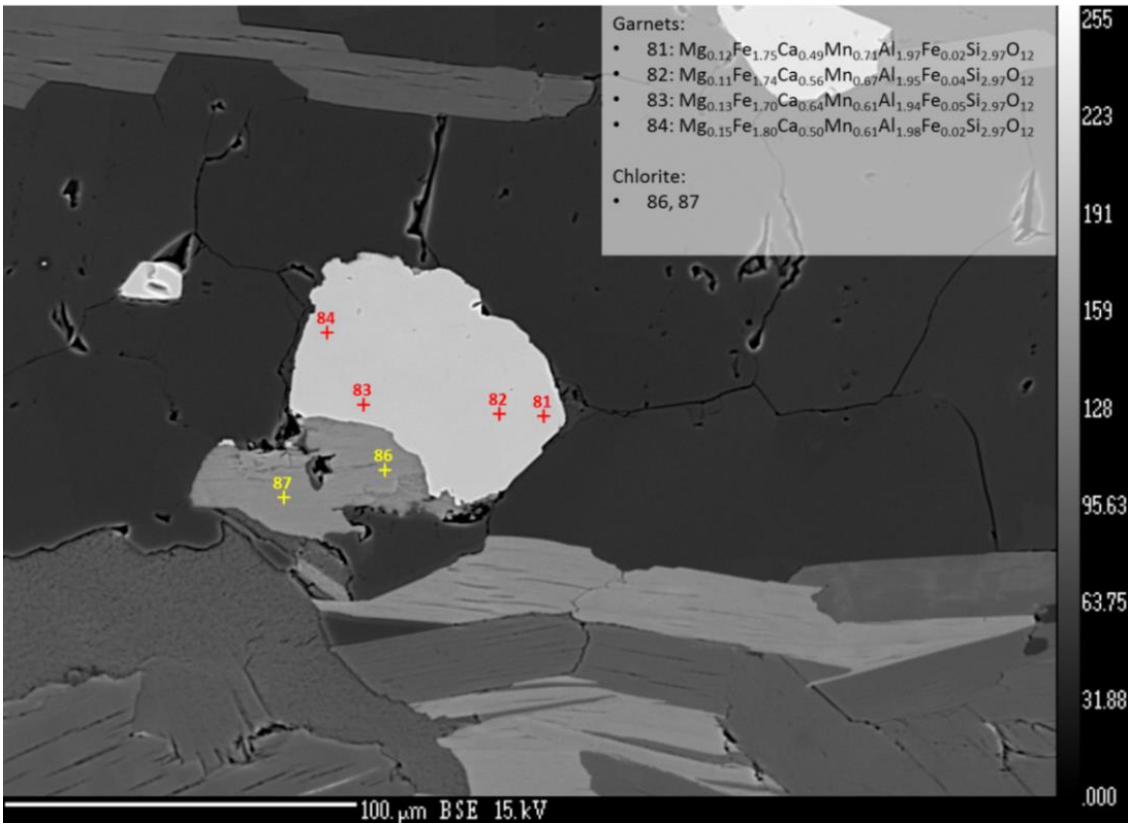

Figure 20: Electron back scatter image of a garnet analysed for zoning in the garnet schist unit. No significant zoning is observed in the BSE image colour nor in the calculated formulae.

The abundance of muscovite combined with the presence of garnet indicates that this protolith was a fine-grained relatively clay-rich sedimentary rock. Since muscovite is the dominant mineral phase, the protolith was probably a clay rich, most likely, marine sediment deposited in a basin which at times received little coarse clastic material.

3.2.4. Quartz schist unit:

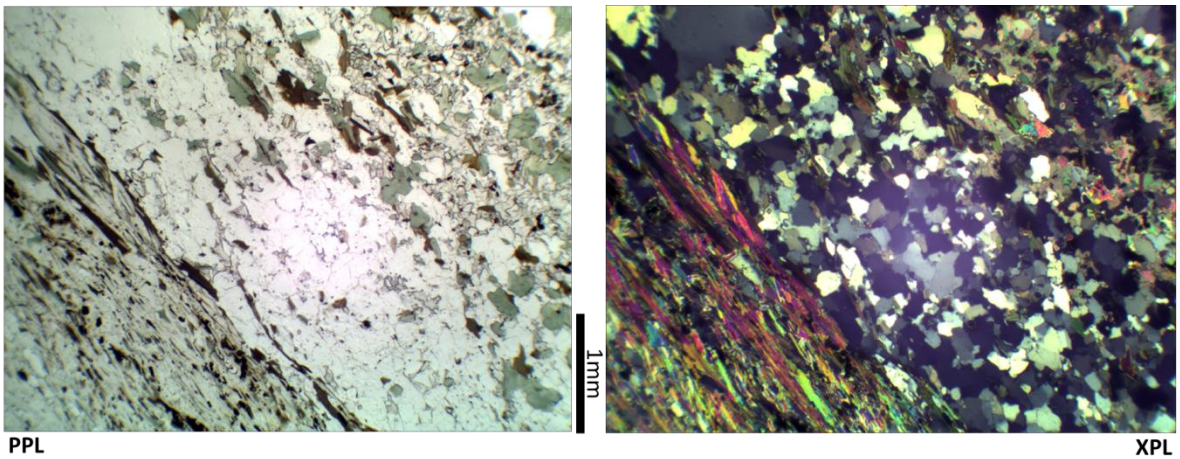

Figure 21: Thin section micrograph of the quartz schist in plane and cross polarized light. The foliation and lithological banding of the unit is visible here, where muscovite is concentrated in the band to the left, quartz in the middle and carbonate and chlorite to the right.

This unit has a higher proportion of quartz and feldspar than the other units mapped (at least half of the bulk composition). Chlorite is present with biotite and muscovite, and together the three sheet silicates make up ca. 25 modal % of the rock. Carbonate is commonly seen in the quartz/feldspar matrix, however it is mostly absent from the muscovite/biotite rich bands (e.g. Figure 21). Ilmenite is an abundant accessory mineral and occurs as elongate grains in line with the foliation.

Foliation is well developed; however, there is also a primary compositional layering preserved showing alternation of quartzo-felsic layers with micaceous layers (see Figure 22 below).

Figure 22: Thin banding in quartz schist showing alternation of quartz-feldspar rich bands and micaceous bands. Crenulation is also seen showing a top to west shear sense.

3.2.5. Graphitic schist unit:

Figure 23: Field picture of the graphitic schist unit showing a graphite rich matrix with sheared quartz veins. The rusty appearance is probably caused by sulphides.

The quartz schist unit grades down into the graphitic schist unit structurally below it. This unit is mainly made up of graphite, quartz and muscovite.

In the transition between the graphitic schist and quartz schist, there is more quartz and muscovite, the latter of which is distributed throughout the rock. In the graphitic schist proper, however, graphite dominates the lithology and the quartz is present as coarse veins as well as a fine grained matrix fill. The muscovite is fine grained and is concentrated along bands. Sulphides and non-crystalline iron oxides give the rock its rusty appearance (e.g. orange coloured quartz vein in Figure 23).

The presence of graphite together with muscovite indicates that the unit must have formed in a stagnant, reducing, most likely marine environment.

3.2.6. Serpentinite unit:

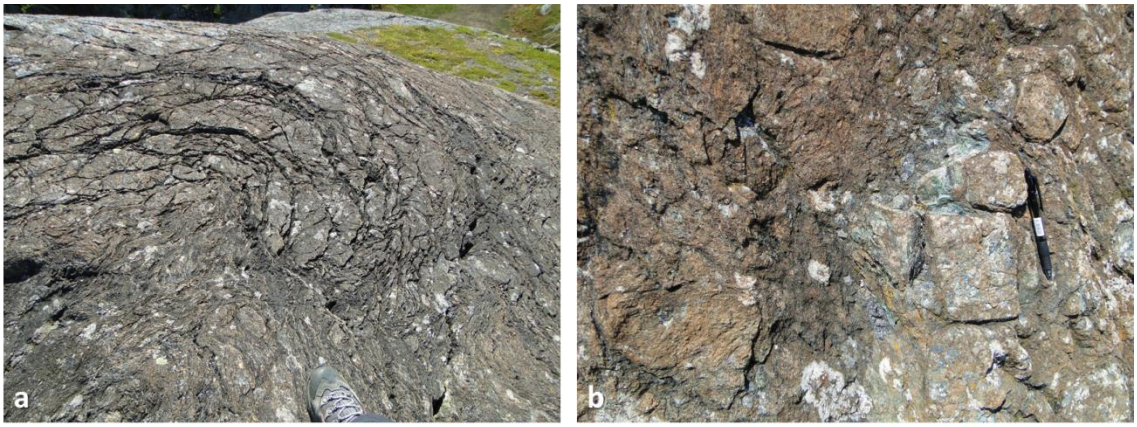

Figure 24: Field pictures of the serpentinite unit. The serpentinite is strongly fractured and veined. b) shows serpentinite brecciation, the green serpentinite can be seen where the orange weathering crust has been chipped away in the middle.

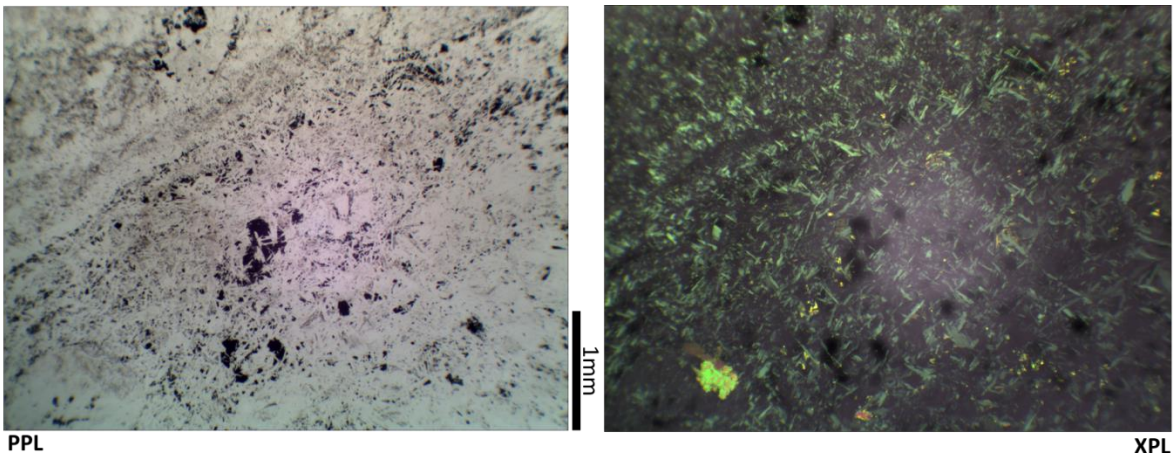

Figure 25: Thin section micrograph of serpentinite in plane and cross polarized light: Mostly serpentine, some magnetite (opaque in PPL) and talc (bright green in XPL).

The serpentinite unit shows some variability. The dominant lithology is serpentinite; however, there are local occurrences of talc schist and soapstones. Since these lithologies share a common

peridotite protolith, they have been grouped in one unit. Additionally, the changes from one lithology to another occur over distances in the order of 1-10m and on a small scale, where the talc schists are often only 1m thick. Thus, it is more practical to consider them one unit. There is no preserved, unaltered peridotite found and so it was not possible to determine with certainty what type of peridotite the protolith was. The variation seen now (serpentinite to talc schist) appears to be related to variation in petrological alteration. The talc schists seem to occur where the serpentinite underwent a greater degree of ophicarbonate alteration(Clerc et al., 2014). Hence, they have larger amounts of carbonate present (e.g. Figure 26). The less carbonated serpentinites, however, are dominantly made up of serpentine and often show a mesh serpentine structure together with magnetite (e.g. Figure 25).

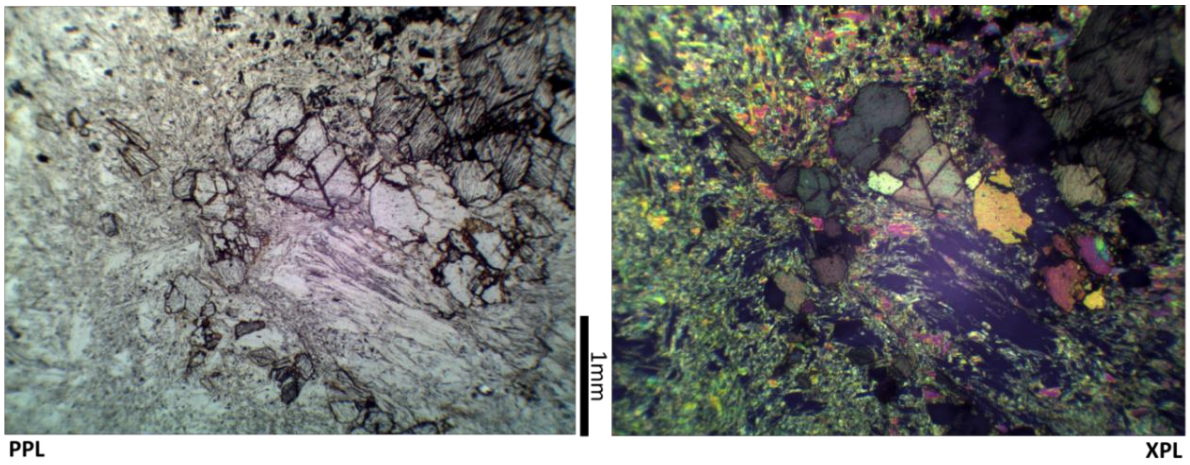

Figure 26: Thin section micrograph of a talc schist in plane and cross polarized light: Talc (matrix to the left), carbonate (high relief crystals in the middle and right) and magnetite (opaque grains in the top of the PPL picture).

While most of the serpentine in the serpentinites occurs in the matrix, there are also abundant serpentine veins throughout this unit. These often show slickensides in the field indicating that the veins accommodated some shear motion. Thin section images of these show two generations of vein fill, where the most recent vein fill formed by shear motion along the fracture, while the first generation formed during tensile opening of the fracture (see Figure 27 below).

The serpentinites that have undergone ophicarbonate alteration show breccia structures, the intensity of which depends on the degree of ophicarbonation. An example is shown in Figure 24b. Ophicarbonation is discussed further in Chapters 1 and 5.

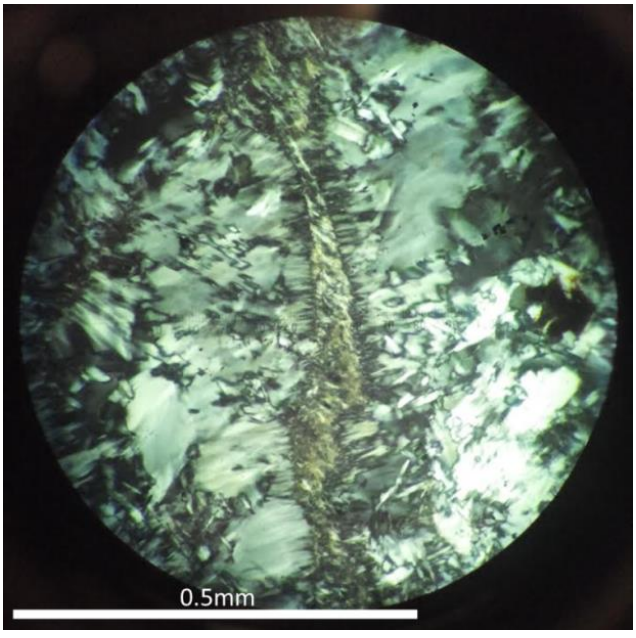

Figure 27: Thin section micrograph in XPL showing a serpentine vein with two generations of growth. The first generation occurred during mode I tensile opening (fibres orthogonal to fracture walls). The second generation occurred during mode II shear opening (fibres at a 30° angle to the fracture walls).

3.2.7. Actinolite schist unit:

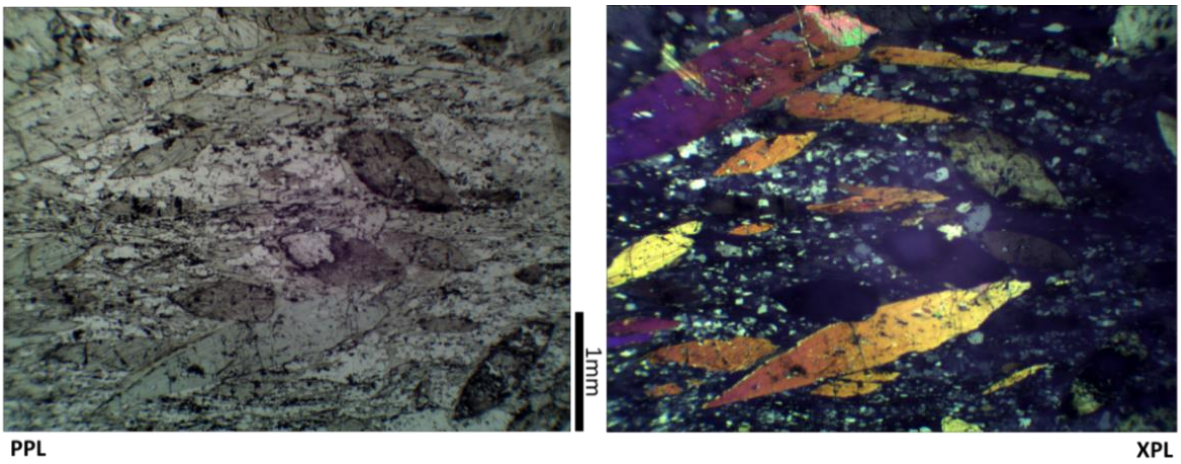

Figure 28: Thin section micrograph of actinolite schist in plane and cross polarized light: Well crystallized actinolite (higher interference colours) with a garben texture in an albite matrix. Taken from the contact between the southern serpentinite body and the garnet schist.

Where the garnet schist and serpentinite contact is exposed, a thin amphibole schist is found. In the mapped area, this unit is seen as a discrete 3-5m thick band between the serpentinite and garnet schist (both northern and southern occurrences). Exposures of other lithologies nearby indicate that it is not a continuous unit. It is therefore more likely to be a metamorphically recrystallized alteration zone rather than a stratigraphic unit. Since it is only observed at the contact with the garnet schist (and not along the contact with the graphite schist), it has probably formed as a product of black wall alteration due to a chemical gradient between the schist and serpentinite during regional metamorphism. There is also evidence of hydrothermal activity which probably aided alteration. Black wall alteration commonly leads to Mg enrichment around peridotites and serpentinites, creating amphibole rich contacts (Beinlich et al., 2010). It is possible that this lithology is not limited to the serpentinite-garnet schist contact, and is not observed elsewhere simply for lack of exposure, however, since it is exposed at several places between the serpentinite and garnet schist (while none of the other contacts are exposed), the weathering susceptibility is taken as an additional lithology indicator.

This unit is invariably made up of actinolite and albite. Figure 29 shows a representative example of mineral chemistry. The grain sizes, however, vary from place to place. Figure 28 above shows an example of well crystallized grains reaching several millimetres in length. This image is from the contact zone of the southern serpentinite body with the garnet schist. In contrast, Figure 30 below shows a very fine grained actinolite and albite matrix taken from the contact of the northern serpentinite body with the garnet schist unit.

Additionally, there is some variation in the remaining, where the northern contact shows more epidote (e.g. band at the top of Figure 30), chlorite and biotite, while the southern body shows more calcite. All of these minerals, however, occur in small quantities. The two occurrences of this unit have been grouped into one unit since they are found in the same structural position. Additionally, the rock forming minerals -namely actinolite and albite- show the same proportion and chemistry in both occurrences, supporting the idea that it is the same unit. The differences in grain size might be due to recrystallization, as the southern occurrence (larger crystals) is associated with a zone of

strong hydrothermal alteration and quartz veining. This would have been an event of elevated temperature and fluid pressure, maybe enabling the actinolite crystals to grow. The northern occurrence (smaller grains), however, does not seem to show the same degree of hydrothermal alteration.

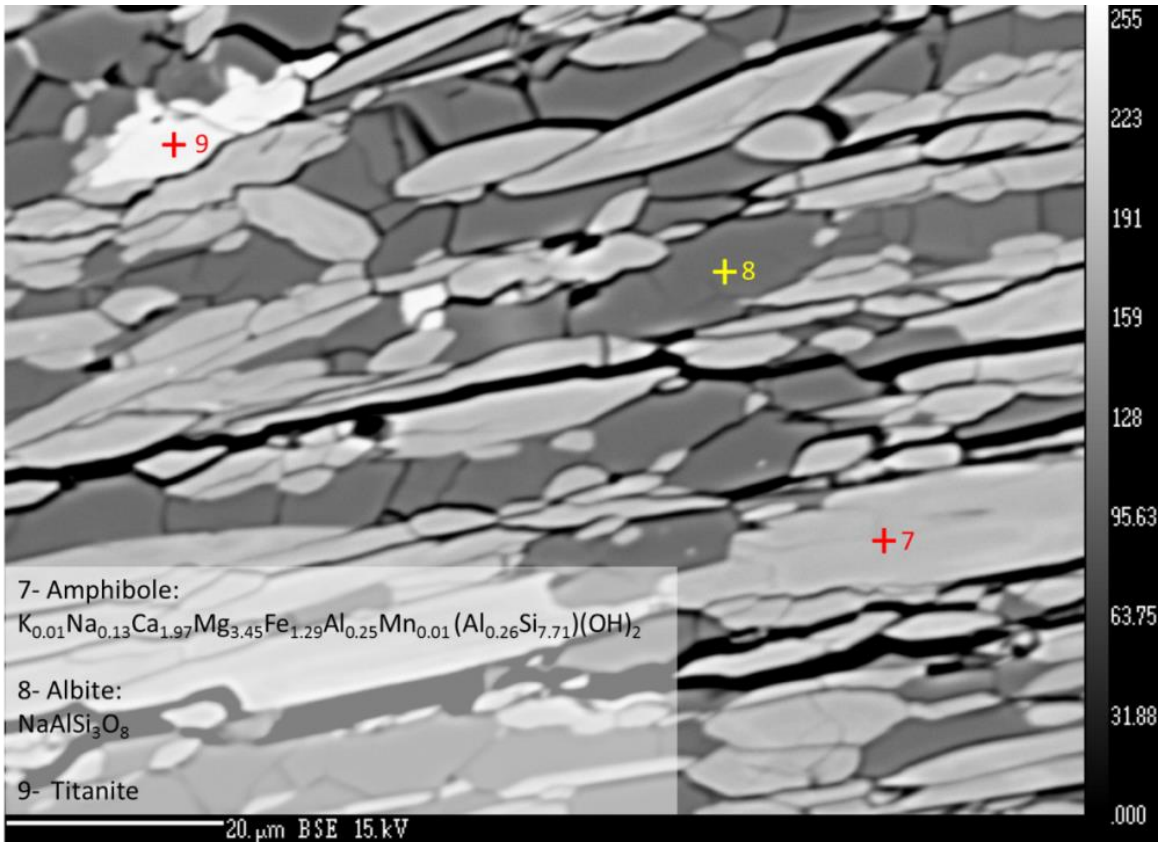

Figure 29: Electron back scatter image showing EMP analysis from the northern actinolite schist unit. The chemistry of the minerals analysed is representative for this unit, however, the small grain size in this northern occurrence contrasts to the larger grain size of the southern occurrence of similar chemistry.

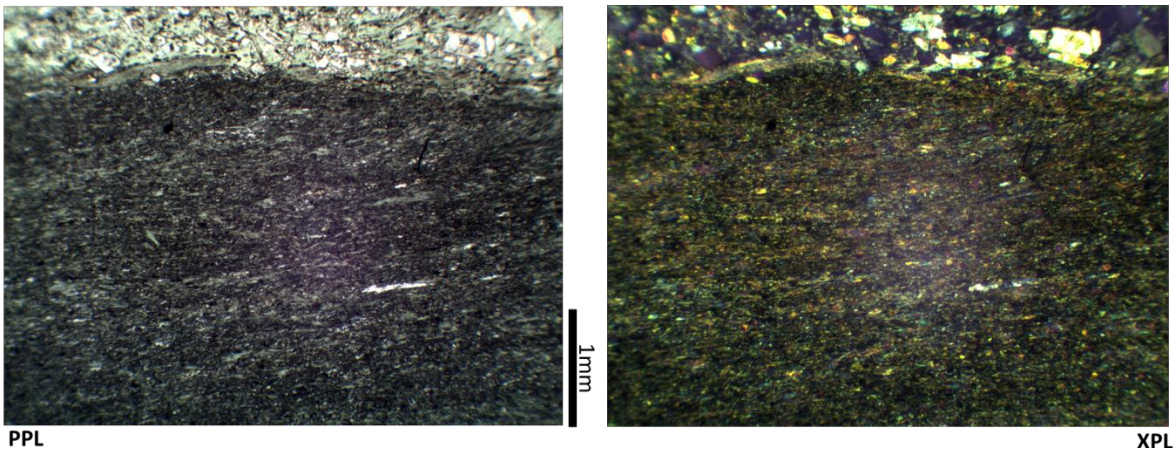

Figure 30: Thin section micrograph of the northern actinolite schist contact: very fine grained actinolite and albite matrix with a band of large epidote grains to the top of the image.

3.3. Structure:

The entire region shows strong multiphase deformation. The overall structure is dominated by a NE-SW strike with a ca. 30°dip towards the E- SE. This means that the units to the SE are structurally higher than those to the NW.

The rocks are strongly foliated and crenulated, where at least two phases of foliation development can be seen in most units. The older generation shows a top to the east shear sense (e.g. Figure 31, Figure 32 and Figure 33), while the younger shows a top to the west direction (e.g. Figure 34).

This most likely represents Caledonian thrusting (top to E-SE), overprinted by top to W-NE shear related to post collisional extensional collapse (Andersen, 1998b, Andersen and Jamtveit, 1990, Fossen, 2010).

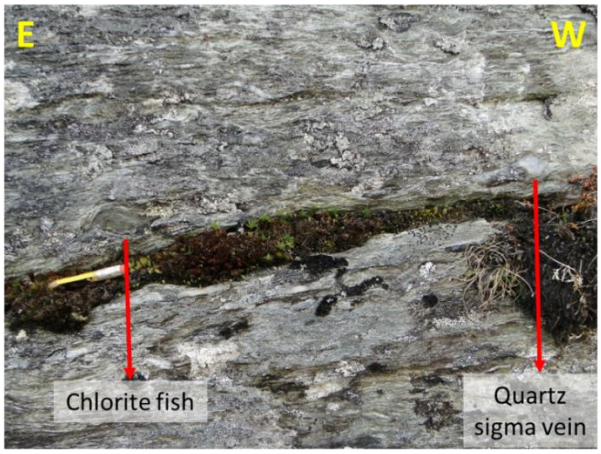

Figure 31: Garnet schist unit shear kinematics: chlorite fish and quartz sigma vein with a top to E-SE shear sense.

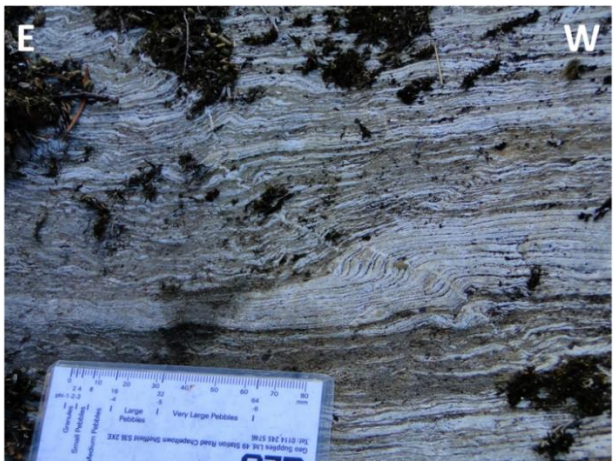

Figure 32: Quartz schist kinematics: Foliation crenulating with a top to E-SE sense of shear.

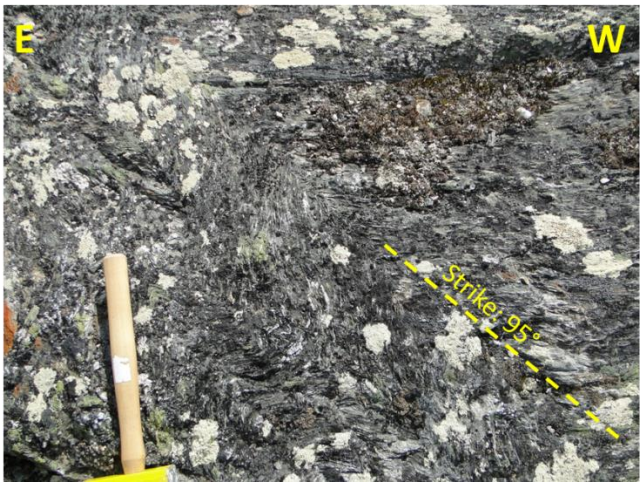

Figure 33: Chevron crenulation in Garnet schist unit with a top E-SE shear sense. The hinge of the chevron microfolds strikes 95°-275°.

Figure 34: Quartz schist unit: Crenulated foliation fish with a top to the W-NW shear sense.

The rocks also show polyphase folding, which is locally seen in microfolds and locally in larger, meter-sized folds. An example of this is shown in Figure 35 below. Quartz veins are also ubiquitous in the

area, however, their sizes vary largely from one exposure to another. An example is shown in Figure 36 below.

Figure 35: Polyphase folding in quartz schist unit, exemplifying the structural complexity of the area.

Figure 36: Garnet schist unit: folded foliation later fractured and filled with vein quartz, which is also deformed.

The structure of the area is, therefore, complex and riddled with several phases of deformation. This complexity is well documented in the literature and lies outside the scope of this thesis. The structures and faults have, therefore, not be been mapped extensively, however the main (and relevant) structures are documented where appropriate.

3.4. Interpretation of association:

The lenses of ultramafic rocks in Bøverdalen are in contact with several metamorphosed sediment units (refer to the lithological map in Figure 9). Figure 37 presents a pseudo-stratigraphic log showing the present succession and stratigraphic thicknesses of the mapped units. This is based on an average Caledonian dip of 30° towards the south east (140° dip azimuth).

One of the purposes of the detailed mapping of the meta-sediments around the meta-peridotites here was to investigate the nature and contact relationships between the variable metasedimentary units in the area. Particular attention has been directed to understand to what extent the vertical succession is structural stacking versus stratigraphic layering.

Since the units dip towards the south east, the structurally lower units are in the north west of the area. The lowermost exposed unit is the garnet schist. According to the NGU map, there is a phyllite unit below the garnet schist, however, we do not find an outcrop of this in the mapped area, and so the exposed north-western edge of the garnet schist unit marks the limit of the mapped area to the NW.

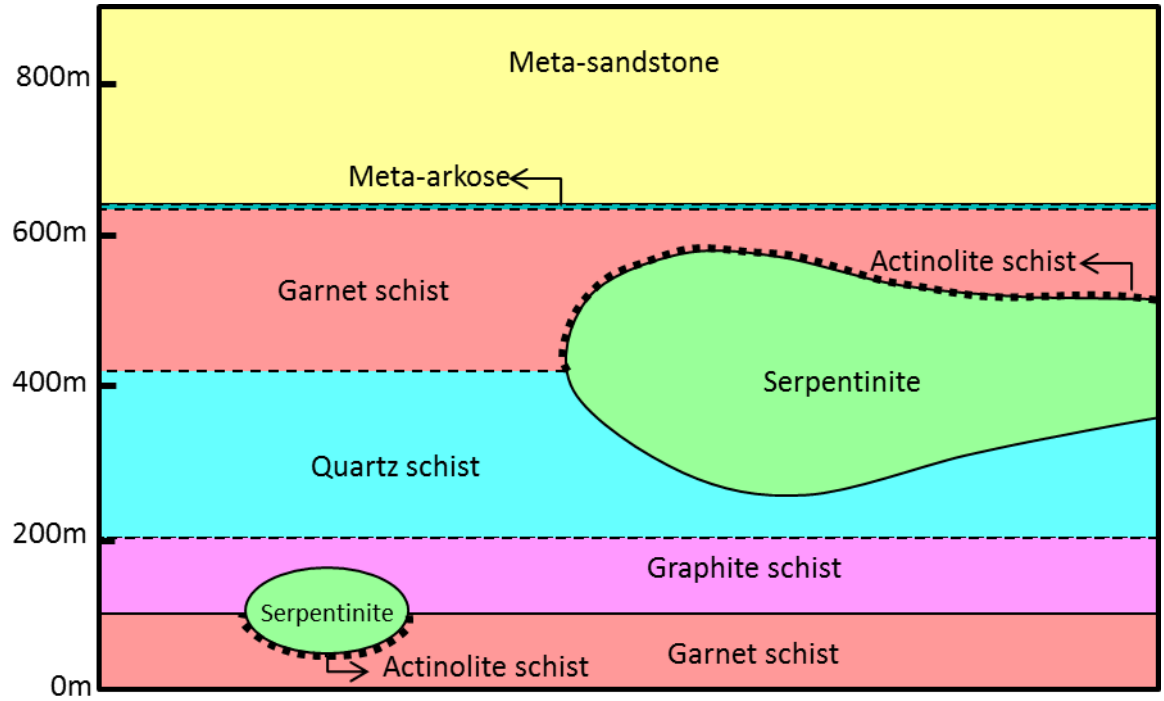

Figure 37: Pseudo-stratigraphic log of the mapped units in Bøverdalen showing their succession and stratigraphic thicknesses based on an average dip of 30° towards 140°. See text for discussion.

The garnet schist is an alumina-rich unit with >50% muscovite. It probably originated as a shale, indicating deep marine conditions (or at least low influx of coarse clastics).

Above this, we find the graphitic schist suggesting an even more stagnant depositional environment. This is most likely of deep marine origin in a basin with limited water circulation and anoxic conditions. The graphite schist grades up into a more quartz rich schist, also likely of a deep marine siliciclastic protolith. This unit contains carbonate in the matrix. The carbonate in its current form is probably secondary, however, its presence in higher amounts in this unit (in contrast to the adjacent garnet schist, for example) indicates that the protolith also probably had carbonate. This may indicate that this unit was deposited in water that was shallower than the carbonate compensation depth (CCD) (Nichols, 1999). The contact between the quartz and graphitic schists is transitional and shows interfingering of quartz and graphitic schist. This indicates that the contact is stratigraphic rather than tectonic. This also indicates that the clastic input varied considerably before the quartz-carbonate rich sedimentation dominated.

A garnet schist also occurs above the quartz schist to the south east. It is not clear from this small area whether it is a repeated unit or a separate unit. The two units have very similar compositions, textures and topographical expressions and so a tectonic repetition cannot be ruled, but is not demonstrated.

There is a thin band of meta-arkose above the garnet schist and below the meta-sandstone. Both the meta-arkose and meta-sandstone are semi-pelites with a large proportion of quartz and feldspar. This indicates a sedimentation environment where continental material was supplied abundantly. A source area with continental and most likely granitoid rocks providing the erosional products must have, therefore, been the provenance area for these sediments. There are no preserved primary sedimentary structures, so an exact interpretation of the depositional environment is not possible.

The meta-arkose has coarser clastic grains suggesting a supply of more coarse-grained material. This would correspond to an interval with more energetic transport than the background sedimentation of dominantly finer grained materials. This was probably due to a brief change in sediment supply, as there is no clear tectonic boundary where the contact is exposed between the two units.

The serpentinites, therefore, lie within metamorphosed marine sediments of varying compositions that probably reflect variation in sediment influx.

There is no evidence of magmatic activity in the Bøverdalen area. Some meta-gabbroic occurrences are found further north east in the Vågåmo-Otta (Jotunheim complex, mapped by the NGU as part of the Jotun-Valdres nappe complex) and south east in the Høyvatnet area (Fortun-Vang thrust) as shown in Figure 38. These also show evidence of marine sedimentation prior to metamorphism, as well as Mid-Ordovician shelly fauna alluding to Iapetan microcontinents (Harper et al., 2008). The Høyvatnet area is presented in more detail in the section below.

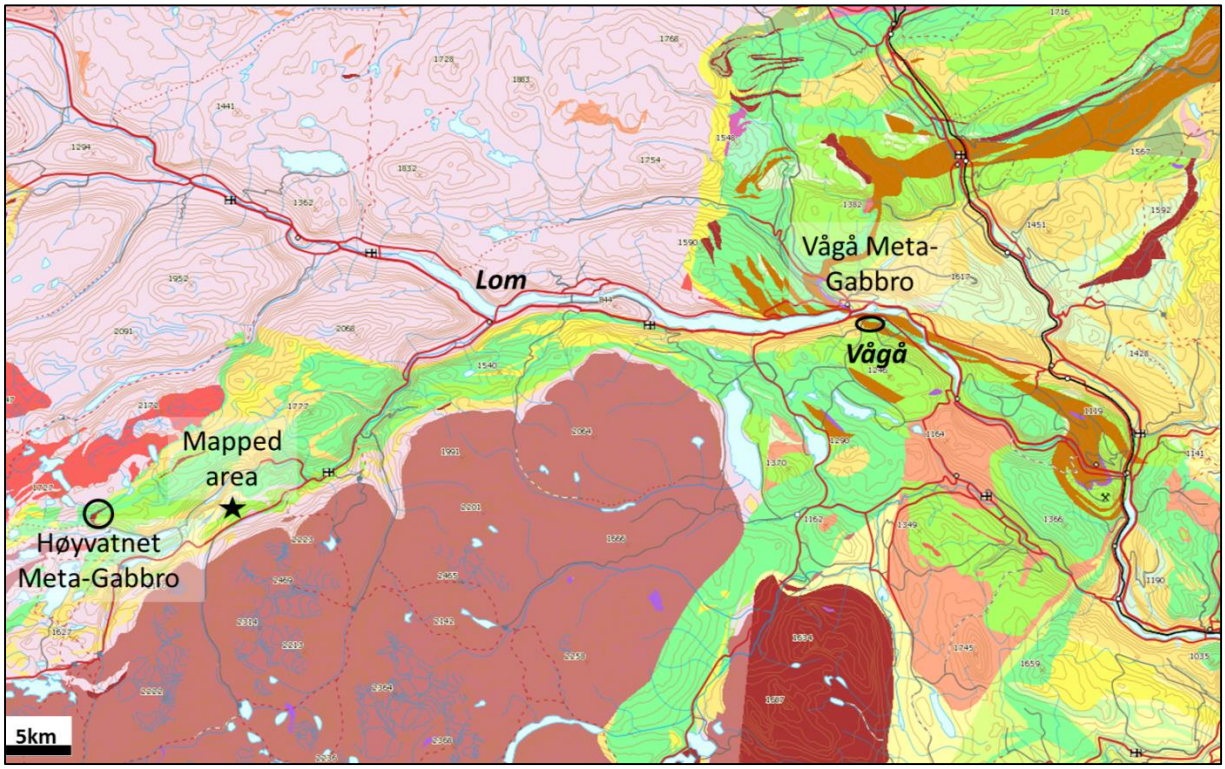

Figure 38: Location of the mapped area and the closest magmatic rocks in Vågå and Høyvatnet.

4. Høyvatnet

4.1. The Høyvatnet meta-conglomerate

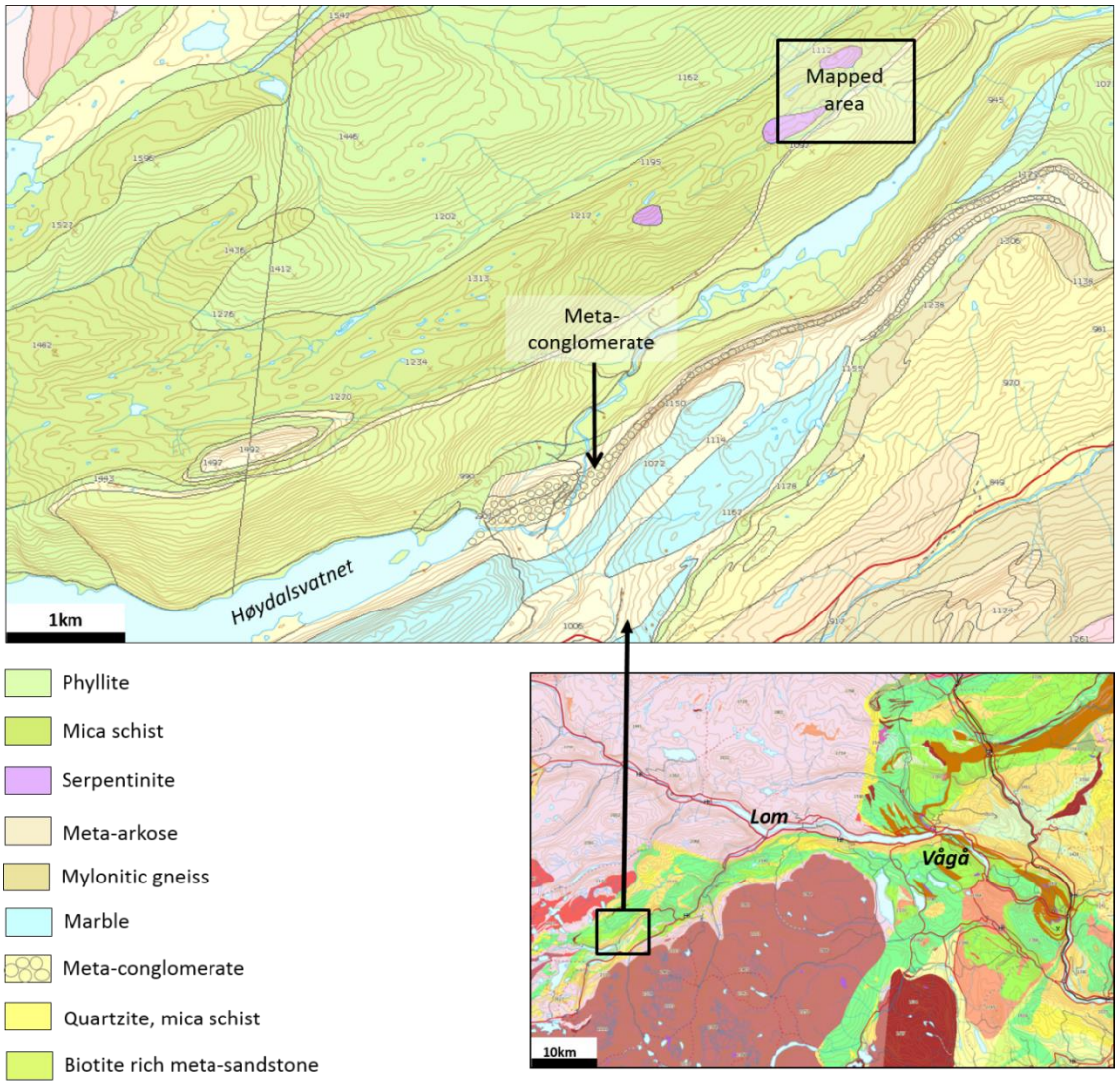

Figure 39: Location of Høyvatnet meta-conglomerate unit relative to the mapped area.

The area at the north eastern end of Høyvatnet (south west of the mapped area) includes a unit of strongly deformed and metamorphosed conglomerate interlayered with coarse- to fine-grained meta-sandstone. On the NGU map (Figure 39) this unit can be traced several kilometeres both to the east and west. Using an average dip of 30° towards the SE, the unit is ca. 430 m thick. The unit shows an excellent outcrop at the northeastern outlet of the Høydalsvatnet lake, which has been selected for further examination.

4.1.1. Lithologies/bedding

There are two main lithologies in this outcrop; meta-conglomerate and meta-sandstone layers. The conglomerate layers are much thicker (range from 1-5 m). The sandier layers are laterally persistent but often only around 20-40 cm thick. The thicker conglomerate layers therefore dominate this outcrop, as is shown in Figure 40.

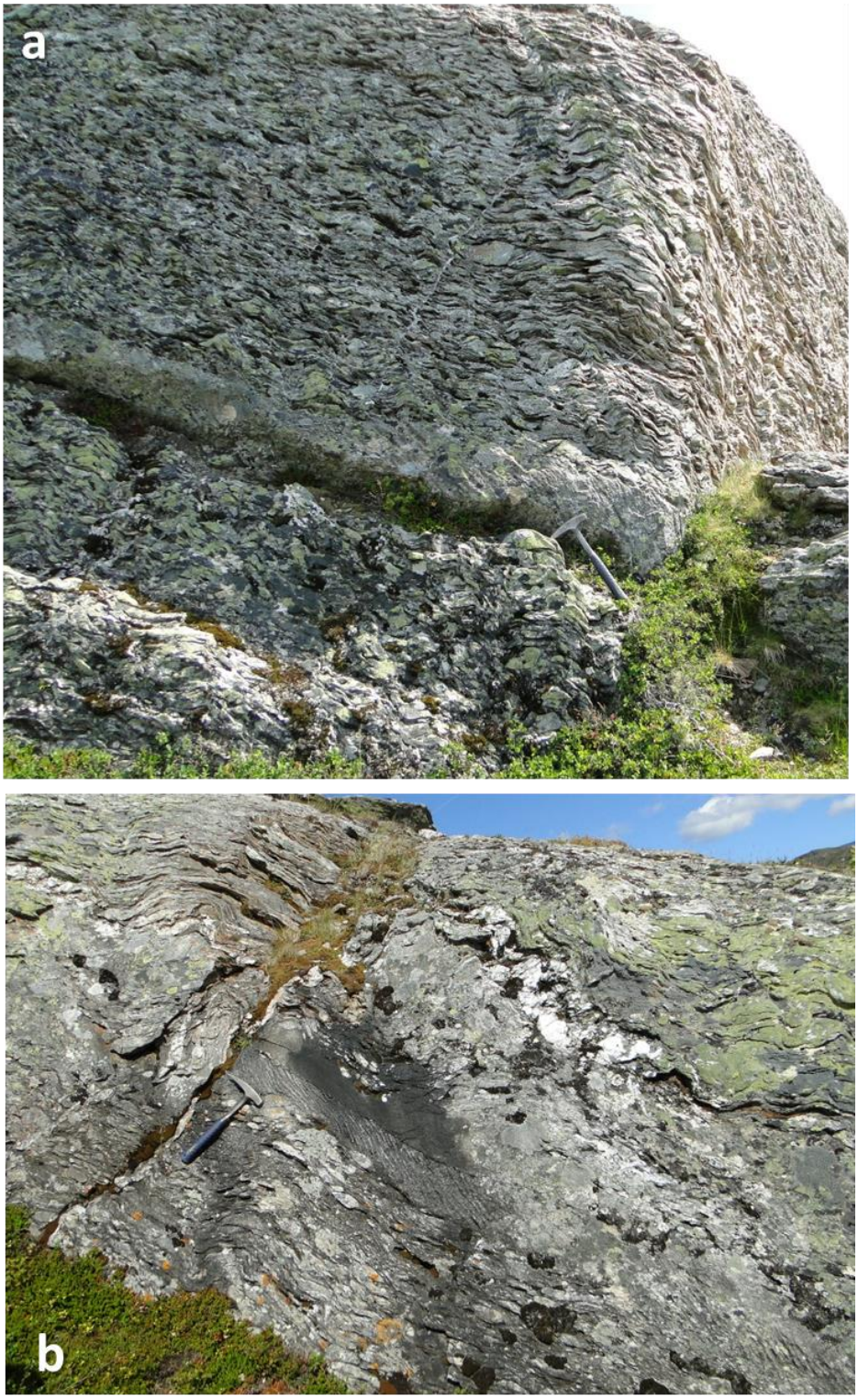

Figure 40: Distribution of deformed meta-conglomerate vs. meta-sandstone layers at Høyvatnet. The pebbles in the conglomerate show wavy deformation and elongation. a) Typical distribution showing 30cm thick sandy layer in between thicker meta-conglomerate layers that are ca. 4m thick. Pronounced foliation created by flattening of the pebbles (see below), as well as crenulation type folding of the foliation. b) 1-2m thick meta-conglomerate with two thinner sandier layers just above the hammer (coarse sand at the hammer head, medium sand above). A spaced crenulation cleavage is seen in the semi-pelite layer at the hammer head. Folded quartz veining visible higher in the outcrop.

The conglomerate layers are mostly clast supported (e.g. Figure 40), however, locally interfinger with matrix supported layers (e.g. Figure 41). The conglomerate layers may show both fining upwards and coarsening upwards sequences. An example of a possible upwards fining sequence is shown in Figure 42. It is to be noted, however, that the outcrop does not show a statistical occurrence of in situ fining/coarsening upwards sequences to conclude the dominant sedimentary grading.

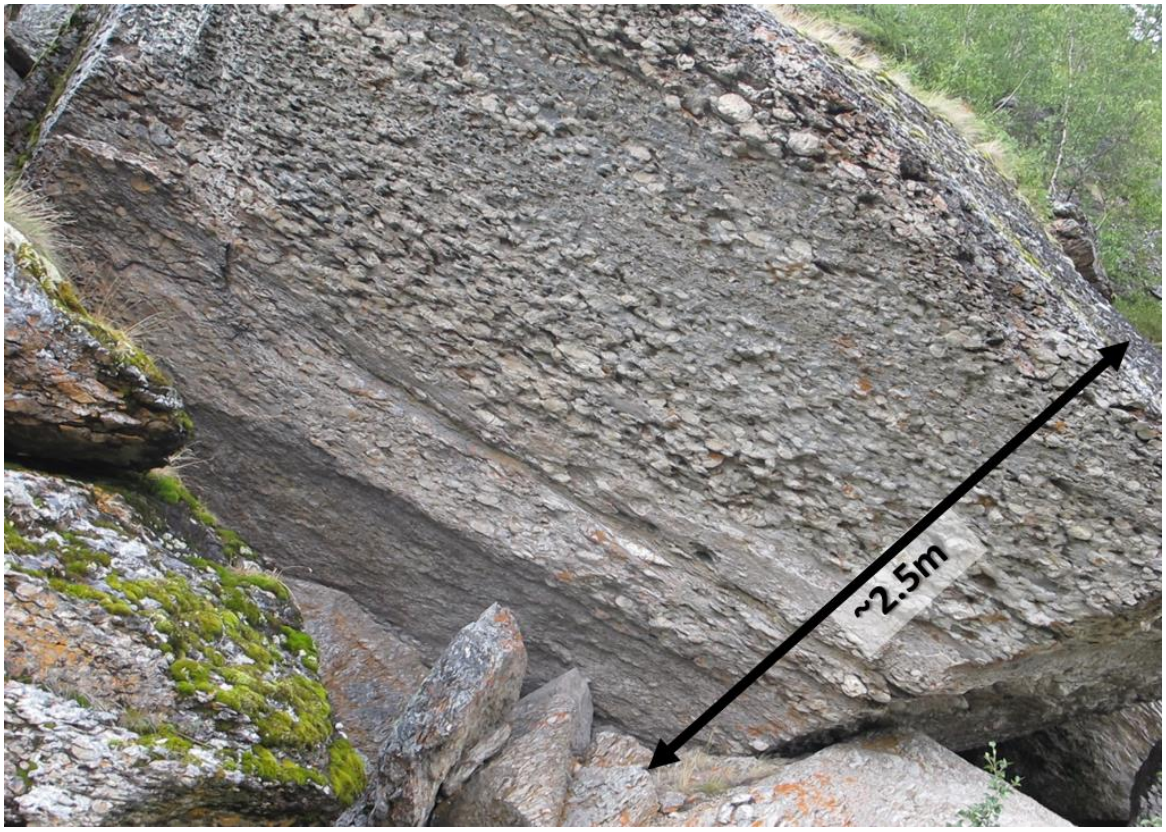

Figure 41: Clast supported conglomerate layers with finer matrix supported layers in between. Photo by Torgeir B. Andersen, 2014.

Figure 42: Possible fining upwards sequence from conglomeratic (wavy foliation) to sandy layers (strong cleavage refraction in sandy layer no. 3, indicating upwards fining of the layer), followed by a new package of conglomerate at the top.

4.1.2. Composition

The sandy layers are mostly made up of coarse sand, with some layers showing medium-fine sand. Some layers also show grading of medium to fine grained sand which is reflected in the intensity of the cleavage refraction developed during deformation (e.g. Figure 43). The sandy layers contain quartz, feldspar, biotite and carbonate.

The conglomeratic layers contain three types of clasts; quartzite clasts, vein quartz clasts and dolomite clasts, where the dolomite clasts are sparser than the quartz dominated clasts.

Quartzite & vein quartz clasts: These clasts are shown in Figure 44 below where the milky white clasts are the vein quartz clasts and the grey clasts are the quartzite clasts. The clasts originated as well rounded pebbles, as can be in the figure (rounded edges and contacts between adjacent clasts). They are mostly 5-10 cm but can reach up to 30 cm along their axes. They appear to be made entirely of quartz, indicating a mature source that has been water worn and transported (to achieve the rounding).

Dolomite clasts: These occur both as small, angular-subrounded pebbles as well as large angular fragments. They weather out of the meta-conglomerate more easily (e.g. Figure 46), creating a pitted appearance in layers that have higher concentrations of them. The smaller pebbles are mostly 5-10 cm large, however, the larger fragments can be up to 2m in size and are often crossed by quartz veins (see Figure 45).

Figure 43: Grain size grading in a sandy layer reflected in the intensity of cleavage refraction developed during deformation. The grain size is coarser at the base and fines upwards. The crenulation cleavage is more pronounced in the top of the layer due to the larger proportion of mica which was more intensely foliated before the secondary crenulation formed. Note the outsized pebble clast in the sandy layer. Photo by Torgeir B. Andersen, 2014.

Figure 44: Cross section of meta-conglomerate layer in Høyvatnet showing dominance of quartzitic clasts (greyish clasts) and vein-quartz pebbles (milky white clasts). The edges of the clasts show the pebbles are originally well rounded.

Figure 45: Conglomeratic layer at Høyvatnet with a large dolomitic clast intersected by quartz veins.

Figure 46: The small dolomite clasts (brown) in the meta-conglomerate are more susceptible to weathering and leave holes where they have fallen out. Some layers contain higher concentrations of the dolomite clasts than others, such as the bottom layer of the image to the left. The image to the right also shows outsized quartzite clasts in the finer grained layers.

4.1.3. Deformation

The meta-conglomerate-sandstone unit is strongly affected by deformation. The resulting flattened, and folded clasts create the conspicuous wavy, planar fabric of the unit (e.g. Figure 40, Figure 43 and Figure 44). A systematic record of pebble shape and deformation is beyond the scope of this thesis, however, qualitative observations show that the pebbles have been mainly flattened with a smaller element of elongation (X ≥ Y > Z). This is shown in Figure 47 where some of the pebbles' axes have been measured and plotted on a Flinn diagram (Flinn, 1962). This creates the planar fabric, while folding (probably later) creates the wavy appearance.

The sandy layers show strong cleavage refraction which is more intense in the finer grained layers. This is illustrated in Figure 43, where sandy layer with grain size grading which fines upwards has developed cleavage which also intensifies upwards. The cleavage in the sandy units is steeper than the primary bedding, indicating that the unit is the right way up and is not overturned.

The whole unit is heavily crossed by quartz lined veins and faults. The veins occur in several generations. The faults (where offset is visible) occur mostly perpendicular to the primary bedding (e.g. at the top and bottom of the dolomite clast in Figure 45).

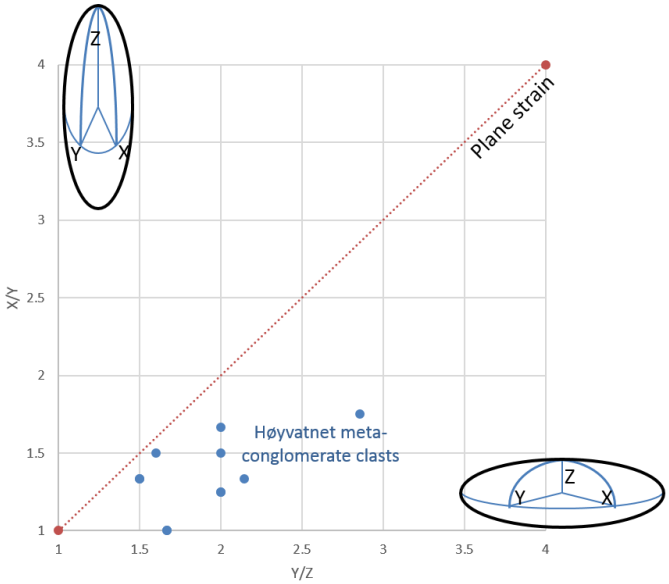

Figure 47: Flinn plot of the Høyvatnet meta-conglomerate. Principal axes measured from the deformed pebbles. The Flinn plot shows the pebbles have dominantly undergone flattening with some elongation (X ≥ Y >> Z).

4.1.4. Base of the unit:

The quartz conglomerate is underlain by a fine grained graphitic schist. The contact between the conglomerate and the schist is sharp (see Figure 48), however, the upper 3 m of the graphitic schist (towards the contact) contains some sandy lenses. There are no fragments of graphitic schist in the overlying conglomerate, indicating that this contact is not an erosional unconformity, but more likely results from a change in sediment supply from the hinterland.

Figure 48: Contact between the conglomerate and the weathered graphitic schist below.

4.1.5. Depositional environment

As shown above, the Høyvatnet meta-conglomerate section is strongly deformed, but the bedding and some original features of the sedimentary architecture are preserved. These features of primary origin suggest that the section is right-way-up. The basal contact to the graphitic schist is in general quite sharp. There are, however, several pebbly to sandy layers near the top of the original black shale, suggesting that the change in deposition was not entirely abrupt. Additionally, there are no clasts of graphitic schist in the overlying meta-conglomerate. It is, therefore, unlikely that the change in sediment supply represents an unconformity/hiatus, but rather resulted from a change in sediment supply in the hinterland.

There are no indications that the conglomerate was deposited in a fluvial environment (no channel bedding or profiles). There are also no indications of tectonic changes in the basin itself (such as uplift or regional erosion). It is, thus, likely that there was a change in sedimentation in the marine realm (where the schist was deposited) triggered by a high energy event, such as a submarine fan.

The deposited conglomerate has three main populations:

1. Quartz vein + quartzite clasts which are ubiquitous and always occur together.
2. Dolomite clasts.
3. Sandy layers.

The quartz dominated clasts (population 1) are mature sediments that have been well rounded. These have probably been water worn and transported far. The sandy layers, however are less mature (rich in feldspar). The dolomite clasts are also probably derived from a closer source as indicated by their larger sizes and angularity. The sandy layers and dolomite clasts probably originated on the shore. The quartz dominated clasts are more likely to be a redeposited conglomerate, which was probably in the vicinity of the sand/dolomite. A high energy event could have triggered a canyon, down which the sediments were transported and deposited together in deeper parts of the basin as part of a submarine fan.

5. Reiggehaugen

5.1. The Reiggehaugen serpentine conglomerate, Vågå (61°47'18.21"N, 9° 5'42.51"E)

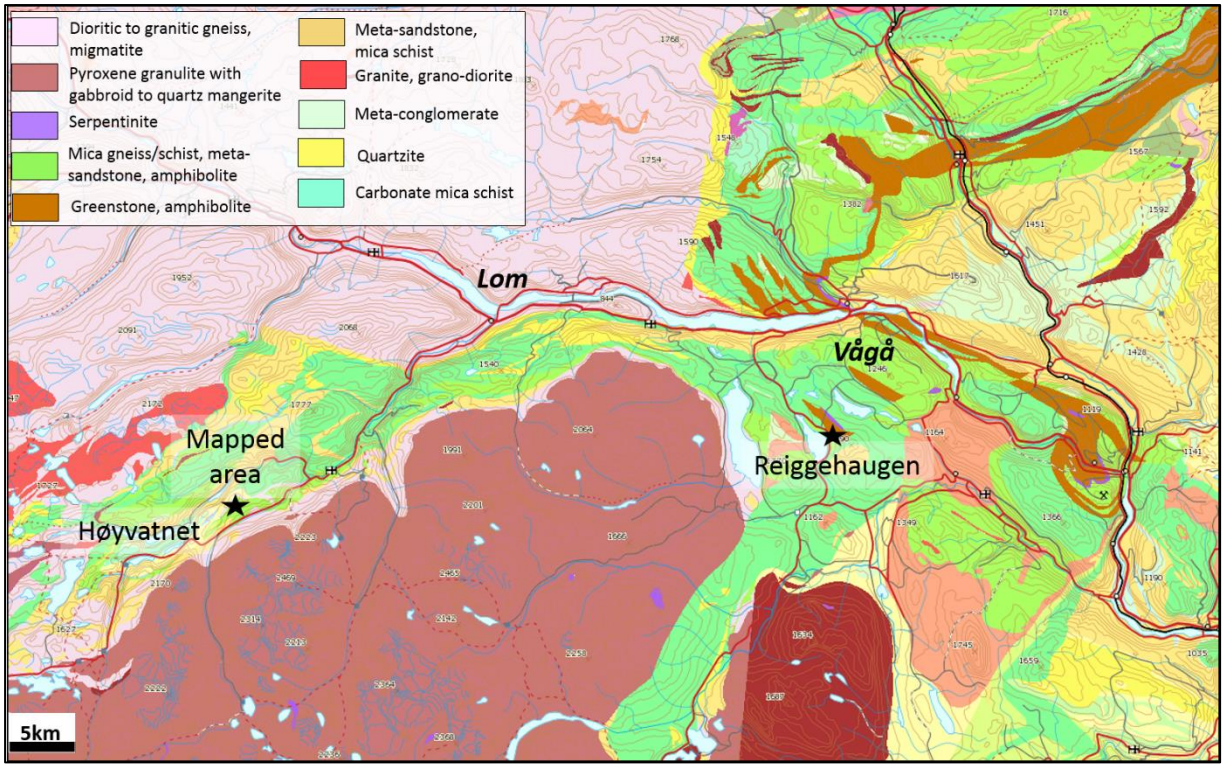

Figure 49: Location of Reiggehaugen ultramafic conglomerate, which lies in the mélange unit in Vågå.

Reiggehaugen is a serpentinite conglomerate hill in Vågå (location shown on Figure 49). Its commercial value as decoration stone was assessed by the NGU in report 2002.031 (Henderson et al., 2002) . This assessment involved sawing several meter sections in the outcrop, exposing non weathered surfaces and allowing detailed study of the serpentinite conglomerate and sandstone (Figure 50).

The rock shows a dominance of pebble-cobble size conglomerate with thinner sandy beds. The rocks are variably fractured and veined and show additional matrix replacement by talc or carbonate concentrated along bands and veins. The structural features are summarized in the next paragraph as documented in the NGU report (Henderson et al., 2002):

> The conglomerate is dipping 50°-70° towards the north. A sandy schist sits structurally on top (northwards), however the contact is not exposed. Structurally underneath (southwards), there is a thin zone of talc schist followed by a green serpentine conglomerate. Further south, there is a thin quartzite and a thicker schistose serpentinite unit (yellow and brown units respectively on Figure 52). The rock is cut by several north-south orientated faults that show increasing displacement towards the east. A perpendicular set of low angle faults (25°-30°) cut the rock with an east-west trend. There are also a series of east-west oriented shear zones throughout the outcrop (foliation/bedding parallel). They are mostly <1-5 mm thick but can be

as thick as 30 cm. Additionally, brittle fractures are observed lined with talc, chlorite and biotite, while wider veins (few millimetres – several centimetres wide) have a talc, chlorite and calcite fill. These are often related to the edges of shear zones and sandstone layers and are less well defined closer to the conglomerate layers. The main features are shown on the geological map in Figure 52.

A description of the rock and its composition is presented below. Sedimentological definitions and classifications are from (Nichols, 1999). An interpretation is proposed at the end of this section.

Figure 50: Sawed outcrop allowing detailed study of the serpentinite conglomerate making up Reiggehaugen, Vågå.

Figure 51: Reiggehaugen conglomerate, weathered vs. cut surface. Photo courtesy of Torgeir B. Andersen.

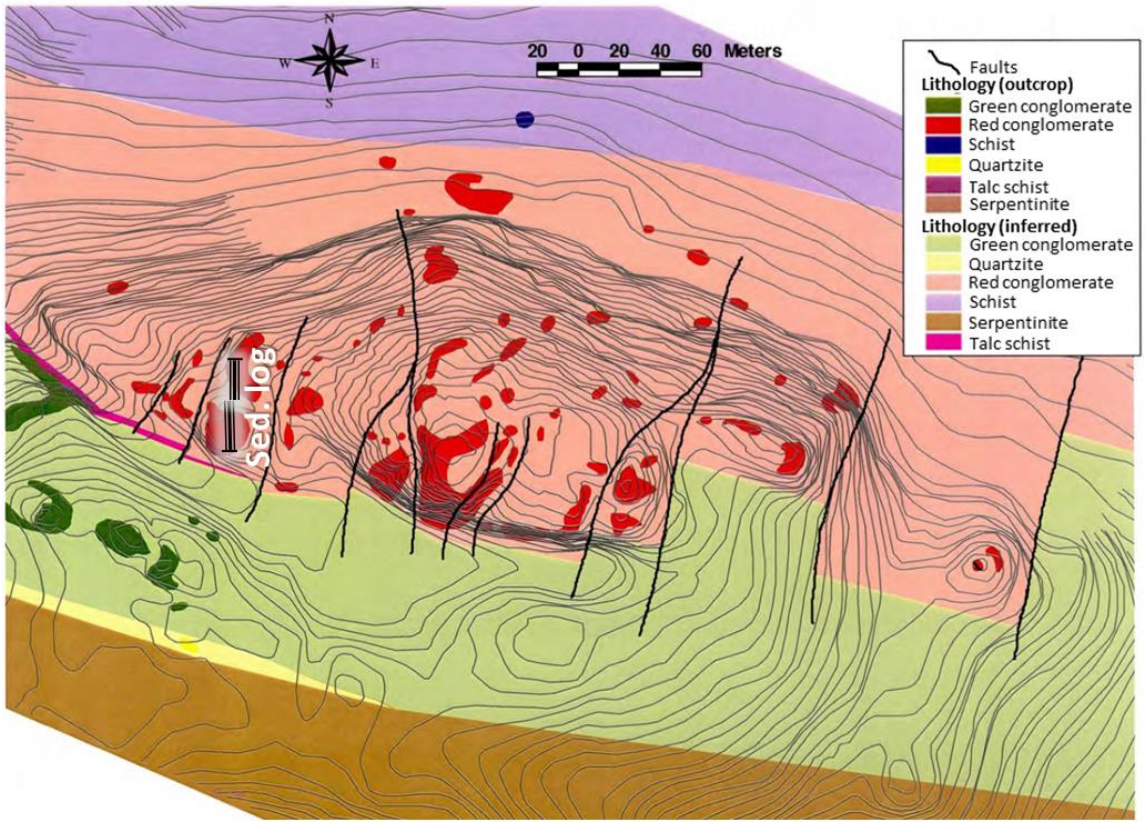

Figure 52: Geological map of Reiggehaugen from Henderson et al. (2002) showing the distribution of lithologies, faulting and location of the sedimentary log which is shown in Figure 55.

5.2. Sedimentology

5.2.1. Layer distribution:

The outcrop shows alternating layers of granule-cobble conglomerate and sandstone, where the coarser cobble conglomerates are dominant. These are clast supported with clast sizes ranging from 5-10 cm. The finest grained layers consist of medium sand sized particles (sand particles around 0.5 mm in size). These layers do not exceed half a meter in thickness, but are often thinner. The coarsest layers are boulder conglomerates (clasts ~20 cm large). The conglomerate layers are poorly sorted, clast supported and often include discontinuous sand stringers (e.g. Figure 53). Most of the layers show an even distribution of clasts, however, some of the layers have an erosive base and fine upwards, where the top is often more matrix supported (e.g. Figure 54). The fining upwards sequences indicate that the layers are the right way, which is also concluded by Bøe et al. (1993).

Sedimentary logging was done on 45m of the outcrop from south to north in the direction of dip. The location of the log is shown on Figure 52 and the log is shown in Figure 55.

Figure 53: Layered sand-gravel layers in the Reiggehaugen ultramafic conglomerate. Many of the pebbles are pitted by other pebbles due to compression. Most of the clasts have a white, talc rim.

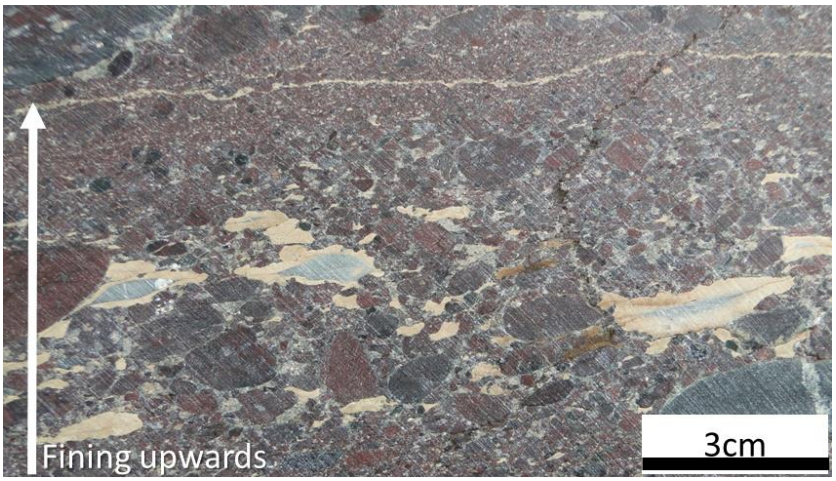

Figure 54: Conglomerate layer fining upwards into a sandstone in Reiggehaugen.

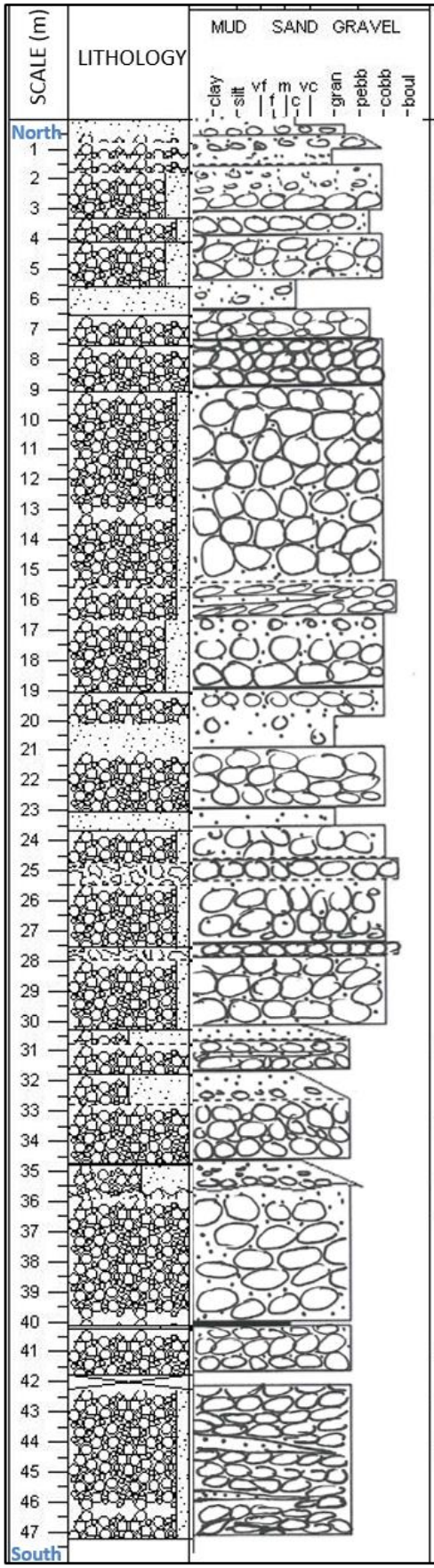

STRUCTURE	NOTES
	Conglomerate with pebbles on top.
300 (strike, top of layer).	Discontinuous sand body on top. Sandier matrix.
	Poorly sorted, well rounded and foliation.
303 (strike)	Foliated sand at the top. More sand in the matrix. Sand fingers.
Veins: 234	Some pebbles.
	Poorly sorted, well rounded and foliation.
	5-10m west of lower profile. Rounded and flattened/stretched. Very poorly sorted. Clasts up to 10cm large. Sand stringers.
	sand stringers
	sandy top
	Sandy layer with some clasts
	Less sand, slightly larger clasts.
292/39	Sand stringers.
	Less sand in base, more on top. Poorly to moderate sorting.
283/43	Moderately sorted, less sand in matrix. Clasts up to 5cm large.
vein in foliation: 293 (strike)	more foliated.
Some sand stringers.	Clasts up to to 2cm large. Higher amount of sand in matrix -Rugby ball clasts. Very poorly sorted. Also veined.
279/39	3m east of bottom of log.
Base: 263/54. Vein (talc fill?): 257/43. Conjugate fracture sets: 238, 301, 270, 246.	Rugby ball shaped clasts at top, rounded and sheared clasts at base (fish shape). Sand fingers. Poorly sorted.

Figure 55: Sedimentary log of Reiggehaugen showing the sedimentary variation in the ultramafic conglomerate.

5.2.2. Clasts:

In the conglomerate, four end members of the clast populations are found:

- Green serpentine clasts
- Red serpentine clasts
- Talc clasts
- Carbonate clasts

The clasts are variably zoned and are thus often a mixture of two or more of the end members. Most of the clasts are well rounded, but some of the green partly talcified clasts are more angular (e.g. green clasts in Figure 58 and Figure 60). In the coarsest layers logged, the clasts can reach 20 cm in length; however 5-10 cm is more common.

Some of the clasts have been sheared, which is locally seen as fractures and veins (e.g. Figure 56). Most of the shearing, however, is expressed in clast reshaping from rounded to variably elongated and flattened fish shaped fragments. The variation in clast shape and size makes it difficult to estimate the deformation aspect ratio, particularly since the original shape is uncertain; however it is probably in the order of 3:2:1.

Clast composition is described below.

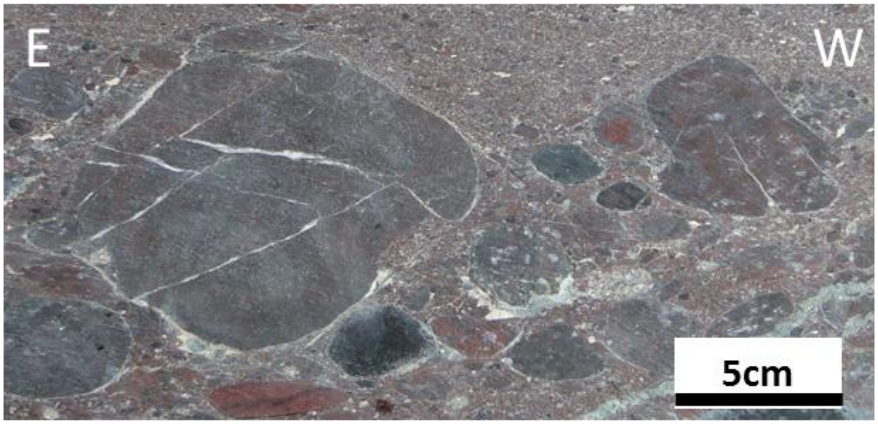

Figure 56: Veining resulting from brittle shearing of a serpentine clast in the Reiggehaugen ultramafic conglomerate. Vein orientation and fibrous growth indicate a top to W-NW shear sense.

5.3. Composition

5.3.1. Matrix:

The matrix mineralogy is made up of serpentine, talc, chlorite, dolomite, magnesite, chromite and magnetite. The matrix grain size varies from fine to granule sized particles. The matrix is shown in a thin section micrograph as well as electron back scatter image in Figure 57. These demonstrate the variation in grain size and mineralogy. The matrix often has a strongly red colour and this seems to be a result of the abundance of relatively large chromite grains (e.g. Figure 57a).

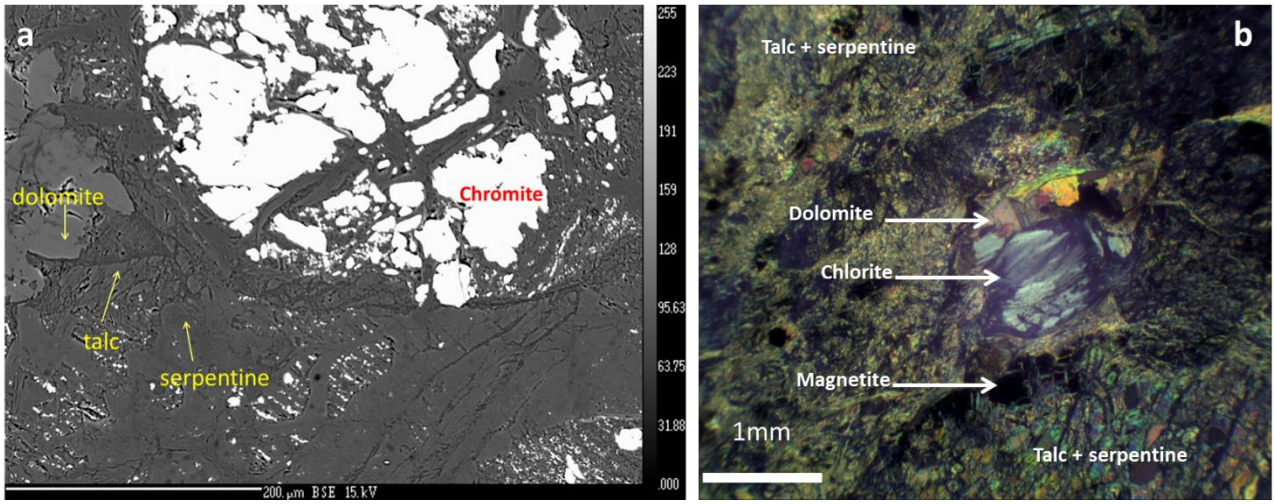

Figure 57: Reiggehaugen conglomerate granule matrix. a) Electron back image shows dolomite, talc, serpentine and chromite. b) Thin section micrograph in cross polarized light showing chlorite and magnetite are also present. The talc and serpentine have the smallest grain sizes present.

In places, there are bands (wider than fractures) filled with magnesite, dolomite and talc. The larger clasts are mostly preserved along these bands (Figure 58) indicating that the carbonate and talc fill is replacing matrix rather than filling a vein.

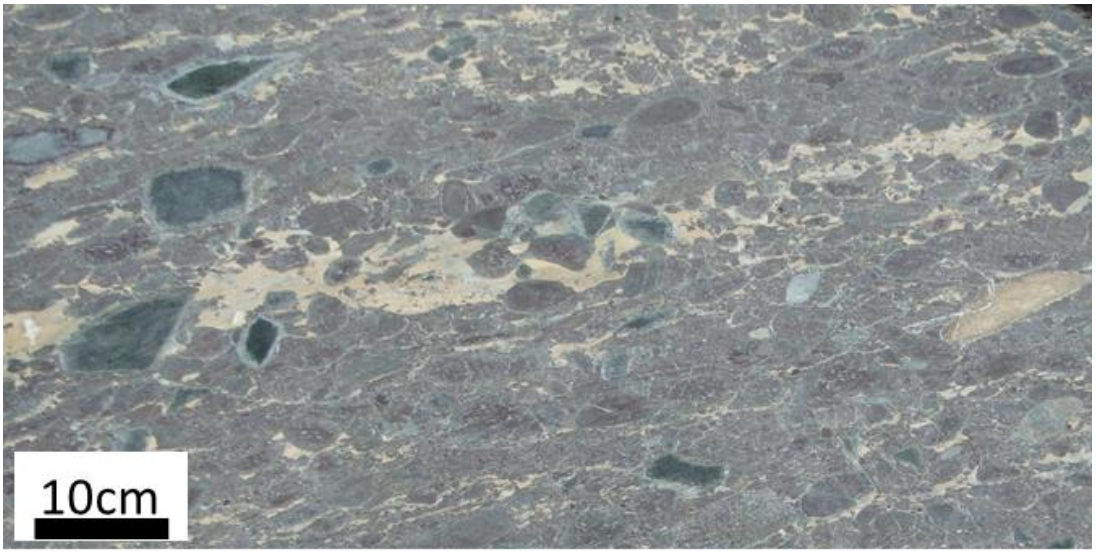

Figure 58: Field picture of Reiggehaugen conglomerate showing a band of matrix replaced by dolomite (beige band going across the picture).

The talc bands are less common than the carbonate bands and seem to be genetically related to fractures from which talcification propagated. An example is shown in Figure 59.

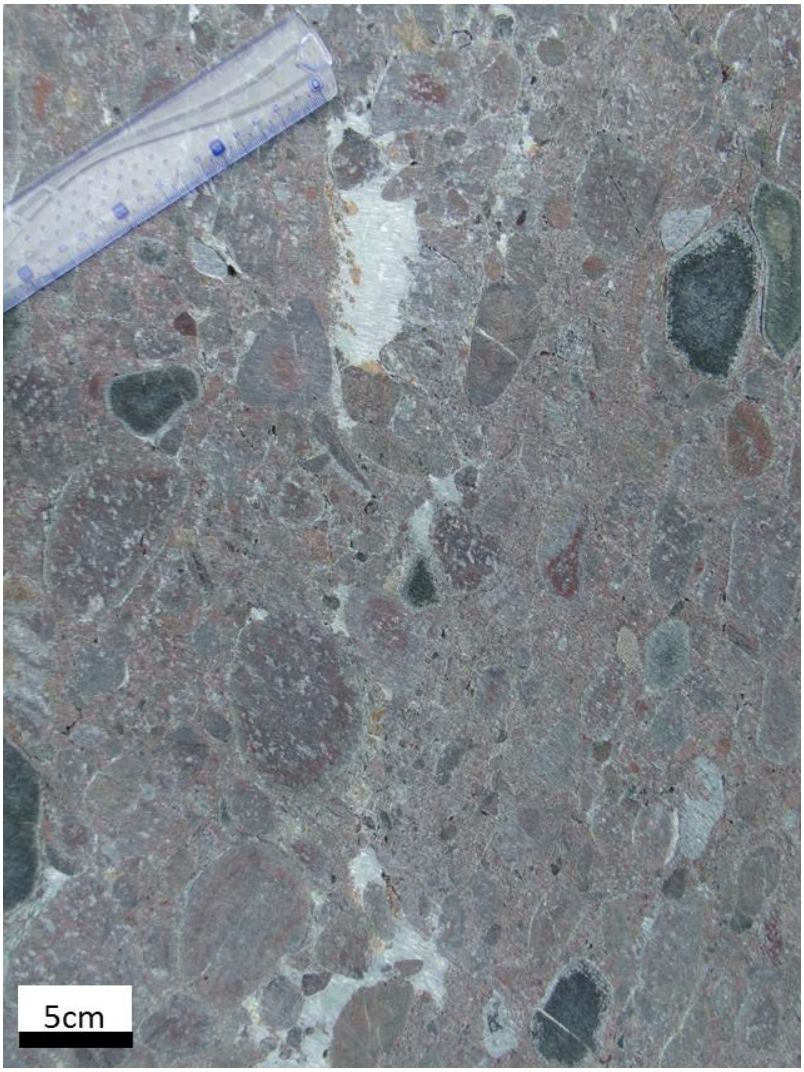

Figure 59: Talc replacement of matrix (grey band in the middle, wider at the top), possibly originating from a fracture in the Reiggehaugen ultramafic conglomerate. Note also concentric zonation in the green clasts where talc (white rim) is replacing serpentinite, also seen in Figure 60.

5.3.2. Clasts:

The clasts have been classified into four end members: Green serpentinite, red serpentinite, talc and carbonate clasts. Most of the clasts show zoning and mixing of more than end member. Notably, talc is often found mineralized in most of the other clasts to varying degrees. Most clasts are either a mixture of talc and carbonate, or more commonly, green and red serpentine. The colour difference may be due to differences in chlorite and hematite contents (Clerc et al., 2014) as well as chromite and talc.

A description of each population is given below.

Green serpentine clasts:

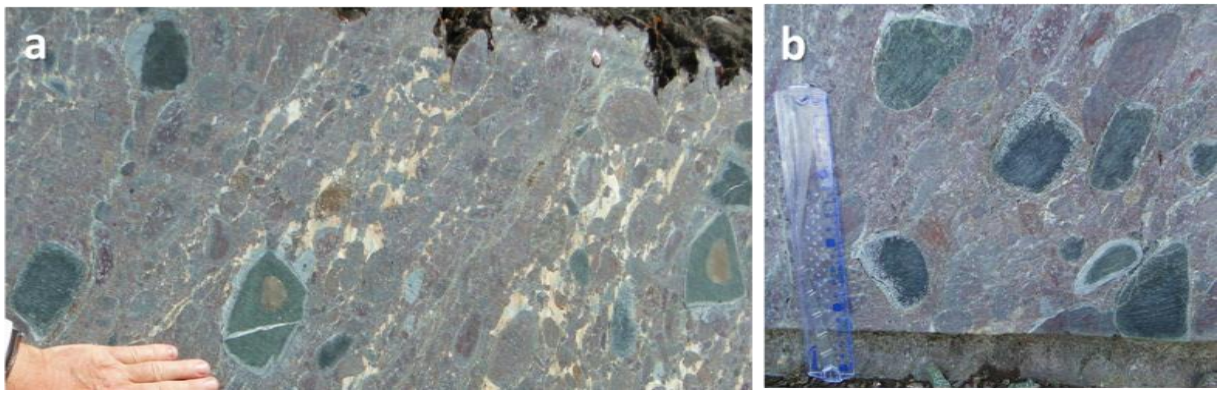

Figure 60: Green serpentine clasts in Reiggehaugen ultramafic conglomerate (scale in (b) is 30cm). They are often larger and more angular than their red counterparts, and some include a yellowish carbonate core, as is seen in (a). b) The talc rim is seen both sharp and grading into the centre of the clast from a specific direction. This may be a mineralization front related to fluid migration from the matrix into the pebbles.

The green serpentine clasts are often larger and slightly more angular than their red counterparts. They almost always have a talc rim and some also have a carbonate core. The talc rim is sharp in some clasts, but grades into the centre of the clast in others, where it is usually more strongly developed in one side of the clast. This may relate to a talcification front moving in associated with metasomatism. Since no specific talc rim orientation was found in the conglomerate, it is more likely that this took place before final deposition of the conglomerate as it is found today. Alternatively, talcification may not have been strongly directional at this scale, however this is considered to be less likely.

Red serpentine clasts:

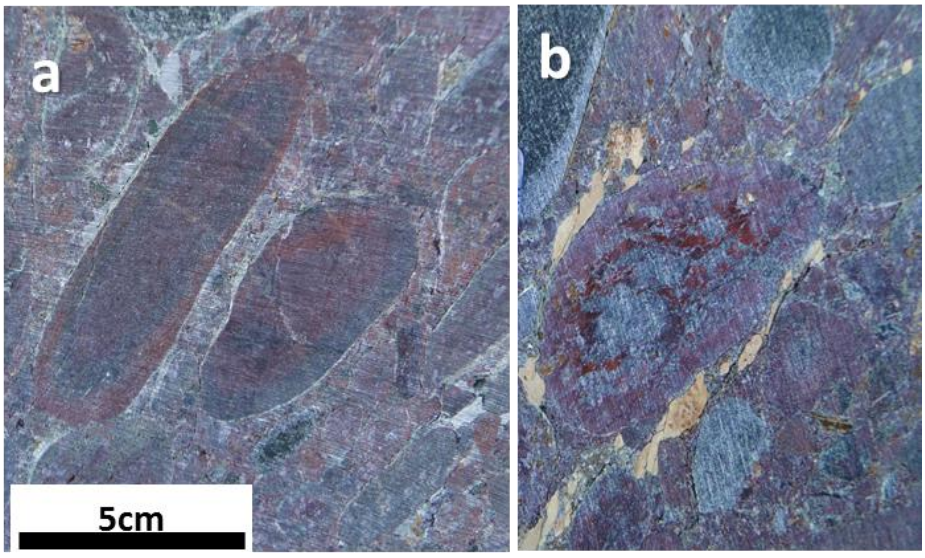

Figure 61: Red serpentine clasts in Reiggehaugen ultramafic conglomerate. a) Elongate, round, red serpentine clasts. b) Strongly zoned, red and green, rounded clasts.

The red serpentine clasts are generally more rounded and often elongate. They are typically smaller than the green clasts, where the clasts shown in Figure 61 are typical. They often also show talcification, however this is usually expressed in zoning of the whole clast rather than just forming a rim. Zoning is also often seen with green 'serpentine', which may be related to varying chlorite and

hematite content (Clerc et al., 2014) The colour variation also seems to be related to the amount of talcification, which seems to give a dominantly green colour. The analysed thin sections from Reiggehaugen indicate that the red clasts (and matrix) mainly get their colour from chromite. An example of a strongly zoned red clast is shown in Figure 62 and Figure 63. The drill core thin section scan (Figure 62, left) shows colourless minerals (talc, carbonate, and serpentine), black magnetite and red chromite.

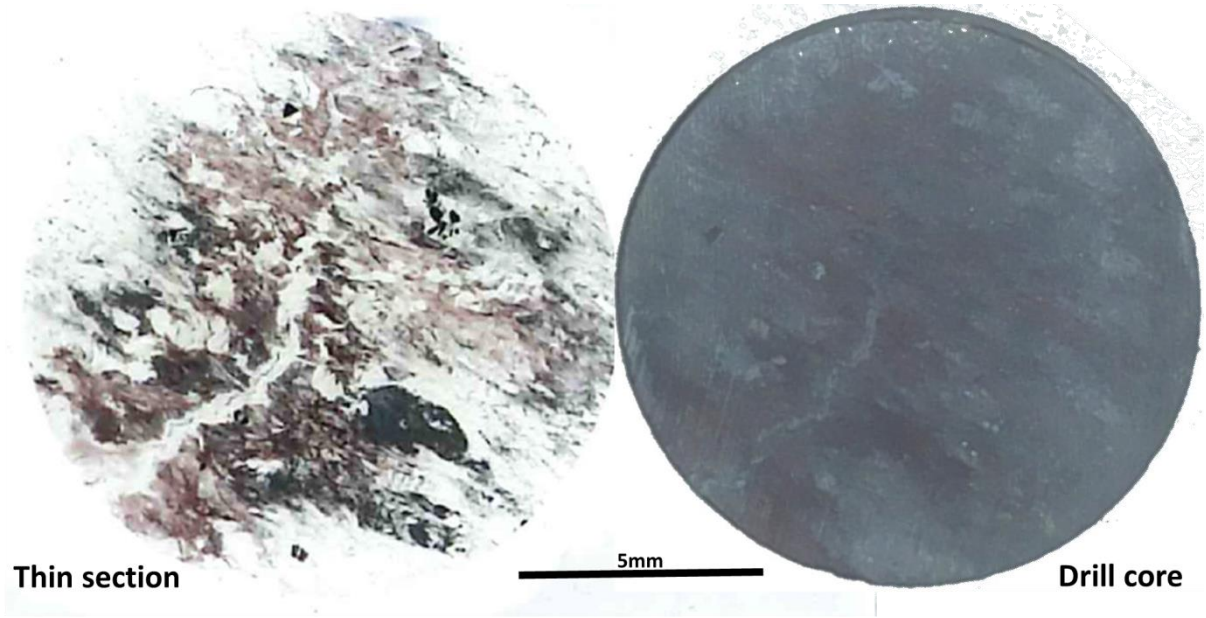

Figure 62: Reiggehaugen conglomerate: strongly zoned red clast and a scan of the thin section made from it. The black mineral is magnetite while the red mineral is chromite.

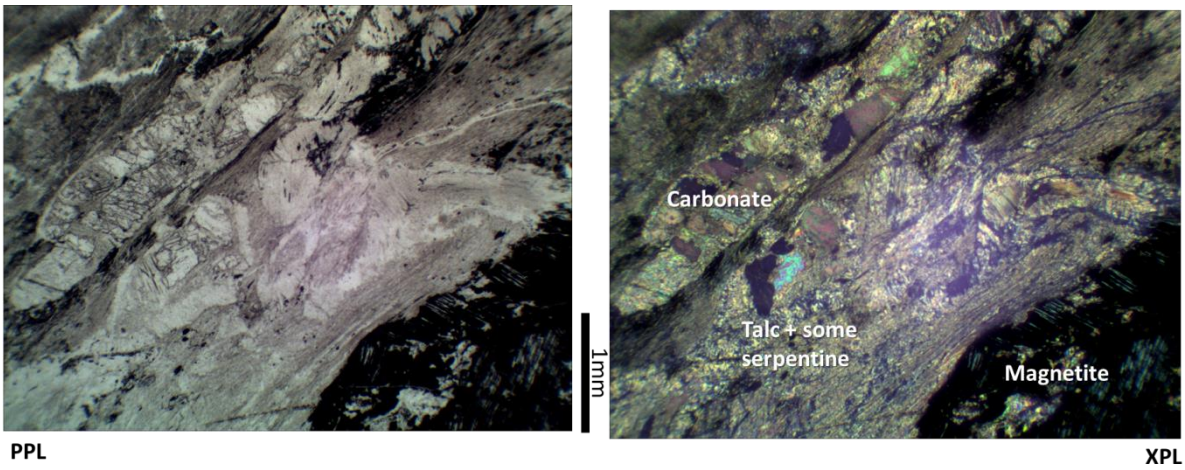

Figure 63: Thin section micrograph of the zoned red clast shown in Figure 62. Most of the serpentine has been replaced by carbonate and talc.

Talc clasts:

Figure 64: Talc clasts (grey) in Reiggehaugen ultramafic conglomerate. These show varying shapes and degrees of rounding, however none are truly angular.

The talc clasts are usually well rounded, but have variable shapes, as is seen in Figure 64 and are less abundant than the serpentine clasts. Some of these have a coarse dolomite core, while the talc that makes up the clast is very fine grained. A beautiful example of this is shown in Figure 65 where a strongly pitted talc clast has a crystalline dolomite core. This clast is also shown in thin section in Figure 66 where the coarse grained dolomite core is visibly contrasted to the finer grained talc matrix around it.

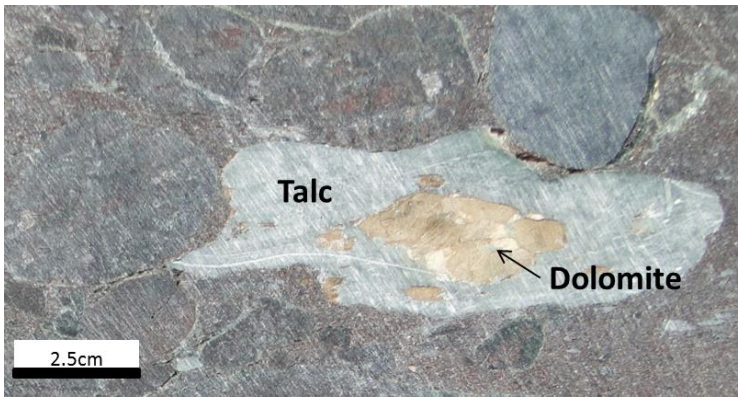

Figure 65: Field picture of a talc clast with a dolomite core. Strong pitting is visible on top of the clast where it is in contact with darker clasts.

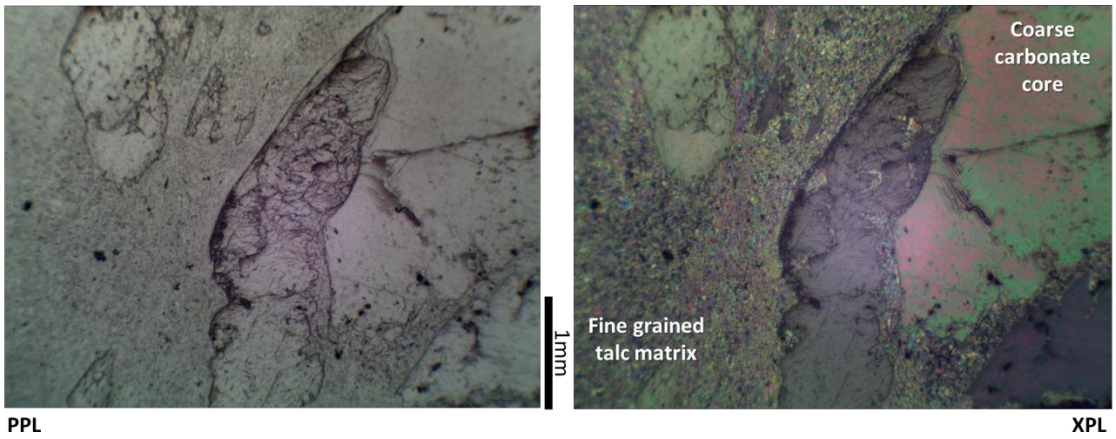

Figure 66: Thin section micrograph of the talc clast in Figure 65. The dolomite core is very coarsely grained (>1mm) and is surrounded by a very fine grained talc matrix.

Carbonate clasts:

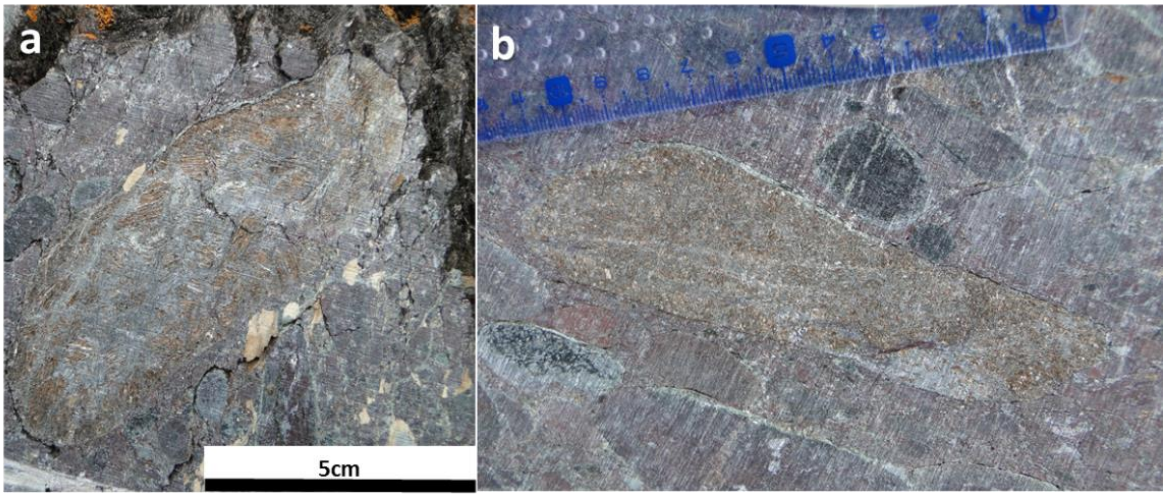

Figure 67: Carbonate clasts in Reiggehaugen ultramafic conglomerate. a) Clast with lamination texture. b) Massive, coarse crystalline clast.

The carbonate clasts show varying textures and amounts of carbonate in the clasts. These clasts consist of dolomite, serpentine, talc and magnetite. Some of the clasts show a more massive, but coarse crystalline texture, such as (b) in Figure 67. Other clasts show lower proportions of carbonate and a crenulated lamination texture, such as (a) in Figure 67. This texture was analysed more closely in thin section and by the electron microprobe. The dolomite is inter-grown with serpentine and talc, and the three are crenulated together (see Figure 68 below). Magnetite mineralization emphasizes the crenulation as it has mainly grown between the laminae.

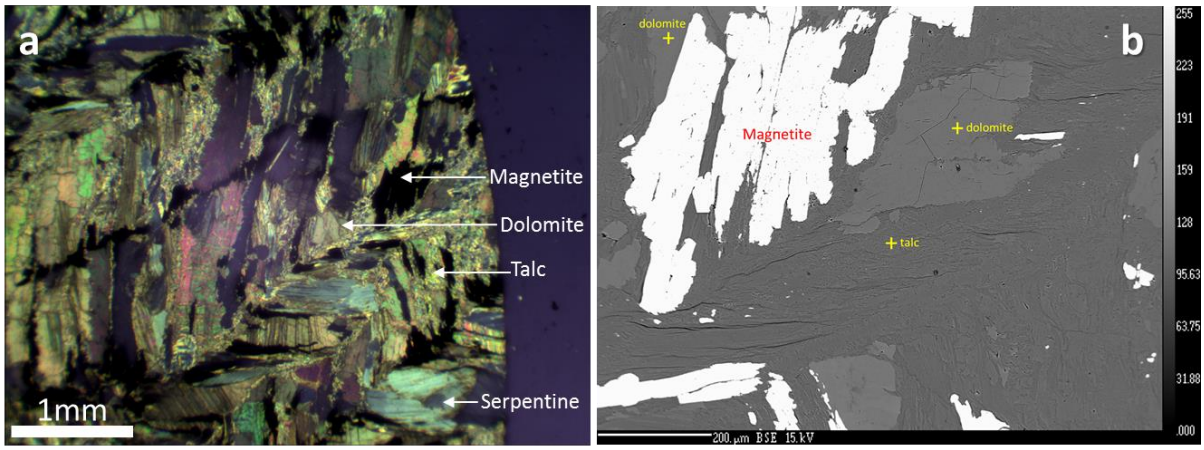

Figure 68: a) Thin section micrograph in cross polarized light and b) electron back scatter image of the laminated carbonate clast shown in Figure 67.a. The clast shows lamination development of talc, serpentine and dolomite, while the magnetite mineralization emphasizes the crenulation.

5.4. Formation

The serpentinite conglomerate studied here was previously assigned to the Sel Group.. The stratigraphy of the area has been documented by Strand (1951) as follows from top to bottom:

- The Sogn-Jotun crystalline complex
- The gabbro conglomerate of the Valdres Sparagmite
- The Sel, conglomerates and Heidal group (named the Vågåmo ophiolite by (Sturt et al., 1991)
    - Sel micaschist
    - Serpentine conglomerate
    - Greenstone conglomerate
    - Greenstones
    - Heidal Series
- The "mio-geosynclinal" sequence:
    - The dark & light sparagmites: phyllites, schistose sparagmites and quartzites, with a single limestone occurrence. The dark sparagmites are underlain to the south and overlain to the north by light sparagmites. The latter are epidote bearing.
    - The Cambro-Ordovician deposits: dominated by gray phyllites with local occurences of black carbonaceous schists. Some of the phyllite sections are interbedded with quartzite
- Basement gneisses

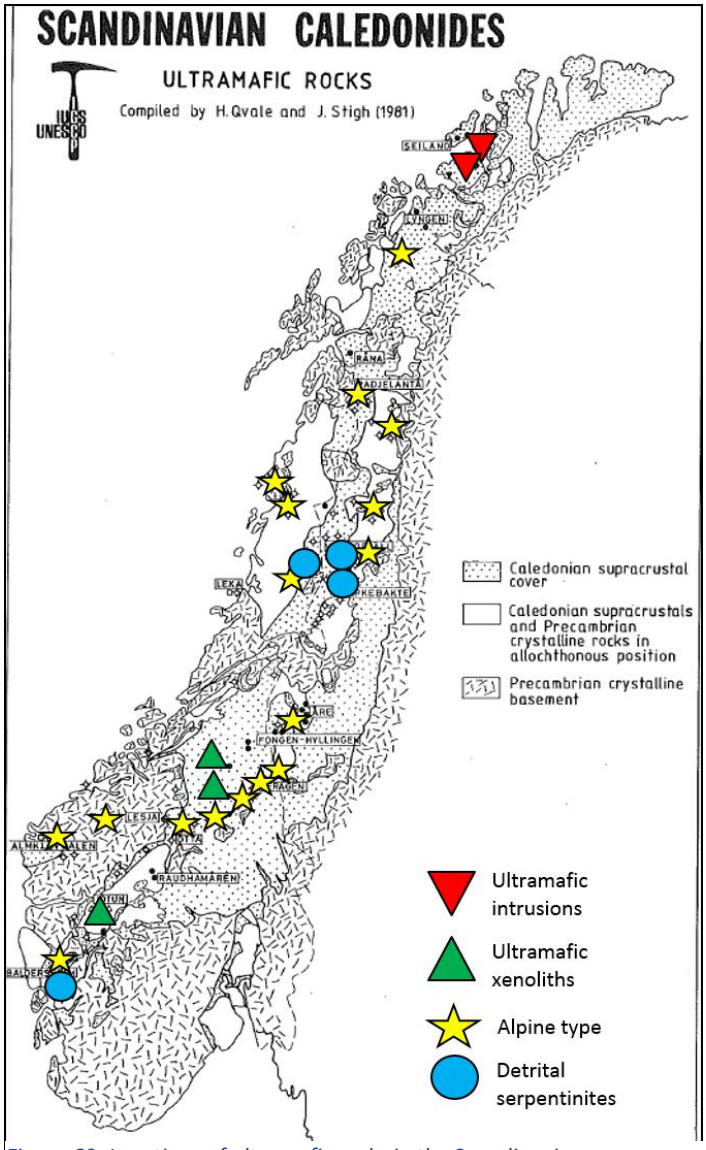

Figure 69: Locations of ultramafic rocks in the Scandinavian Caledonides. Note the locations of the detrital serpentinites in solid black circles. Modified after Qvale and Stigh (1985).

Detrital serpentinites are not limited to Otta-Vågå in the Scandinavian Caledonides, they are observed along the length of the Caledonides. This is shown in Figure 69 along with occurrences of other ultramafic rocks (which are often associated with the detrital serpentinites).

The Reiggehaugen conglomerate is a monomict ultramafic conglomerate (Otta conglomerate facies). Both the clasts and matrix here are made up of serpentine, talc, chlorite, dolomite, magnesite, magnetite and chromite. Strand (1970) documents some quartz rich outcrops in the Otta serpentinite conglomerate as well as fossiliferous portions with Ordovician fauna. He, along with other authors, have suggested volcanic origins for the conglomerate, either combined with

sedimentary processes or as a pyroclastic deposit (e.g. Oftedahl, 1969). Later authors (e.g. Qvale and Stigh, 1985) suggested the serpentinites are part of an ophiolitic sequence that provided the source for conglomerate sedimentation. This was later considered to represent a terrane-linking unconformity (e.g. Sturt et al., 1991, Bøe et al., 1993, Sturt and Ramsay, 1999). In the latter scenario, outboard oceanic terranes are thought to have accreted onto the Baltican margin followed by an erosional unconformity linking the continental and oceanic terranes. In this interpretation, the serpentinite conglomerate sits above the unconformity and the clasts would have been derived from the underlying ophiolitic terrane (see Figure 70). Sturt and Ramsay (1999) defined the age of the unconformity as Upper Cambrian based on geochronology and fossils found in the overlying conglomerates (e.g. Bjerkgård and Bjørlykke, 1994, Bruton and Harper, 1981).

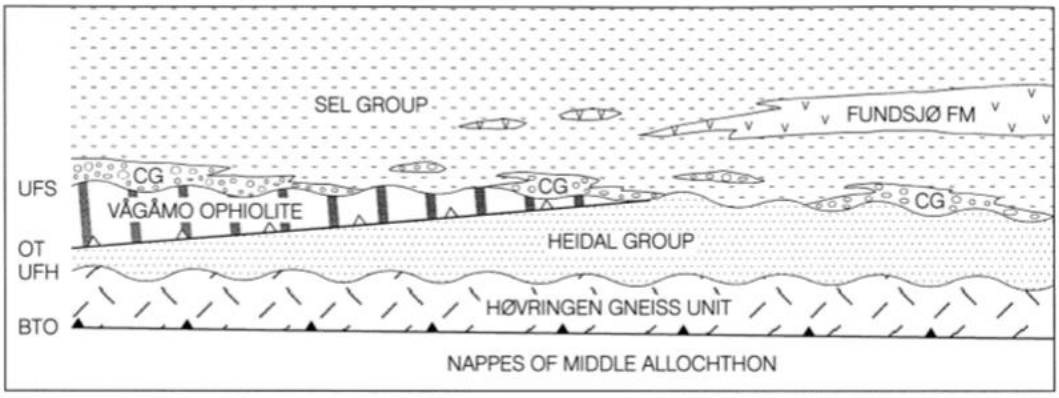

Figure 70: The tectonostratigraphic units in the terrane-linking unconformity interpretation of the serpentinite conglomerate, as illustrated in Sturt and Ramsay (1999). The serpentinite conglomerates here is thought to have formed at the base of the Sel Group, which is a terrane linking unconformity post-dating ophiolite obduction. The clasts of the conglomerate were thought to have been derived from the underlying ophiolite.

This interpretation, however, is not in agreement with the tectonostratigraphy of the area, as it would place the serpentinite conglomerate on top of the Caledonian nappe stack, while it is in fact, underneath the Jotun nappe, as documented by Strand (1951). Also, the serpentinite conglomerate is too old to postdate nappe stacking and ophiolite obduction, as the Caledonian collision which emplaced these (Upper Silurian) is much younger than the serpentinite conglomerate (Early-Mid Ordovician). This is additionally alluded to by the current distribution of the detrital serpentinites along the length of the Caledonides in a similar tectonostratigraphic position, suggesting they were part of a terrane that predated the Scandian Orogeny. Therefore, a new interpretation for the formation of the ultramafic conglomerate is needed.

The monomict composition of the ultramafic conglomerate as well as poor sorting indicates a limited sedimentary catchment. The rounding of the clasts, however, would normally indicate lengthy transport. Additionally, a serpentinite source as part of an ophiolitic assemblage is problematic here as there no other indicators of an ophiolitic origin (notably, no meta-basalts and gabbros). Thus, the emplacement of the serpentinite source must first be resolved. The detrital serpentinites in the Scandinavian Caledonides are mostly found in association with the solitary 'alpine type' serpentinites Figure 69, such as those studied in Bøverdalen. The solitary serpentinites are, thus, the most likely source. The conglomerates in the Sel group are inarguably sedimentary as they show clast imbrication, grading, cross bedding, heavy mineral concentration and fossils (Qvale and Stigh, 1985, Bruton and Harper, 1981).

The poor sorting and lack of extensive lateral grading indicate rapid deposition (Qvale and Stigh, 1985) such as in debris flows. The presence of clast imbrication and grading where the layers often fine upwards indicates sub-aqueous deposition, such as in a sub marine fan.

Serpentinized mantle can be exhumed to the sea floor in a hyperextended margin (see Chapter 1 for an explanation of the process). If this took place on the Baltican margin during the opening of the Iapetus, a serpentinite ridge in the early basin could have sourced sedimentation. In this setting, the serpentinized mantle is known to undergo brecciation related to ophicarbonate alteration (e.g. Clerc et al., 2014, Picazo et al., 2012, Lemoine, 1980). This is observed in the solitary serpentinites in the Caledonides (e.g. in Bøverdalen, Figure 71c). Such brecciation would expedite the rounding of the clasts, eliminating the need for lengthy transport to achieve the observed rounded conglomerate. The deposition of the conglomerate would, thus, be achieved in proximity to a serpentinite ridge, limiting the catchment, but showing clast rounding from the alteration and brecciation of the source. An example of such a source is shown in Figure 71c which can be compared to the ultramafic conglomerate from Reiggehaugen in Figure 71a-b.

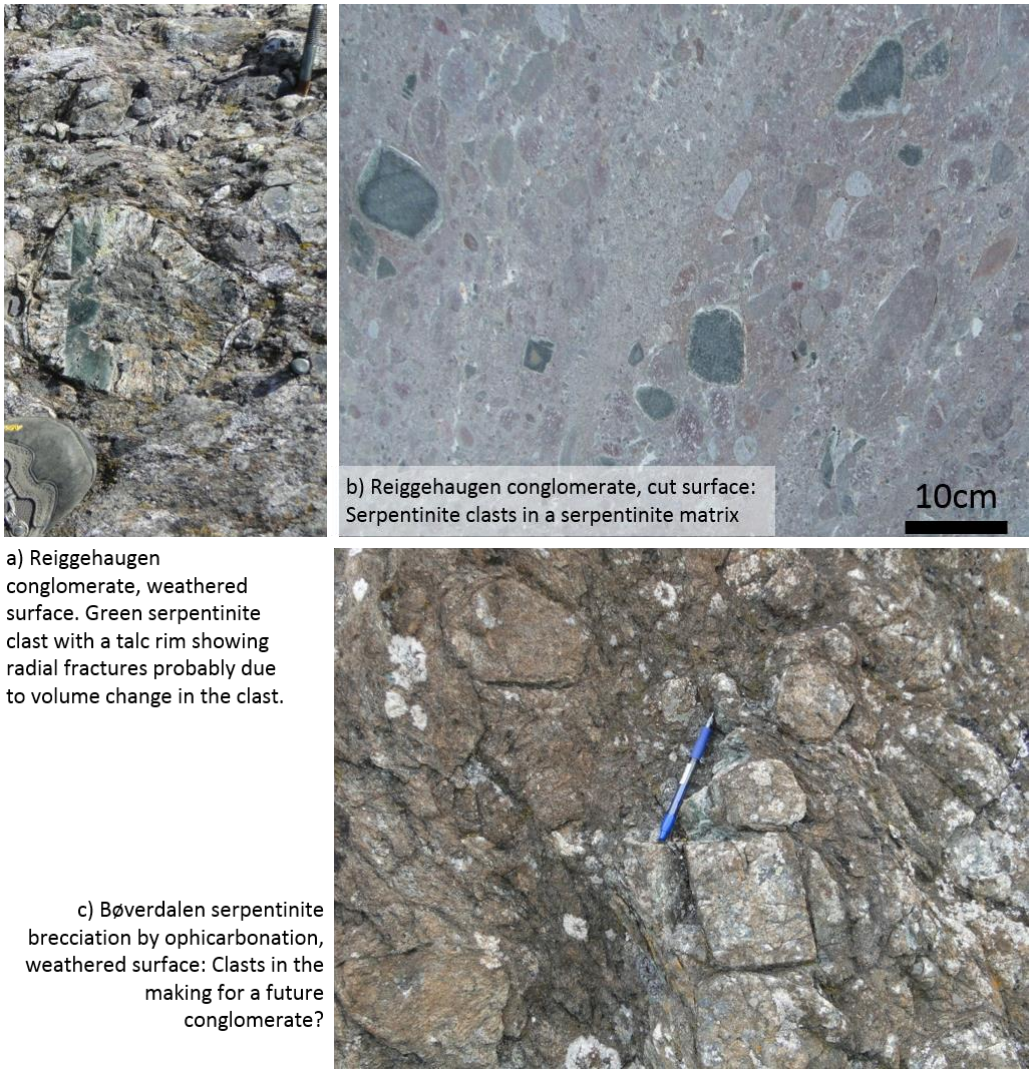

Figure 71: Comparison of the Reiggehaugen ultramafic conglomerate (a & b) to the ophicarbonated Bøverdalen serpentinites (c). In situ brecciation of the ophicarbonated serpentinites may provide the first stages of conglomerate formation, as weathering the former would provide the clasts for the latter. This would eliminate the need for lengthy water transport mechanisms, allowing a nearly pure ultramafic conglomerate to form with limited sedimentary catchment.

6. Geochronology

6.1. Geology of the Samnanger area

An age constraint is needed for the formation of the mélange unit to aid interpretation and tectonic reconstruction. If it did in fact form on the young Iapetan passive margin, it should have an age that is younger than the Proterozoic Sveconorwegian event but older than the onset of subduction of the Iapetus.

As there are no datable elements in the meta-peridotites themselves, we have searched for datable magmatic rocks in the mélange unit. These are sparse in the immediate vicinity of the mapped area. Figure 38 in Chapter 3 shows the closest previously mapped meta-igneous rocks to the mapped area: The Høyvatnet meta-gabbro and the Otta gabbro. The former, however, has an age of around 500 Ma and thus appears to be a Sveconowegian tectonic sliver incorporated in the nappe stack (Fernando Corfu, unpublished work). The Otta gabbro (previously refered to as the Vågåmo ophiolite by Sturt et al., 1991) was sampled, however, no datable minerals were found. A related gneiss gives an age of about 1100 Ma, suggesting it is an older tectonic sliver (Andersen & Corfu, work in progress).

We have, thus, dated samples from a different locality that are thought to be part of the same mélange unit but with more abundant magmatic rocks. The dated samples were collected in the Bergen arc area from Hana near Trangereid and Samnanger (refer to Figure 72 for locations). The tectonostratigraphic map of southern Norway (Figure 6 in Chapter 1) shows that this area lies along the same mélange unit mapped in Bøverdalen. Additionally, a very similar rock association is found where alpine type peridotites are interleaved with mica and graphitic schists (Færseth et al., 1977, Andersen et al., 2012). This unit is, thus, thought to be equivalent to the unit mapped in Bøverdalen.

The dated samples are from the Samnanger Complex in the Major Bergen Arc. A description of the regional geology in the Samnanger area is summarized from Færseth et al. (1977):

The Samnanger Complex:

The Samnanger Complex consists of lenses of meta-peridotite amongst a sequence of meta-sediments:

- Mica schist: The most common rock type in the Samnanger Complex. Dominated by quartz-albite-muscovite-biotite-chlorite-calcite schist, locally containing garnet, graphite, epidote and actinolite.
- Albite-mica schist: Restricted to the westernmost part of the Samnanger Complex. Same mineralogy as the mica schist but with less quartz and more albite (40-50% of the rock).
- Quartz schist: Restricted to the west of the Haukenes Gneiss. Prominent foliation defined by alternating quartz and mica rich layers. Quartz forms 50-80% of the rock with the rest made up of albite, white mica, biotite, chlorite and calcite.
- Quartz meta-conglomerate: Does not occur extensively. Consists of quartz pebbles in a pelitic matrix identical to the surrounding mica schist. Strongly deformed with the pebbles' long axes lying parallel to the foliation.

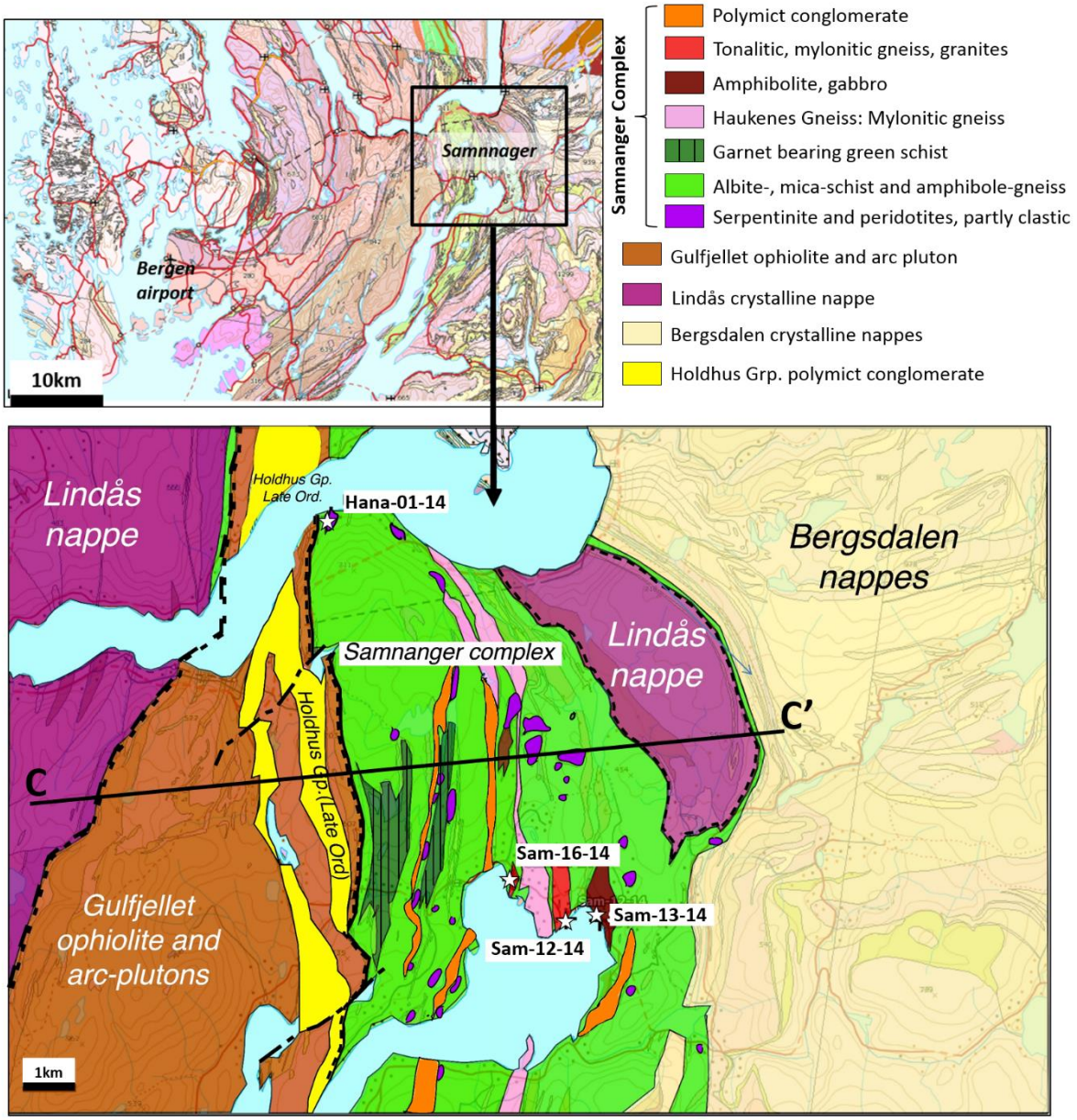

Figure 72: Location of the dated samples from the Samnanger Complex. The generalized geological map shows the tectonic units around the Samnanger Complex. A simplified cross section along C-C' is shown below.

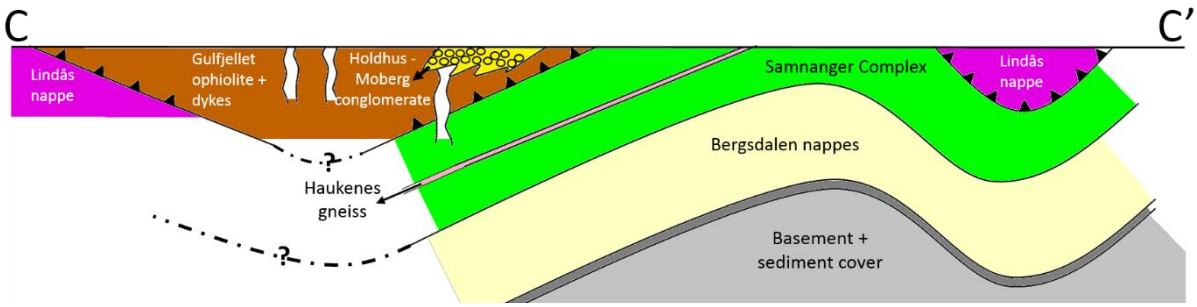

Figure 73: Simplified cross section of the Samnanger area (location shown in Figure 72 above) showing the position of the Samnanger Complex above the Bergsdalen nappes and below the Gulfjellet ophiolite. The Holdhus Group sits unconformably above the Gulfjellet ophiolite (modified after Færseth et al., 1977).

- Amphibolite: Occurs extensively in the Samnanger Complex often as thin bands (<1m). Mainly consists of actinolite, albite, epidote and quartz with minor carbonate, biotite, chlorite, garnet, sphene, apatite and rutile.
- Greenstone: Occurs in the west of the Samnanger Complex. Consists of actinolite, albite, epidote and chlorite with minor quartz, carbonate, biotite and sphene. Small lenses of gabbro (a few metres in size) also occur within the greenstone.
- Gneiss: Occurs in the eastern part of the Samnanger Complex. Mostly forms lenticular sheet-like bodies interlayered with mica schists, however, the Haukenes Gneiss forms a belt with a minimum length of 40km. The gneisses occur as quartzo-felsdpathic gneisses with augen textures and as anorthositic gneisses with gabbroic parts

The sequence is cross cut by intrusive trondhjemitic rocks (Kolderup and Kolderup, 1940), while meta-gabbros and quartz diorites are also present (Færseth et al., 1977).

The meta-peridotites in the Samnanger Complex are mostly serpentine rocks found in the lower mica schists. These are serpentinized dunites, massive and schistose serpentinites, and soapstones with serpentine, talc, chlorite and magnesite (Kolderup and Kolderup, 1940). These are found as more than 40 lenses which are up to 2 km in length and 300 m in width. Their long axes occur parallel to the foliation of the country rock. Some of the larger massive lenses show forsteritic olivine relics (dunitic origin. The contacts between the serpentinites and the host meta-sediments are often phyllonitic and chlorite rich, with additional albite growth in the host rock near the contacts. The meta-peridotites were strongly affected by Caledonian deformation together with the host meta-sediment (Færseth et al., 1977).

Gulfjell ophiolite:

Occurs to the west of the Samnanger Complex and consists of island arc tholeiites and gabbros considerably altered by saussuritization and amphibolitization (Thon, 1985). There are also meta-peridotites present as cumulates in the ophiolite. This unit is intruded by several generations of basic dykes (mainly made up of amphibole, albite and epidote), quartz dioritic dykes (most extensive in the area), quartz augen gneiss (essentially quartz, plagioclase, epidote, clinozoisite and white mica), and quartz diorites (also intrude the Samnanger Complex but absent (?) in the Holdhus Group). The Gulfjellet ophiolite has been dated at 485-475 Ma (Dunning and Pedersen, 1988).

The Holdhus Group:

Consists of the Moberg conglomerate passing up into marble. The higher levels of the marble contains Upper Ordovician fossils. The conglomerate contains a mixture of igneous and metamorphic clasts in a medium grained lithic and feldspathic greywacke. The clasts include gabbro, greenstone, meta-dacite and quartzite. Above the marble, this group contains schists (mostly muscovite and chlorite with thin lenses of granoblastic quartz and plagioclase), meta-graywacke (mainly quartz, feldspar, micas and epidote minerals), porphyritic greenstone (albite from saussuritized plagioclase, epidote and clinozoisite), and pebbly quartzite.

6.2. U-Pb dated samples:

The Samnanger Complex is thought to be part of the mélange unit and the following four samples from this complex were dated (locations shown on Figure 72):

- Tonalite (sample Sam-12-14)
- Gabbro pegmatite from the Samnanger complex (sample Sam-13-14)
- Well preserved granitoid in Samnanger complex (sample Sam-16-14)
- Quartz granitoid (sample Hana-01-14)

Each sample and its measured age are described below, while Table 3 shows the detailed results of the analyses.

6.2.1. Tonalite: Sample Sam-12-14

(60°23'46.72"N, 5°44'57.09"E)

The target was to date the Haukenes Gneiss sheet, the continuous belt that cuts through the Samnanger Complex. The sample was collected at an outcrop which shows less deformation. This was an attempt to capture the granitic core of the gneiss which was probably intrusive and would maybe give the intrusion age. The map, however, was misread, and the sampled outcrop is separated from the main mylontic gneiss body by a thin body of mica schist (refer to Figure 72). The sampled rock is a tonalitic, relatively fine-grained, porphyroclastic and mylonitic gneiss. It is made up of quartz, plagioclase, muscovite, chlorite, carbonate and epidote (see Figure 74). The Haukenes Gneiss, by contrast, is a mylonite with remnants of orthopyroxene (now bastite) with porphyroclasts of string perthite and mesoperthite (observed by Færseth et al., 1977). This mineralogy and texture were not observed in the sampled rock, and together with the separation of the outcrop by the mica schist body, indicates we did not sample the Haukenes Gneiss, but a separate tonalite body. This is an error to be corrected in future work by resampling. The sampled meta-granitoid is strongly deformed and share the main features observed in the Samnanger Complex.

Nonetheless, the sample was dated and gave an age of 476.23 ± 0.84 Ma.

Table 3: U-Pb data, Samnanger samples

Properties	Weight	Pbt	U	Th/U	Pbc	Pbcom	206/204	207/235	2 sigma	206/238	2 sigma	rho	207/206	2 sigma	206/238	2 sigma	207/235	2 sigma	207/206	2 sigma	Disc.
	[µg]	[ppm]	[ppm]		[ppm]	[pg]			[abs]		[abs]			[abs]		[abs]		[abs]		[abs]	[%]
Tonalite: Sam-12-14																					
57: Z EU SP AA 1GR	1	33	426	0,32	0,00	0,3	6619	0,59634	0,00228	0,07653	0,00020	0,82	0,05651	0,00013	475,4	1,2	474,9	1,4	472,6	4,9	-0,6
58: Z EU SP AA 1GR	1	19	244	0,33	0,00	1,0	1169	0,60038	0,00406	0,07683	0,00022	0,59	0,05667	0,00032	477,2	1,3	477,5	2,6	478,8	12,3	0,3
59: Z TIP AA 1GR	1	5	63	0,35	0,00	0,3	1166	0,59677	0,00564	0,07683	0,00029	0,52	0,05634	0,00046	477,1	1,7	475,2	3,6	465,7	17,9	-2,6
60: Z TIPS AA 1GR	1	7	91	0,35	0,00	0,3	1554	0,59853	0,00408	0,07660	0,00028	0,65	0,05667	0,00030	475,8	1,7	476,3	2,6	478,8	11,5	0,7
Gabbro pegmatite from the Samnanger complex: Sam-13-14																					
52: Z SPHERE AA 1GR	8	1	9	0,42	0,07	1,1	367	0,60568	0,00801	0,07844	0,00029	0,47	0,05600	0,00067	486,8	1,7	480,8	5,1	452,4	26,2	-7,9
53: Z AA 1 GR	15	1	10	0,27	0,00	1,5	527	0,61073	0,00819	0,07843	0,00023	0,49	0,05648	0,00069	486,7	1,3	484,0	5,2	471,3	26,9	-3,4
54: Z AA 1GR	2	15	190	0,48	0,00	1,7	1137	0,61058	0,00426	0,07798	0,00021	0,57	0,05679	0,00033	484,1	1,3	483,9	2,7	483,3	12,9	-0,2
Well preserved granitoid in Samnanger complex: Sam-16-14																					
13: Z LP AA 1GR	1	20	310	0,14	0,06	2,1	650	0,51167	0,00548	0,06740	0,00018	0,50	0,05506	0,00053	420,5	1,1	419,6	3,7	414,7	21,5	-1,4
62: Z LP AA 1GR	1	20	302	0,23	0,00	1,2	1101	0,51415	0,00371	0,06773	0,00018	0,55	0,05506	0,00034	422,5	1,1	421,2	2,5	414,5	13,7	-2,0
Quartz granitoid: Hana-01-14																					
15: Z LP AA 1GR	1	4	38	0,18	0,00	0,8	357	0,95728	0,01734	0,10713	0,00045	0,50	0,06481	0,00106	656,1	2,6	681,9	9,0	768,1	34,2	15,3
16: Z R AA 1GR	1	23	371	0,00	0,00	0,9	1777	0,51483	0,00271	0,06747	0,00017	0,65	0,05534	0,00023	420,9	1,1	421,7	1,8	426,1	9,0	1,3
17: Z AA 1GR	1	15	111	0,66	1,23	3,2	259	1,02022	0,01639	0,11222	0,00046	0,48	0,06594	0,00096	685,6	2,7	714,0	8,2	804,4	30,1	15,6
18: ZZ TIP AA 1GR	1	5	39	0,99	1,17	3,2	91	0,79538	0,04324	0,09475	0,00052	0,57	0,06088	0,00313	583,6	3,1	594,2	24,2	635,1	107,0	8,5

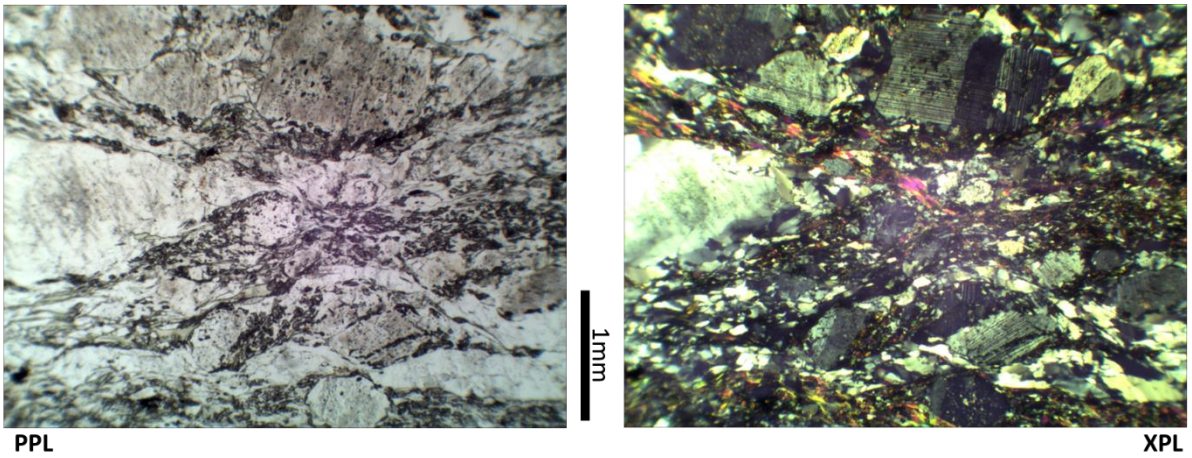

Figure 74: Thin section micrograph of Sample Sam-12-14: Tonalite dominated by quartz (~30%), plagioclase (~20%), muscovite, epidote and some carbonate and chlorite. Most of the quartz is recrystallized however some original strained grains are observed.

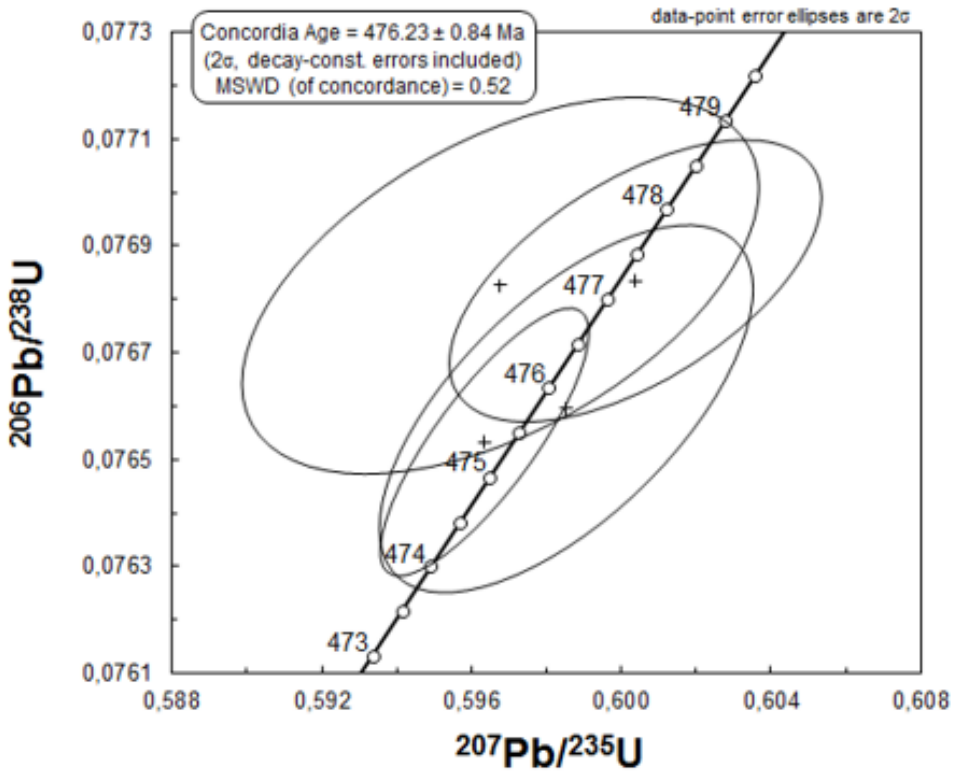

Figure 75: Tonalite from the Samnanger Complex (sample Sam-12-14) U-Pb age: concordant, 476.23 ± 0.48 Ma.

6.2.2. Gabbro pegmatite: sample Sam-13-14

(60°23'48.56"N, 5°45'39.20"E)

Coarse gabbro cut by doleritic dykes, preserved as a ca. 2km long lens within the mélange mica schist matrix. The rock is very retrogressed and altered showing a large degree of recrystallization but locally with a preserved texture.

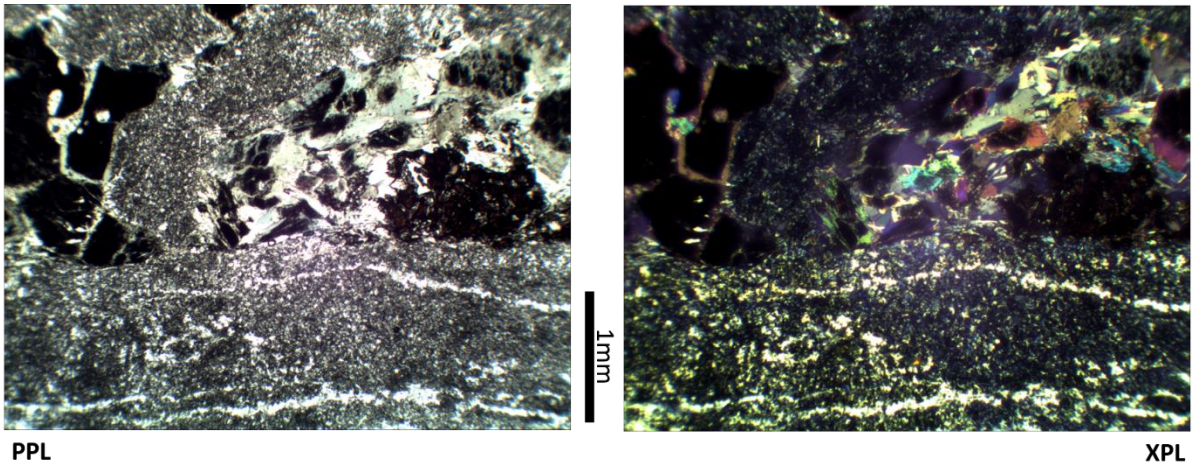

Figure 76: Thin section micrograph of Sample Sam-13-14: Retrogressed gabbro pegmatite. Almost entirely recrystallized but the texture is preserved. Primarily consists of actinolite, chlorite, epidote, Fe-oxide, titanite and some rutile.

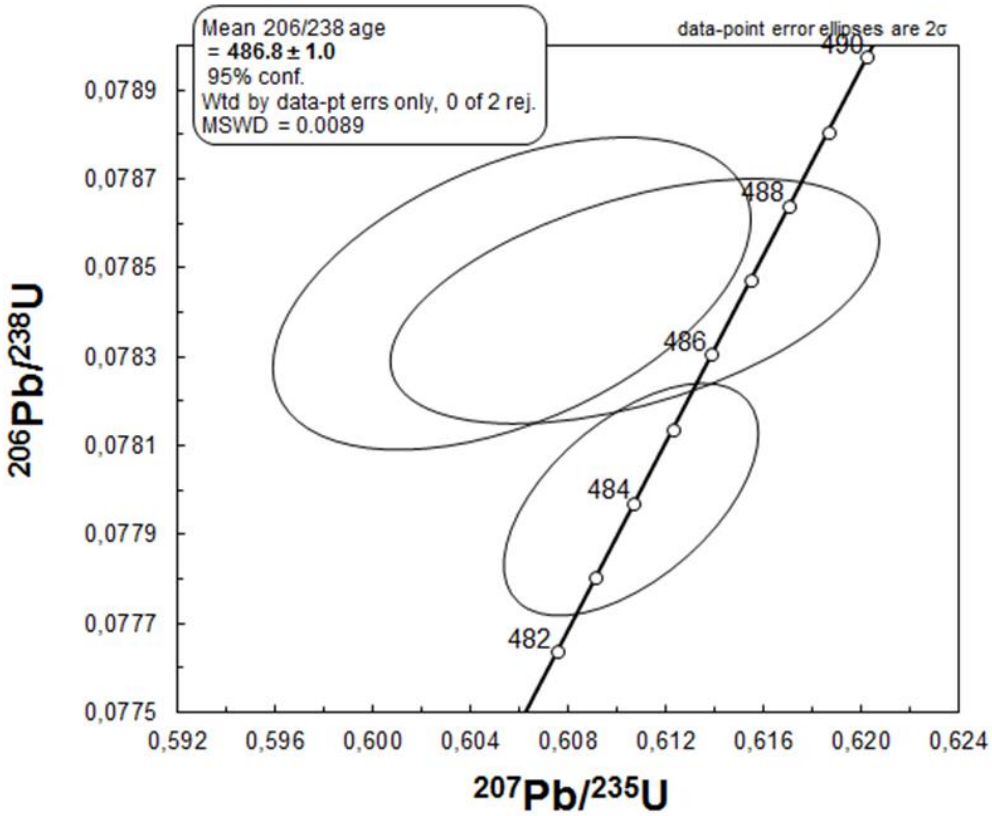

Figure 77: Gabbro pegmatite from Samnanger complex (sample Sam-13-14) U-Pb age: concordant, 486 ± 1 Ma

6.2.3. Well preserved granitoid: sample Sam-16-14

(60°24'5.91"N, 5°43'44.40"E)

Well preserved granitoid in the Samnanger complex made up of K-feldspar, plagioclase, quartz, calcite and muscovite.

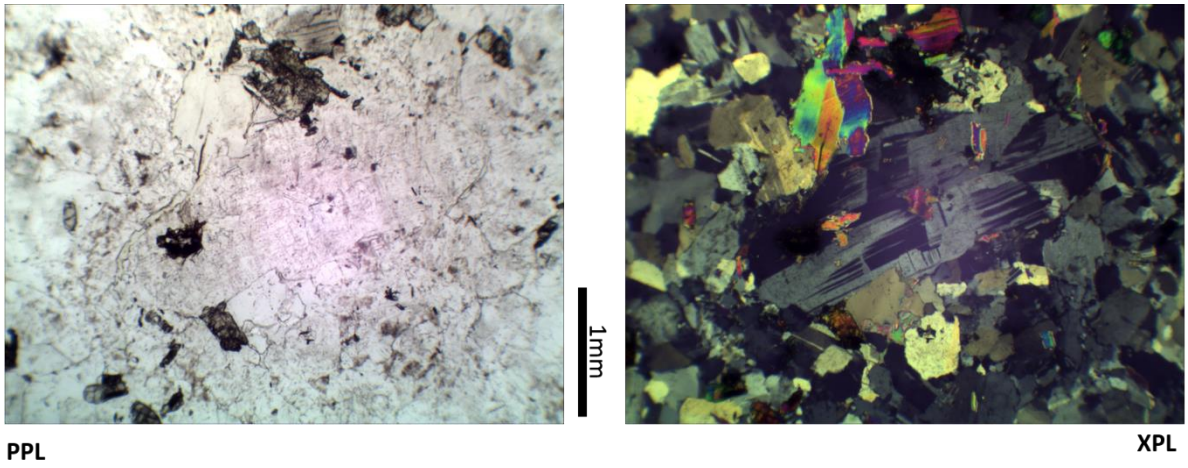

Figure 78: thin section micrograph of sample Sam-16-14: Well preserved granitoid primarily made up of K-feldspar, plagioclase, quartz, calcite, muscovite and some epidote.

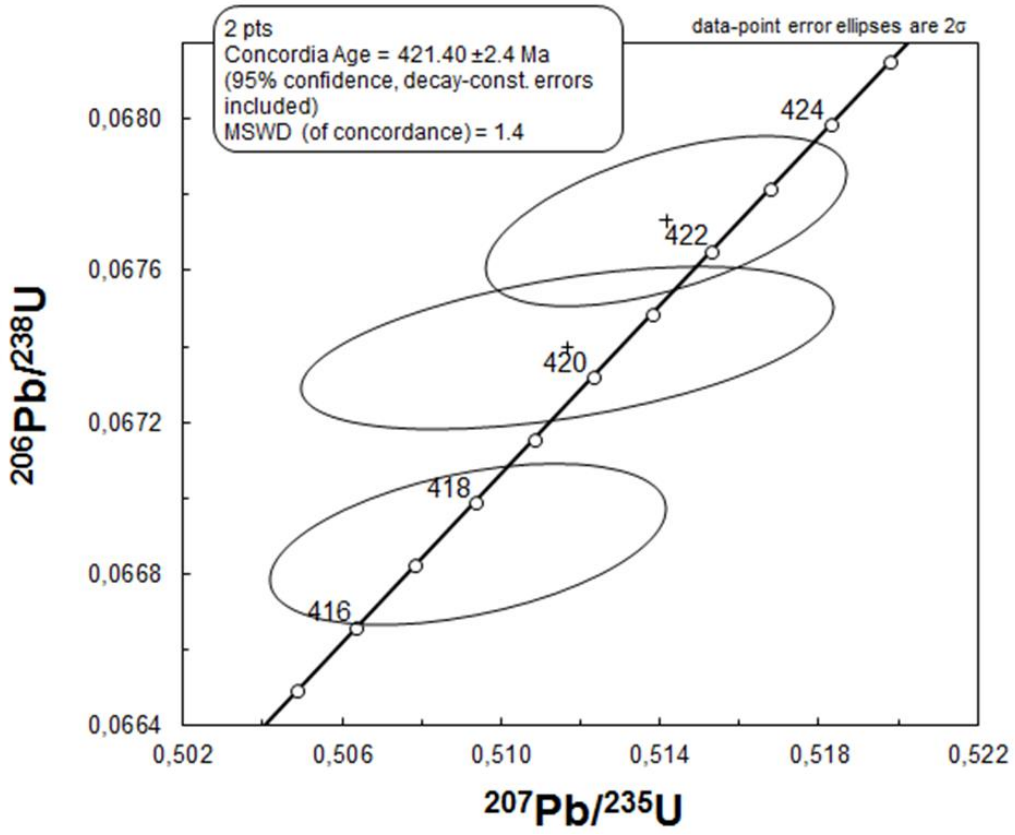

Figure 79: Preserved granitoid in Samnanger complex (sample Sam-16-14) U-Pb lead age: concordant, 421.4 ± 2.4 Ma.

6.2.4. Quartz diorite: sample Hana-01-14

(60°27'31.55"N, 5°38'55.52"E)

This quartz diorite is little deformed, altered and consists of plagioclase, quartz, secondary muscovite, chlorite and epidote. It was sampled at a probably sheared contact with soapstone conglomerate, although the contact itself is not exposed.

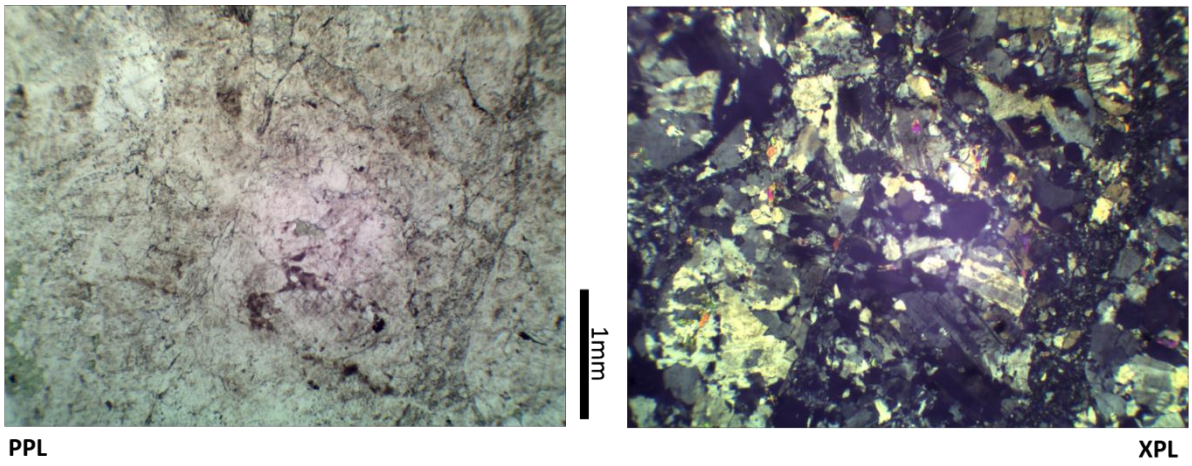

Figure 80: Thin section micrograph of Sample Hana-01-14: Little deformed and altered quartz diorite. Mainly consists of plagioclase, quartz, secondary muscovite, chlorite and epidote.

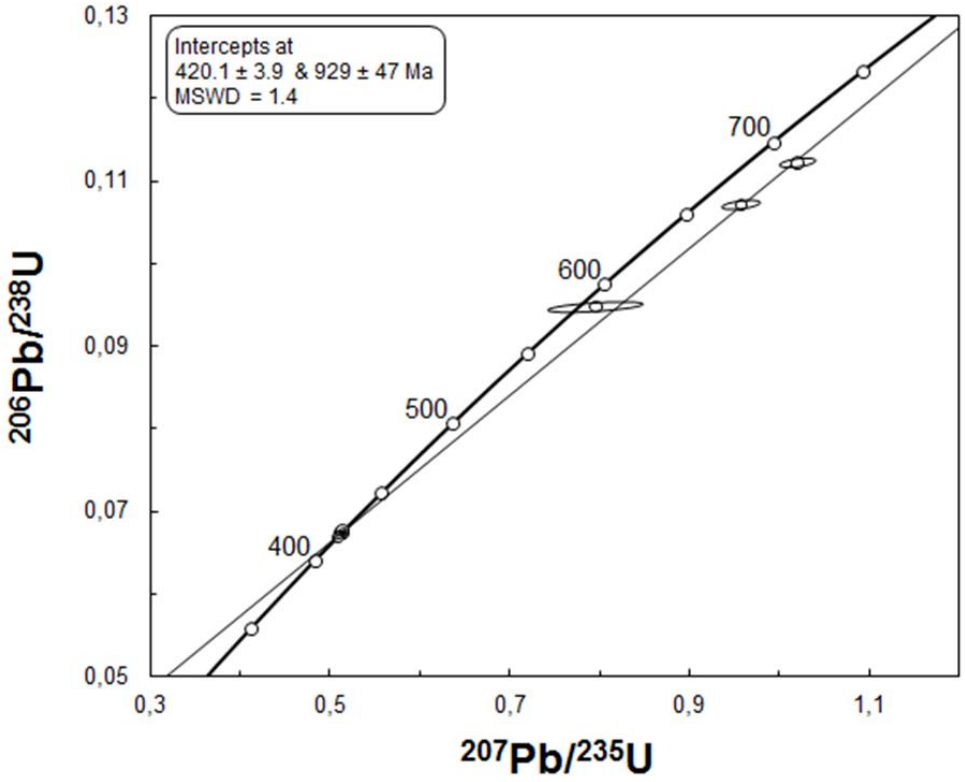

Figure 81: Quartz granitoid (sample Hana--01-14) U-Pb age: discordant, intercepts at 420.1 ± 3.9 and 929 ± 47 Ma indicating resetting and inherited ages.

6.3. Interpretation

The dated samples have given two age groups, both of which are later than the onset of subduction in the Iapetus:

- Samnanger granitoid and the Hana granitoid: **421.4 ± 2.4 Ma & 420.1 ± 3.9 Ma, respectively, with the latter showing inheritance from 929 ± 47 Ma**
- Tonalite and Gabbro pegmatite: **476.23 ± 0.84 Ma and 486.8 ± 1 Ma, respectively.**

6.3.1. The first age group ~420 Ma:

The dated granitoid samples formed around 420 Ma. This is contemporaneous with the Scandian orogeny and most likely represents partial melting associated with the orogeny. The Sveconorwegian inheritance observed in the Hana granitoid supports this (dated 420.1 ± 3.9 Ma with an upper intercept age of 929 ± 47 Ma). This is also observed elsewhere in the Major Bergen Arc as well as in the Lindås and Jotun Nappes. Kuhn et al. (2002) document 425 Ma trondhjemitic dykes found in the nappes (but not the Baltican basement). They interpret these to have formed as crustal partial melts resulting from hydration during Scandian collision. Similarly, Lundmark and Corfu (2007) have measured a U-Pb age of granitic dykes intruding the Upper Jotun Nappe at 427 ± 1 Ma. Here they show that previous Sveconorwegian age calculated by Rb-Sr resulted from mixing, where the granites are derived from partial melting of Rb-poor sediments of Baltican affinity overridden by the nappes during thrusting, explaining the presence of the dykes in the nappes but not in the basement. The granitoid samples dated in this thesis probably also formed in this way; by partial melting of Sveconorwegian basement (probably Baltican) during the Scandian collision.

6.3.2. The second age group ~476-487 Ma

This age group coincides with the age of subduction related magmatism, arc and ophiolite formation observed in the south western Caledonides and can be interpreted in more than one way.

Either it correlates to the age of the ophiolite, indicating the mélange in the Samnanger area is related to ophiolite obduction. The ophiolites have been dated at ca. 500 – 440 Ma where the dated samples include plagio-granites differentiated from melt, island arc tonalities and trondhjemites and gabbro intrusions (Dunning and Pedersen, 1988). In the current structural interpretation of the Samnanger area (refer to the cross section in Figure 73), the Samnanger Complex is overlain by the Lindås nappe which in turn is overlain by the Gullfjellet ophiolite. The Lindås nappe, however, is missing between the Samnanger Complex and the Gullfjellet ophiolite at these locations. This could be due to excision, out of sequence thrusting or inherited discontinuity from the extensional phase. Alternatively, the current structural interpretation based on Færseth et al. (1977) is wrong and needs revision.

If the Samnanger complex is not a mélange related to ophiolite obduction, but rather a hyperextension related mélange that formed before the onset of subduction, the calculated age would not correspond to the mélange formation age. Instead, it may be an intrusion age related to subduction arc magmatism. While the main subduction was most likely further outboard (creating the future Gulfjellet and other ophiolites), it is possible minor subduction took place in other weak parts of the distal parts of the basin. This could be sufficient to generate subduction related

magmatism. Since we find no evidence of high pressure metamorphism in the mélange unit (no blue schist-eclogite facies metamorphism, unlike other parts of the Caledonides that underwent deeper subduction), we favour the latter interpretation of the calculated age. In spite of this, further work is needed (both structural and geochronological) to better understand the age and setting of the various units in and around the mélange.

7. Discussion

The mélange unit in the southern Scandinavian Caledonides is thin but laterally continuous above the Lower Bergsdalen Nappe and below the Upper Bergsdalen, Jotun and Lindås Nappes. Since it maintains its structural position along a large part of the Caledonides and shows strong flattening and attenuation by deformation, it inevitably must have formed before the Scandian orogeny and was thrust into its present position during the orogeny. This unit has been historically overlooked or unexplained as it was considered ophiolitic (exhumed oceanic lithosphere) or of outboard origin. It sits, however, structurally below the allochthonous crystalline nappes (most importantly the Jotun nappe) that have been traditionally considered of Baltican affinity. Particularly problematic is the origin of the ultramafic bodies throughout the mélange unit. These occur as solitary bodies (Alpine serpentinites) as well as detrital deposits. Their emplacement has been previously considered either ophiolitic or volcanic (e.g. Qvale and Stigh, 1985). A volcanic origin is geochemically problematic, as the serpentinites are metasomatised from a peridotite protolith that either represents dry mantle or restite (dunitic protolith). An ophiolitic origin is more likely than a volcanic origin as there are known ophiolites thrust on top of the serpentinized peridotite bearing mélange (e.g. Dunning and Pedersen, 1988). The classical Penrose pseudostratigraphy of an ophiolite, however, includes serpentinites, gabbros, sheeted dykes, pillow basalts and deep marine sediments (Dilek and Furnes, 2011). From this pseudostratigraphy, the mélange unit is missing the sheeted dykes, the pillow basalts and does not have an abundance of gabbros. It is possible that this is a question of preservation, however, a non-ophiolitic origin should be explored.

It has been shown in this thesis that the ultramafic bodies are surrounded by metamorphosed marine sedimentary rocks. It has also been shown that at least some of the contacts are stratigraphic rather than tectonic, implying that the lithological association is probably a primary association. The ultramafic bodies are thus expected to have always been intimately associated with the marine sedimentary rocks since their exhumation. This association predates the Scandian Orogeny and places the ultramafic bodies in a marine basin long before 430 Ma when the final Scandian collision started (e.g. Corfu et al., 2014a, Corfu et al., 2006). This means that the ultramafics probably originated along the Iapetan margin sometime before ~430 Ma (unless they are older than the Iapetus, in which case their preservation would be unlikely). Alternatively, if Baltica was upside down in the latest Proterozoic (refer to the Introduction), the mélange unit could have also originated along the Ægir Ocean, with remnants dragged along the Baltican margin during rotation to its current position before the final Caledonian orogeny.

The lithological association we find here where Alpine serpentinites and detrital serpentinites are interleaved with siliciclastic and carbonate marine sediments shown both in Bøverdalen, Høyvatnet and the Samnanger Complex can occur in a magma-poor hyperextended margin. This is seen in both

ancient preserved hyperextended margins as well as in modern hyperextended margin. Additionally, the Reiggehaugen ultramafic conglomerate may be the product of ophicarbonate alteration, as argued in Chapter 5, which would also strongly suggest formation in a hyperextended basin. In order to assess this, comparisons can be made to modern and fossil hyperextended margins.

The Iberian passive margin is the type locality for modern hyperextended margins. It has been drilled and dredged, providing lithological information. Manatschal et al. (2001) and references therein document the lithological drilling results from ODP Legs 149 and 173. This is summarized in the next paragraph, however, it is to be noted that this is not a complete sedimentological record since the drilling targets were the basement highs in the basin.

7.1. Lithological association in a modern hyperextended margin

7.1.1. The example of the Iberian passive margin, summarized from Manatschal et al. (2001)

The pre-rift sediments are dominated by shelf deposits on (normal thickness) continental crust. These are made up of variably cemented claystones, thin layers of sandstone and conglomerates.

Mass flow deposits are found consisting of reworked serpentinized peridotite and with a minor amount of basalt clasts. These are thought to have formed by submarine slope failure on a large fault scarp. The matrix here is older than the onset of seafloor spreading, suggesting formation during earlier rifting (Whitmarsh and Miles, 1995).

There is an abundance of breccias in the Iberian Abyssal Plain. These are found in various tectonic positions suggesting formation by different mechanisms. There are sedimentary breccias which occur both as clast and matrix supported rocks. These consist of clasts derived from continental crust: meta-gabbro, meta-anorthosite, amphibolite, minor meta-tonalite and arkosic wacke in a calcareous matrix. These are thought to have formed as mass flows, rock falls and talus deposits (Whitmarsh et al., 1998) and then tectonized at depth. At the base, the tectonic breccias are juxtaposed against serpentinized peridotite.

There are also breccias that are cut by gouge horizons and grade down into massive serpentinized peridotite. These only consist of serpentinites clasts and some rare gabbro clasts. They are poorly sorted and embedded in calcite cement, with a fabric similar to alpine ophicalcites (e.g. Bernoulli and Weissert 1985, Lemoine et al., 1987). Calcite is also seen to replace serpentine, but no sedimentary structures are discernible, suggesting that these are tectonic breccias from the serpentinite basement.

Lower crustal rocks: Here we find foliated and brecciated meta-gabbros, variably deformed and brecciated amphibolites (of gabbroic origin), meta-tonalite and meta-anorthosite. The meta-gabbros show variable Mg-numbers and ratios of compatible vs. incompatible elements (Whitmarsh et al., 1998). The lower crustal rocks are also found as clasts in breccias which are probably derived from the nearby highs, as they show similar mineralogy and petrographic structures.

Serpentinized mantle peridotites (based on descriptions by Manatschal et al. (2001), Cornen et al. (1996) and de Kaenel and Bergen (1996)):

- The drilled serpentinized mantle peridotites show variable petrological and tectonic evolutions. They comprise spinel dunite and harzburgite, spinel plagioclase harzburgite, lherzolite and pyroxenite.
- In places, the entire ultramafic section is serpentinized. There are transitions from carbonate rich serpentinites associated with serpentinites breccias at the top to massive serpentinized peridotites with local plagioclase and clinopyroxene enrichment at the base. The serpentinized peridotite often occurs below tectonized breccias and shows more deformation/brecciation to the top. This is locally expressed as a serpentine gouge with strong foliation, which disappears at depth where veined serpentinites preserve the high-T foliation marked by spinel grains.
- The breccia overlying massive serpentinized peridotites is often poorly sorted, clast supported and contains clasts of the same underlying rocks and is cemented by blocky calcite (ophicalcites). Serpentine gouge was observed between the ophicalcites and the underlying massive serpentinites, with clasts of the gouge also occurring in the breccia above.
- Some of the massive serpentinites contain pegmatitic gabbro (probably intrusive), consisting of altered plagioclase, clinopyroxene, amphibole and ilmenite.
- Ultramafic rocks were also found in breccias and as olistoliths of serpentinized peridotite (several tens of meters in size) amongst sediments.
- The peridotite protolith is thought to have originated either as sub-continental mantle or at a very slow-spreading ridge (c. 20mm a^{-1}), as the composition shows low (<10%) degrees of partial melting and depletion (Cornen et al., 1996).
- In addition to brecciation, some of the rocks show a history of lower granulite/upper amphibolite facies deformation evolving to sea-floor conditions, recording exhumation. There is also evidence for greenschist-facies mylonitization. Brittle deformation is seen as well as ductile deformation. Veining is extensive, where pervasive calcite veining (late syn- to post-kinematic) occurred at/close to the sea floor (Skelton and Valley, 2000). This overprints an earlier generation of veins consisting of epidote, chlorite, plagioclase, iron oxide and rare calcite. Cataclasites and pseudotachylites are also observed. Much of the brittle deformation is thought to have formed under greenschist and subgreenschist facies conditions until final exhumation to the sea floor.

Syn-rift magmatism does not seem to have played a major role in the Iberian Abyssal Plain (Pinheiro et al., 1996).

7.1.2. Comparison of the Caledonian mélange to the modern Iberian hyperextended margin:

This association presents strong similarities to the lithological association observed in the Caledonian mélange unit. Most striking is the intimate association of serpentinized peridotite and marine sediments. Shelf deposits have been described from the Iberian margin (claystone, sandstone and conglomerate). A similar association is found in the Caledonian mélange, where we also find a large abundance of now metamorphosed deep marine sediments (analogous to sediments currently being deposited in the Iberian margin). The serpentinites in both the Iberian margin and the Caledonian margin occur as massive bodies as well as ophicalcites (brecciated and carbonated serpentinites). Some lower crustal rocks (meta-gabbro, meta-tonalite, meta-anorthosite) were recovered from the Iberian margin, but similar rocks from the extensional phase in the Caledonian mélange have not yet been found (see Chapter 6 for a discussion of dated samples). Tellingly, however, both margins show

no significant magmatism; a feature that could be due to lack of preservation in the Caledonian margin, but acts as compelling evidence considering all other similarities to the Iberian modern magma-poor margin.

7.2. Ancient hyperextended margins preserved in mountain belts

In order to better understand which elements of a hyperextended margin are preserved, we can look at ancient hyperextended margins in other mountain belts. Orogens are inherently made up of mixed units and terranes, so recognizing a lithological association that predates the orogeny versus one that is juxtaposed to its current position by orogenesis requires specific criteria. Beltrando et al. (2014) sum this up well and state the following requirements for recognizing an exhumed rift related lithological association:

1. Consistency of the lithostratigraphic architecture over large areas. Observing this consistency despite orogenic deformation rules out chaotic mixing during subduction and exhumation.
2. The presence of basement clasts in surrounding meta-sediments. This provides evidence of proximity to the continent during the deposition of the meta-sediment protolith.
3. Evidence of brittle deformation predating orogenic metamorphism both in the continental basement and in the ultramafic rocks.
4. Evidence of a similar tectonomorphic evolution under orogenesis for the ultramafic rocks, continental basement and meta-sediments.

Points 1, 2 and 4 are observed in the Caledonian mélange and have been documented in this thesis, where lithostratigraphic consistency is shown as well as the presence of basement clasts in the surrounding meta-sediments. The entire lithostratigraphic association also shows a similar tectonomorphic evolutions under orogenesis, however, this event seems to have eradicated any pre-orogenic brittle deformation.

While hyperextended margins are recognized in several mountain chains now, e.g. the Alps (Manatschal, 2004, Manatschal et al., 2006); the Pyrenees (Lagabrielle et al., 2010) and the Appalachians (Van Staal et al., 2013, Chew and van Staal, 2014). Some of these are better studied than others. The Caledonian mélange can, thus, be compared to other mountain chains that show evidence of preserved hyperextended crust. In the following section, the Caledonian mélange will be primarily compared to the hyperextended remnants observed in the Alps, but also those documented from the Pyrenees and the Appalachians.

7.2.1. The Alps

The Alpine orogeny is associated with the closure of the Tethyan oceanic to transitional crust basins in the Late Cretaceous-Early Tertiary (Pfiffner et al., 1997). The preserved portions of mafic-ultramafic in the Alps were historically interpreted as ophiolites. These were characterized by smaller amounts of mafic rocks (gabbros and basalts) than typical ophiolites, the absence of sheeted dyke complexes and the frequent occurrence of oceanic sediments stratigraphically overlying mantle-derived peridotites. This is now recognized to represent the ocean continent transition zone in a magma-poor margin (Lagabrielle et al., 2015). This is exemplified in the Tasna unit, where the OCT is made of serpentinized mantle peridotites which are overlain by dark shales, calciturbidites, breccias, siliciclastic sandstones and marly limestones. These are often seen as flysch type sedimentary rocks

which include allochthonous fragments of continental and oceanic basement rocks (Manatschal et al., 2006).

Several specific lithostratigraphic associations have been found in the Alps and Corsica and are summarized by Lagabrielle et al. (2015) as follows: The pelagic sediments and ultramafic-gabbro breccias are observed to overlie a large body of sheared gabbro (with a thin sheared serpentine cap). They are also found to directly overlie exhumed serpentinized peridotite (no magmatic rocks in such sections) where the serpentinite is capped by sheared talc-schists and chlorites. The serpentine, talc-schist and chlorite caps are thought to represent detachment surface shear zones. Olistoliths of gabbro and ultramafic-gabbro breccias are seen at various levels in the sedimentary cover. Basaltic pillow lavas and pillow breccias are also seen overlying serpentinized peridotite and exhumed, layered gabbros. The gabbros and ultramafics are thought to have formed in the rift/hyperextension stage, while pillow lavas are emplaced distally if a spreading axis forms. A conceptual tectonic reconstruction of these lithological associations is shown in Figure 82, where detachment shear zones exhume ultramafic and gabbroic basement, leading to brecciation and mass flows on top. Exhumation to the seafloor results in pelagic sediments being deposited directly on top of the shear zones and breccias.

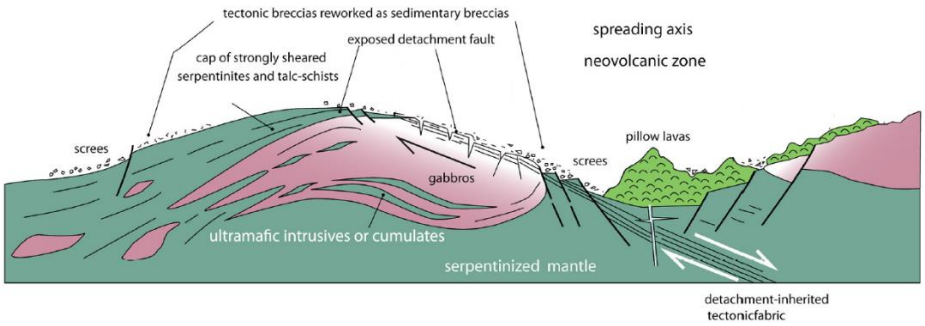

Figure 82: Reconstructed Tethyan oceanic basement based on lithostratigraphic successions observed in Alpine and Corsican meta-ophiolites. The basement includes gabbros and ultramafic rocks and has cover successions of ophiolitic breccias, volcanic rocks and pelagic sediments. This reconstruction is made by Lagabrielle et al. (2015) and is based on a section of a modern ocean core complex: the MARK area in the slow spreading Mid-Atlantic Ridge (Lagabrielle et al., 2015 and references therein).

Additionally, different domains are recognizable in the Alpine Tethys in both the internal and external parts. Tectonic reconstructions (Figure 83) show that two of these domains experienced hyperextension: the Piemonte-Liguria domain and the Valais domain (Mohn et al., 2010).

Different lithological associations can be recognized from the different domains, which may be linked to basin architecture and the processes involved in magma poor rifting. At the time of continental breakup in the early-late Jurassic, the external Piemonte-Liguria domain (proto-ocean) developed a section of cherty-limestones followed by breccias and sandstone which include dolomitic, basement and ophiolitic clasts (e.g. Mohn et al., 2010).

The Adriatic Distal margin is characterized by basement unconformably overlain by sediments (e.g. hardground) which are overlain by carbonate dominated debris flows that develop into siliciclastic sequences upsection, reflecting a major change in the source area related to the exhumation of crustal rocks (Mohn et al., 2010). The transition zone from the Piemonte-Liguria domain to the Brianconnais domain (other side of the proto-Tethys) shows breccias made of basement clasts with an arkosic matrix.

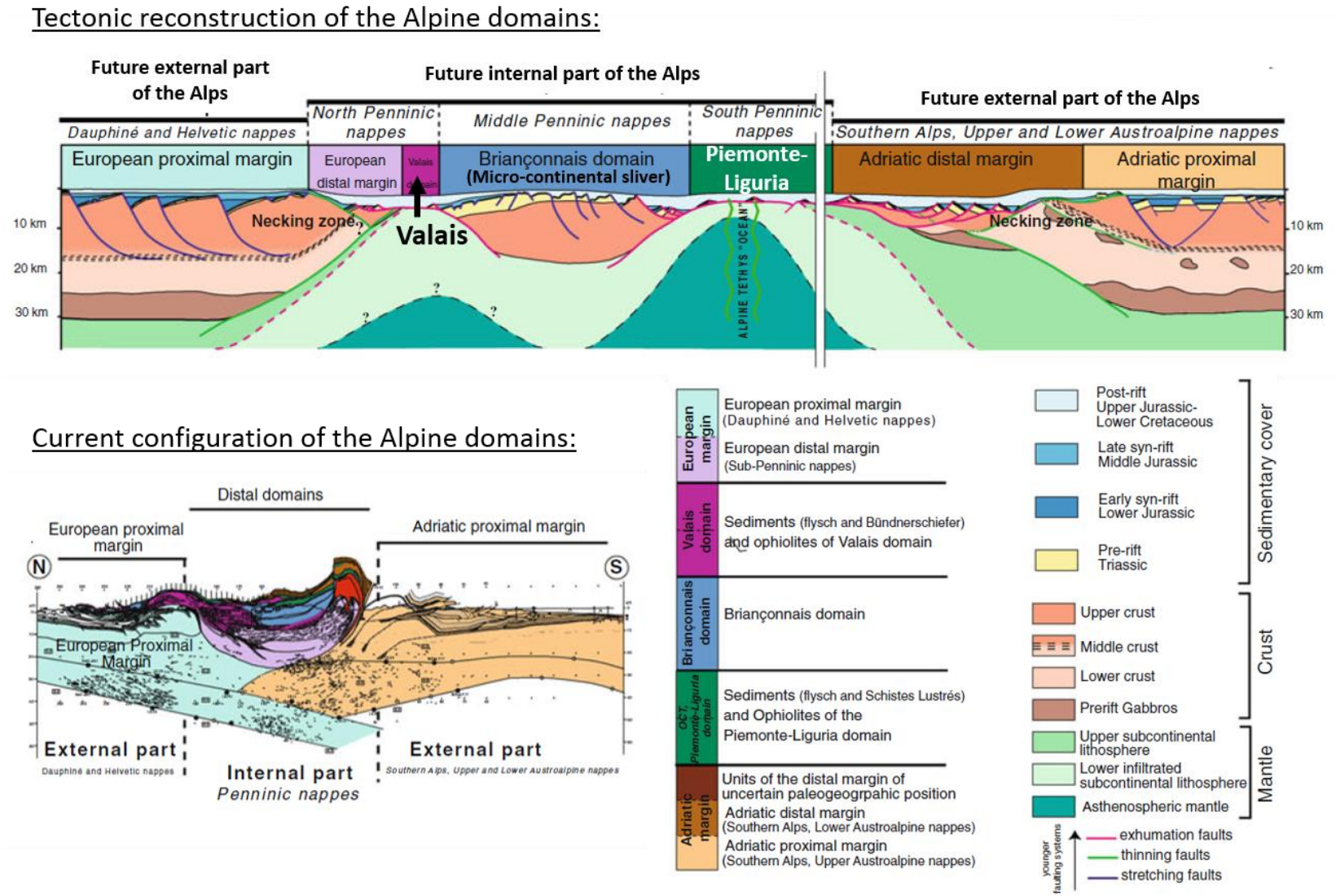

Figure 83: The Alpine Tethys shows various domains in its internal and external parts. Reconstructing this to the Late Jurassic shows two domains of hyperextension in the Piemonte-Liguria domain and the Valais domain. After Mohn et al. (2010).

The serpentinized mantle peridotites are thought to form in at least three types: ancient inherited sub-continental mantle (spinel lherzolites and pyroxenites); inherited and infiltrated mantle (plagioclase lherzolites and subordinate harzburgites); and oceanic depleted mantle (harzburgite-dunite) which is rare (Müntener et al., 2009, Müntener et al., 2004).

The occurrence of mantle rocks underlying crustal rocks was previously thought to have resulted from accretion at a slow-spreading ridge, but it is more likely derived from a former OCT (Manatschal and Müntener, 2009).

7.2.2. The Pyrenees

The north Pyrenean zone consists of numerous ultramafic bodies thought to have been exhumed during rifting (Lagabrielle and Bodinier, 2008). These are found in the form of massive peridotites as well as brecciated and carbonated peridotites (ophicalcites) (e.g. Clerc et al., 2014, Lagabrielle et al., 2010). These are associated with meta-sediments (carbonates, meta-evaporites, clastic conglomerates) unconformably overlain by black flysch sedimentation (Clerc and Lagabrielle, 2014).

These rocks are thought to be remnants of isolated pull-apart basins formed in response to the eastward drifting and rotation of Iberia (anti clockwise relative to Europa) along the north Pyrenean fault (Le Pichon et al., 1970, Choukrane and Mattauer, 1978). Hyperextension here occurred but did not proceed to sea floor spreading, which is why there are no remnants of a proper oceanic domain (Clerc et al., 2015, Vauchez et al., 2013). The basins were later inverted during the Pyrenean orogeny in the late Cretaceous-early Cenozoic (Le Pichon et al., 1970, Choukrane and Mattauer, 1978). Unlike the Alpine case, subduction did not take place in the Pyrenean realm, and so the preserved hyperextended margin has not been overwritten by high pressure metamorphism, allowing the study of the original thermal gradients during thinning (Clerc et al., 2015). The highest temperatures seem to be associated with areas where extension was oblique (increased thermal fluxes) and where mantle exhumation was faster (Clerc et al., 2015). Additionally, the thinning stage led to the formation of crustal boudins now in the north Pyrenean massifs (Clerc et al., 2015).

7.2.3. The Appalachians

Similar to the mélange of the Caledonides, the Appalachians show evidence of an Iapetan hyperextended margin, however, from the Laurentian rather than the Baltican side. This is seen in the Birchy Complex (Newfoundland) and is well documented by Van Staal et al. (2013) who show that serpentinized peridotites lie within a belt of mica schist, psammite, graphitic schist and with lenses of amphibolite. The ultramafic rocks here are commonly metamorphosed to soapstone and carbonate bearing ultramafic schists. Similar to the Scandinavian Caledonian mélange, the serpentinized peridotites lie between meta-sediments and overlying ophiolites dated at ca. 490 Ma (Van Staal et al., 2013).

7.2.4. Comparison of the Scandinavian Caledonian mélange to other orogens containing hyperextended remnants:

The fossil hyperextended margins of the Alps and the Pyrenees is better preserved than the Iapetan mélange in the Scandinavian Caledonides, however, strong similarities can still be drawn. Primarily, the association of ultramafic rocks with metamorphosed pelagic sediments that are continuous over large areas. Many of these sections do not contain magmatic rocks, which resemble the scarcity of magmatic rocks in the Caledonian mélange. Many of the sections that do contain magmatic rocks (mainly in the Alps), are thought to many have formed once sea floor spreading was established.

Similarities can also be drawn between the talc schist and chlorite caps in the Alpine serpentinites (thought to be detachment surfaces) and the local occurrences of talc schist and chlorite in the Caledonian serpentinites. These may also be detachment/fault surfaces, however, the structure is obscured by Caledonian deformation.

Additionally, the progression of carbonate debris flows into siliciclastic debris flows upsection resemble changes in source area sedimentation as those inferred from Høyvatnet in the Caledonides (see the Chapter 4).

The lithological association in the Appalachian fossil margin (the Laurentian conjugate margin to the Baltican fossil margin in the Caledonides) shows an almost identical lithological association with serpentinites interleaved with pelagic meta-sediments and overlain by ophiolites.

The level of preservation of the Tethyan OCT in the Alps has permitted extensive study, it has revealed that different lithological associations can be recognized from different Alpine domains, which is can be used to interpret basin architecture. We are still in the early stages of studying the Scandinavian Caledonian mélange, however, mapping other parts of the mélange in more detail may reveal similar relationships between basin architecture and lithological association.

Thus, comparison of the Caledonian mélange to fossil hyperextended margins in other mountains belts as well to modern hyperextended margins shows strong similarities that support the idea that the Caledonian mélange formed in a hyperextended margin before the Scandian orogeny.

7.3. Palaeotectonic implications:

The mélange unit presently sits above the lower Bergsdalen Nappe and below the Upper Bergsdalen, Dalsfjord, Lindås, and Jotun nappes. These nappes have traditionally been considered to be of Baltican affinity, according to the classical tectonostratigraphy which does not take the mélange unit into consideration. The mélange, however, must have originated outboard of Baltica, which would separate the lower nappes by an oceanic basin before thrusting if the Lindås and Jotun nappes are not out of sequence thrust sheets.

If the mélange originated in a hyperextended margin, the ocean must have separated the allochthonous crystalline nappes (Lower Bergsdalen and Upper Bergsdalen-Jotun-Lindås Nappes) by significant distance. This is supported by the Celtic fauna found in the Otta serpentinite conglomerate in the mélange unit. The fossils here show mixed provinciality of an island origin, suggesting deposition on an island outboard of both Baltica and Laurentia in the Mid-Ordovician (470-464 Ma) (Bruton and Harper, 1981). Few fossils have been found elsewhere at this stage, however, detrital clastic serpentinites such as those found in the Samnanger Complex of the Bergen area (e.g. Heldal and Jansen, 2000, Qvale, 1978) or the Reiggehaugen conglomerate described in this thesis strongly indicate the presence of serpentinite ridges or highs providing material for high energy clastic sedimentation. This would be facilitated by hyperextension, which may exhume serpentinized mantle to the sea floor (see Chapter 1 for elaboration), providing serpentinite ridges and perhaps islands. The serpentinite ridges can, in turn, be uplifted further during plate convergence as they are weak and relatively buoyant. This could explain the Celtic Mid-Ordovician fauna found in detrital serpentinite in Otta.

In this scenario, the crystalline nappes of the Jotun-Lindås system must formed as continental ribbons or microcontinents, separated from Baltica by a basin which formed by hyperextension. A similar, but smaller scale, association is documented in the Pyrenees where hyperextension creates crustal boudins separated by basins (Clerc et al., 2015). This introduces additional complexity in the palaeotectonic architecture of Baltica and the Iapetus, which in turn is supported by the current along strike variation of the allochthonous crystalline nappes and the Seve Nappe Complex (Andersen et al., 2012). If Baltica and Laurentia were separated by greater distances than previously postulated, the path leading to their collision would capture additional elements such as microcontinents, island arcs and ocean fragments (Corfu et al., 2014a). This is comparable to the modern day motion of Australia towards Asia or the Cenozoic Himalayan collision (e.g. Roberts et al., 2003, Labrousse et al., 2010, Van Staal et al., 1998). Additionally, the possible rotation of Baltica from the Late Cambrian (Cocks and Torsvik, 2002) introduces additional terranes that may have been captured from the Ægerian margin. This would not only explain the structural position of the mélange and the overlying crystalline nappes, it also implies that suspect nappe units in the Caledonides such as the Seve and Kalak Nappes could have originated in domains other than Baltica and Laurentia (Corfu et al., 2014a). A new pseudo-terrane reconstruction is presented in Figure 84. It shows the minimum number of terranes that would have existed in the Iapetan domain prior to the Scandian orogeny, e.g. around 470 Ma, according to the fossil ages, but likely further back in time before 600 Ma, which is when the first dyke swarms are observed (e.g. Nystuen et al., 2008, Svenningsen, 2001, Baird et al., 2014). The hyperextended margin here separates the Lower Bergsdalen nappe (Baltican) from the Upper Bergsdalen nappe and its accompanying crystalline nappes. The width of the Iapetus here is undetermined and probably extended for significant distances, comparable to the modern North Atlantic margin (Andersen et al., 2012). This permits additional complexity, such as the Celtic fauna island, microcontinents, island arcs or continental slivers to have existed prior to Caledonian thrusting, enabling capture during the orogeny and emplacement into their current position in the Caledonides.

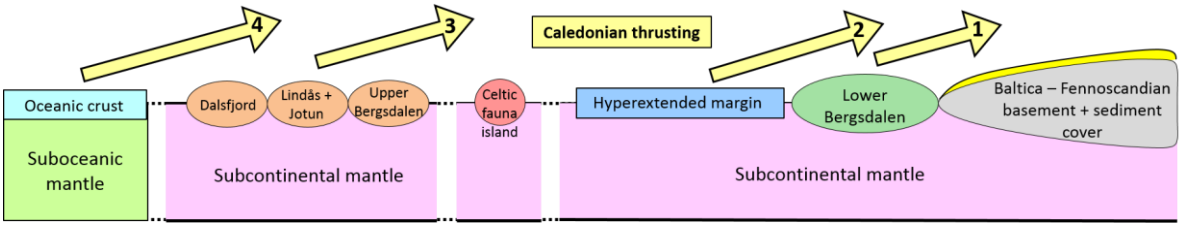

Figure 84: Pseudo-terrane reconstruction for the Baltican margin prior to the Scandian orogeny. The hyperextended margin separates the Lower Bergsdalen nappe from the crystalline Upper Bergsdalen, Jotun, Lindås and Dalsfjord nappe. These crystalline nappes may have been microcontinents or arcs. Additional complexity (such as the isolated islands with Celtic fauna) are permitted in such a setting and this reconstruction shows the minimum terranes that would have existed. Closure of the Iapetus Ocean (whose width is undetermined here) would capture these terranes and thrust them onto Baltica in the Caledonian Scandian event.

Alternatively, the crystalline nappes may have originated on the Baltican margin, placing them adjacent to the Lower Bergsdalen basement, and the hyperextended margin could have been sandwiched in by wedging between the two or by out of sequence faulting. The former involves thrusting the Lower Bergsdalen basement first, followed by the Upper Bergsdalen nappe on top and then thrusting the hyperextended margin in between the two previously thrust nappes (triangle thrust section). This seems highly unlikely as the hyperextended margin is made up of weak serpentinite which is more likely to override crystalline rocks rather then get caught in between. The

second possibility, out of sequence faulting, involves thrusting the Lower Bergsdalen basement first, followed by thrusting the outboard hyperextended margin over the crystalline Dalsfjord, Lindås, Jotun and Upper Bergsdalen units and onto the Lower Bergsdalen thrust and then thrusting the Upper Bergsdalen, Lindås and Dalsfjord nappe on top. This also does not seem likely, as it is difficult to thrust the hyperextended margin over such large continental units. It is more likely that thrusting of the mélange would have stopped on top of the Dalsfjord-Lindås-Jotun-Upper Bergsdalen units and passively rode on top of these as they were thrusted later (piggy-back thrust). Neither of these scenarios would place the mélange between the Lower and Upper Bergsdalen nappes, so we favour the terrane reconstruction shown in Figure 84, where the crystalline nappes are separated by the hyperextended margin as continental slivers, and the various domains are thrust onto Baltica in sequence.

The terrane and oceanic domain complexity shown here as well as the reinterpretation of the mélange unit, the Middle Allochthon and other suspect units in the Caledonides emphasizes the point made by Corfu et al. (2014a) for the need to abandon the classical 4-Allochthon tectonostratigraphy based on tectonic genesis, and adopt terminology that permits re-interpretation using modern ideas of margins, rift systems and polyphase compressional regimes.

7.4. The age problem:

The opening of the Iapetus between Baltica and Laurentia is thought to be the last stage of the break-up of Rodinia. This continental break is marked by emplacement of doleritic dyke swarms along the Baltoscandian margin from ca. 610 - 542 Ma (Nystuen et al., 2008). The oldest dyke swarm documented so far is the Egersund Dyke swarm at ca. 616±3Ma (Bingen et al., 1998). The Seve Nappe Complex shows a series of doleritic-tholeiitic dyke swarms with ages of 610-550 (Paulsson and Andreasson, 2002) as shown on Figure 85 with the relevant references. These have normal to transitional mid ocean ridge geochemical signatures (Baird et al., 2014). Subduction of the Iapetus is thought to have initiated around 508Ma (Van Staal et al., 1998).

It has been shown earlier that the Caledonian mélange unit must have formed before the Scandian orogeny, as the entire unit (meta-peridotites included) shows strong Caledonian deformation. There is, however, little else to constrain the age of the mélange. The mapped area has sparse magmatic rocks, so samples collected from the mélange in the Bergen area have been dated and documented in Chapter 6. The dated samples, however, probably originated in two later events that postdate the onset of subduction (~476-486 Ma and ~420 Ma) (see Chapter 6 for more detail).

Additionally, a conglomerate pebble from the mélange matrix in Stølsheimen has been dated by Andersen et al. (2012). The pebble is a leucogranite pebble from a matrix supported conglomerate containing mainly quartzite and quartz pebbles. The pebble was found to have a zircon crystallization age 1033 ± 22 Ma with rutile giving a secondary age of 958 ± 35Ma and with formation of metamorphic titanite of 410 ± 3 Ma. The crystallization ages of the leucogranite pebble is akin to the age of the Baltican basement and suggests continental provenance (Andersen et al., 2012). This also supports the formation of the mélange on the proto-Iapetan Baltican margin, where continental material could be derived from Baltica and deposited in the rift basin.

Prior to the Scandian orogeny, the Iapetus separated Baltica from Laurentia. The mélange, therefore, most likely originated in the margin of the evolving Iapetus. If the mélange originated in the Iapetan hyperextended passive margin, it must be older than onset of subduction and may have an age closer

to or slightly younger than the early Iapetan dyke swarms (~600 Ma). At the time of writing, there is no information from the Caledonian mélange to directly support or contradict this however, the Laurentian Iapetus margin supports this. Here we find a similar mélange unit in the Birchy Complex (described above) that has been intruded by gabbros dated ~550-565 Ma (Van Staal et al., 2013). The gabbro ages overlap with the last phase of rift related magmatism observed along the Humber Margin (Laurentian Iapetus margin) dated at 615-550 Ma (Kamo et al., 1989, Cawood et al., 2001). This indicates emplacement of the mélange before the onset of rift related magmatism (although by how long, remains an open question).

Therefore, there is no evidence to contradict the formation of the mélange on the proto-Iapetan Baltican margin, however, further work needs to be done before an age can be suggested with confidence.

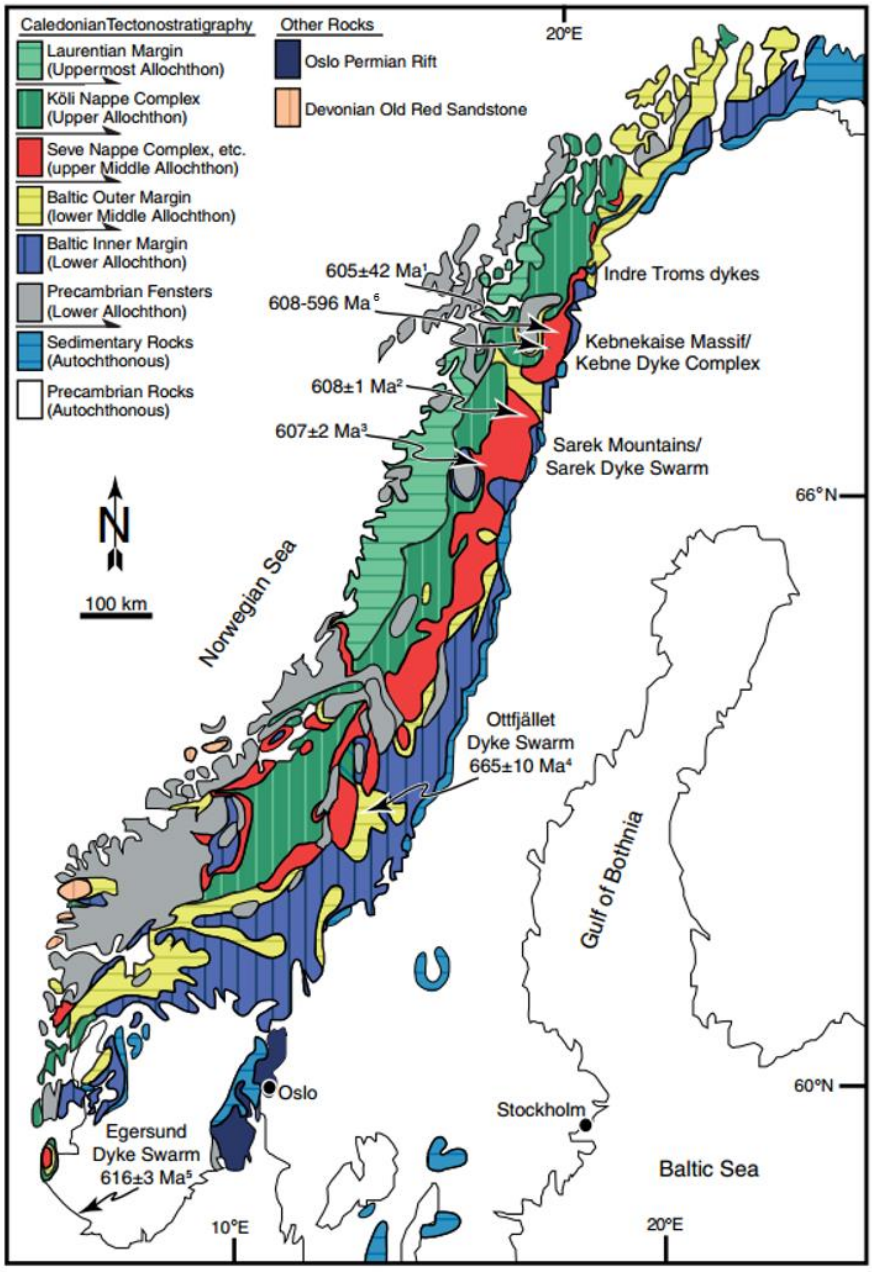

Figure 85: Ages of dyke swarm formation in the Iapetus as found in the Seve Nappe Complex and related rocks. Tectonostratigraphic map after Gee et al. (2013). Ages from: 1-Paulsson and Andreasson (2002); 2-Svenningsen (2001); 3-Root and Corfu (2012); 4-Claesson and Roddick (1983); 5-Bingen et al. (1998); 6-Baird et al. (2014).

Conclusion and way forward

The occurrence of the mélange in the Scandinavian Caledonides, recently identified as a separate tectonic unit, has not been previously studied or explained satisfactorily. Evidence for its formation in a hyperextended passive margin is presented in this thesis. This idea is mainly supported by the lithological association in the mélange, where ultramafic rocks are interleaved with marine meta-sediments partly with continental provenance in an association that precedes the Scandian Orogeny. Formation of the mélange unit on the Baltican hyperextended passive margin implies that some of the crystalline allochthonous nappes traditionally assigned to the Middle Allochthon may have been microcontinents or outboard continental boudins separated by significant distances. The age of the magma poor mélange remains an open question. It is thought to have formed in the Baltican passive margin in the early stages of continental breakup, however, no direct geochronological evidence is found in the Scandinavian Caledonides yet. More work is needed in this area to constrain the age and refine Palaeotectonic reconstructions from this era. Additionally, the origin of the mélange unit could be better understood by structural studies and structural restoration. This would help elucidate the structural setting of the mélange unit before the Scandian orogeny. More pressingly, the mélange unit needs to be mapped along the length of the Caledonides. This may reveal different parts of the basin, giving a clearer picture of basin architecture during the mélange's formation. Comparing this to modern analogues of young oceans such as the Red Sea will give a much better constraint on the processes involved in hyperextension and the role it plays in the history of the Caledonides.

Appendix

I. Preparation of samples for U-Pb dating

I.1. Mineral separation

The samples were crushed in a clean and controlled environment (to avoid contamination) using a jaw crusher followed by a Retsch crusher to reduce the grain size to less than 0.5mm.

The samples were then split into a heavy fraction and light fraction using a Wilfley shaking table.

The heavy Wilfley fraction was then taken for further mineral separation using some or all of the steps below (the steps used for each sample are shown in Table 4 below).

- Hand magnet to take out the most magnetic minerals.
- Free fall magnet up to 1.5 Amperes.
- Sifting away grains larger than 250µm.
- Use of the Frantz magnetic separator in several steps to remove minerals of higher magnetic susceptibility
- Final separation using a heavy liquid. The liquid used was Methylene iodide (CH_2I_2, aka DJM) with an SG of 3.3 (more information about the liquid can be found at chemdata.org).

Sample	Sifted	Hand magnet	Free fall	Frantz steps	Heavy liquid
Ot-1b-14	y	n	y	0.25 A 0.30 A 0.40 A 0.70 A 0.80 A	y
Hana-01-14	y	n	y	n	y
Sam-11-14	y	n	y	0.40 A 0.70 A 0.80 A	y
Sam-12-14	y	n	y	0.40 A 0.60 A 0.80 A	y
Sam-13-14	n	y	n	0.30 A 0.40 A 0.50 A 0.60 A	y
Sam-16-14	y	n	y	0.25 A x2 0.30 A 0.40 A 0.80 A	y

Table 4: Mineral separation steps performed on each sample.

I.1. Grain selection

Following mineral separation, the heaviest fraction of each sample was taken for grain selection. Zircons are primarily targeted; however, rutile was also selected for one of the samples.

The first batch of grains was selected manually and put through mechanical abrasion. Here, some pyrite is added to the sample which is then subjected to compressed air to buff the selected grains overnight.

Once the grains are abraded, the pyrite is removed by dissolution in dilute nitric acid over a hot plate and subjected to infrared light. This speeds up the reaction while evaporating away the reacted pyrite-nitric acid. After this, the sample is ready for final grain selection. The following grains were selected for each sample:

Sample	Selected grains
Ot-1b-14	No zircons found
Hana-01-14	4 zircon grains
Sam-11-14	None (2 zircons found with a large core, deemed undateable)
Sam-12-14	2 zircon crystal tips (to avoid cores) 2 euhedral zircon grains
Sam-13-14	4 zircon grains 2 rutile grains
Sam-16-14	4 zircon grains

I.2. Preparation of selected grains:

All of the selected grains were washed once in water and twice in acetone. They were also subjected to ultrasonic vibrations before each washing step, insuring that any dirt clinging to the grains is removed. The grains are then dried, weighed and individually put in Teflon bombs for dissolution at 195° for single grain analysis. Here we added one drop of nitric acid and twelve drops of hydrofluoric acid. A spike of ^{202}Pb, ^{205}Pb and ^{235}U is also added. The spike has a known constant ratio which allows us to calculate the amount Pb and U in the sample, as the ratios are more easily measured than absolute quantities.

After dissolution, the U and Pb is extracted from samples to be measured using ID-TIMS (Isotope dilution thermal ionization mass spectrometry). For small grains, the U and Pb was not chemically separated, however, chemical separation of U and Pb was done for larger grains (using an ion exchange resin).

Table 5 below shows the grains picked, their weights, amount of spike added and whether or not they underwent chemical separation of U and Pb.

Table 5: Preparation steps of grains for ID-TIMS.

Sam-13-14 zircons					
Grain	**Weight**	**Spike**	**Bomb**	**Chemistry**	**Result**
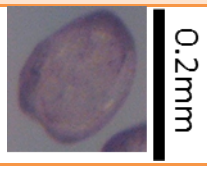	=/< 0.001mg	3.2mg	51	No	Sample lost.

	0.008mg	3.2mg	52	Yes	486.8Ma
	0.015mg	3.2mg	53	Yes	486.7 Ma
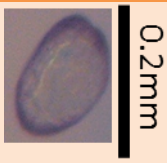	0.002mg	3.2mg	54	Yes	484.1 Ma

Sam-13-14 Rutiles					
Grain	**Weight**	**Spike**	**Bomb**	**Chemistry**	**Result**
	0.137mg	6.1mg	55	Yes	Insufficient uranium.
	0.032mg	6.1mg	56	Yes	Insufficient uranium.

Sam-12-14 zircons (euhedral crystals)					
Grain	**Weight**	**Spike**	**Bomb**	**Chemistry**	**Result**
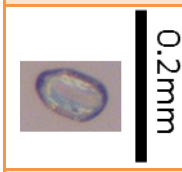	<0.001mg	3.2mg	57	No	475.4 Ma
	<0.001mg	3.2mg	58	No	477.2Ma

Sam-12-14 zircons (tips)					
Grain	**Weight**	**Spike**	**Bomb**	**Chemistry**	**Result**
	<0.001mg	3.2mg	59	No	477.1 Ma

	<0.001mg	3.2mg	60	No	475.8 Ma

Sam-16-14 zircons					
Grain	**Weight**	**Spike**	**Bomb**	**Chemistry**	**Result**
	<0.001mg	3.2mg	61	No	417.3 Ma
	<0.001mg	3.2mg	62	No	422.5 Ma
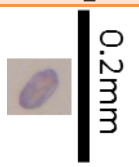	<0.001mg	3.2mg	13	No	420.5 Ma
	<0.001mg	3.2mg	14	No.	Sample lost.

Hana-01-14 zircons					
Grain	**Weight**	**Spike**	**Bomb**	**Chemistry**	**Result**
	<0.001mg	3.2mg	15	No	656.1 Ma
	<0.001mg	3.2mg	16	No	429.9 Ma
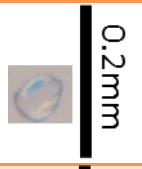	<0.001mg	3.2mg	17	No	685.6 Ma
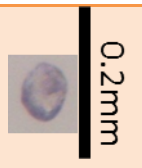	<0.001mg	3.2mg	18	No	583.6 Ma

II. Mineral calculation spreadsheets

The spreadsheet built to calculate each mineral is shown with an example calculation. The mineral structural formula is indicated as well as the number of oxygens the mineral was normalized to. Some of the analyses were done with Ni and Sr, however, the majority were without Ni and Sr, so the example spreadsheets shown below are for the analyses that do not include Ni and Sr. The included elements are shown.

The following atomic weights were used:

O	15.9994
Si	28.0855
Al	26.98154
Ca	40.078
Fe	55.845
Mn	54.93805
Cr	51.9961
Mg	24.305
Na	22.98977
K	39.0983
Ti	47.867
H	1.00794
Ni	58.6934
Sr	87.62

II.1. Muscovite

Mineral formula:	**A1**		**M2**		**T4**		**OH2**			**Normalize to Oxygen #**
Muscovite	K20	0.85518	Al2O3	1.595118	Al2O3	0.889712	F			11
A1M2T4O10(OH)2	Na2O	0.117776	MgO	0.161253	SiO2	3.178571	Cl			
	CaO	-0.00308	FeO	0.244282			OH	2		
			MnO	-0.00065						
Sum	**A**	**0.96988**	**M**	**2**	**T4**	**4.068283**	**OH**	**2**		

DataSet/Point	**SiO2**	**Al2O3**	**CaO**	**FeO**	**MnO**	**Cr2O3**	**MgO**	**Na2O**	**K2O**	**TiO2**	**H2O**	**Total**
75 / 1 .	46.9579	31.1471	-0.0424	4.3152	-0.0114	0.0051	1.598	0.8974	9.9032	0.2643		95.0345
GFW (atomic weight)	60.0843	101.9613	56.0774	71.8444	70.93745	151.9904	40.3044	61.97894	94.196	79.8658	18.01528	
mole units (apfu):	0.781534	0.30548	-0.00076	0.060063	-0.00016	3.36E-05	0.039648	0.014479	0.105134	0.003309		
oxygen units:	1.563067	0.916439	-0.00076	0.060063	-0.00016	0.000101	0.039648	0.014479	0.105134	0.006619		2.704633
normalized oxygen units:	6.357143	3.727245	-0.00308	0.244282	-0.00065	0.000409	0.161253	0.058888	0.42759	0.026918		
atom units:	3.178571	2.48483	-0.00308	0.244282	-0.00065	0.000273	0.161253	0.117776	0.85518	0.013459		

II.2. Biotite

Mineral formula:	**A1**		**M3**		**T4**		**OH2**			**Normalize to Oxygen #**
Biotite	K2O	0.965507	MgO	1.077057	Al2O3	1.339999	F			11
$A_1M_3T_4O_{10}(OH)_2$	Na2O	0.002197	FeO	1.485498	SiO2	2.806632	Cl			
			MnO	0.058166			OH	2		
			Cr2O3	-0.0008						
			TiO2	0.137269						
Sum	**A**	**0.967704**	**M**	**2.757195**	**T4**	**4.146631**	**OH**	**2**		

DataSet/Point	**SiO2**	**Al2O3**	**CaO**	**FeO**	**MnO**	**Cr2O3**	**MgO**	**Na2O**	**K2O**	**TiO2**	**H2O**	**Total**
111 / 1 .	35.4139	14.3462	-0.0139	22.4126	0.8665	-0.0127	9.1163	0.0143	9.5496	2.3023	93.9952	biotite
GFW (atomic weight)	60.0843	101.9613	56.0774	71.8444	70.93745	151.9904	40.3044	61.97894	94.196	79.8658	18.01528	
mole units (apfu):	0.589404	0.140702	-0.00025	0.31196	0.012215	-8.4E-05	0.226186	0.000231	0.10138	0.028827		
oxygen units:	1.178807	0.422107	-0.00025	0.31196	0.012215	-0.00025	0.226186	0.000231	0.10138	0.057654		2.310042
normalized oxygen units:	5.613264	2.009998	-0.00118	1.485498	0.058166	-0.00119	1.077057	0.001099	0.482754	0.274539		
atom units:	2.806632	1.339999	-0.00118	1.485498	0.058166	-0.0008	1.077057	0.002197	0.965507	0.137269		

II.3. Amphibole

Mineral formula:	**A0-1**		**Md2**		**Mabc5**		**T8**		**OH2**		**Normalize to Oxygen #**
Amphibole	K2O	0.007964	Na2O	0	Al2O3	3.010709	SiO2	5.769149	OH	2	23
A0-1Md2Mabc5T8O22(OH)2	Na2O	-0.00271	CaO	3.70509	TiO	0.010682	Al2O3	0.781836	F		
					FeO	1.977835			Cl		
					MgO	-0.00169					
					MnO	0.002461					
Sum	**A**	**0.00525**	**Md2**	**3.70509**	**T4**	**5**	**T**	**6.550985**	**OH**	**2**	

DataSet/Point	**SiO2**	**Al2O3**	**CaO**	**FeO**	**MnO**	**Cr2O3**	**MgO**	**Na2O**	**K2O**	**TiO2**	**H2O**	**Total**
110 / 1 .	36.6906	20.4653	21.9922	15.0406	0.4803	0.0198	-0.0072	-0.0089	0.0397	0.0903	94.8029	amphibole
GFW (atomic weight)	60.0843	101.9613	56.0774	71.8444	70.93745	151.9904	40.3044	61.97894	94.196	79.8658	18.01528	
mole units (apfu):	0.610652	0.200716	0.392176	0.20935	0.006771	0.00013	-0.00018	-0.00014	0.000421	0.001131		
oxygen units:	1.221304	0.602149	0.392176	0.20935	0.006771	0.00039	-0.00018	-0.00014	0.000421	0.002261		2.434501
normalized oxygen units:	11.53838	5.688815	3.70509	1.977835	0.063967	0.003692	-0.00169	-0.00136	0.003982	0.021364		
atom units:	5.769149	3.792545	3.70509	1.977835	0.063967	0.002461	-0.00169	-0.00271	0.007964	0.010682		

II.4. Epidote

Mineral formula:	**A4**		**B6**		**SiO4**		**OH2**		**Normalize to Oxygen #**
Epidote	CaO	2.013636	Al2O3	2.061166	SiO2	3.135407	OH	2	12.5
$A_4B_6(SiO_4)_6(OH)_2$	REE, Sr, Y		FeO	1.074911					
			MnO	0.034765					
Sum	**A**	**2.013636**	**B**	**3.170841**	**SiO**	**3.135407**	**OH**	**2**	

DataSet/Point	**SiO2**	**Al2O3**	**CaO**	**FeO**	**MnO**	**Cr2O3**	**MgO**	**Na2O**	**K2O**	**TiO2**	**H2O**	**Total**
110 / 1 .	36.6906	20.4653	21.9922	15.0406	0.4803	0.0198	-0.0072	-0.0089	0.0397	0.0903		94.8029
GFW (atomic weight)	60.0843	101.9613	56.0774	71.8444	70.93745	151.9904	40.3044	61.97894	94.196	79.8658	18.01528	
mole units (apfu):	0.610652	0.200716	0.392176	0.20935	0.006771	0.00013	-0.00018	-0.00014	0.000421	0.001131		
oxygen units:	1.221304	0.602149	0.392176	0.20935	0.006771	0.000391	-0.00018	-0.00014	0.000421	0.002261		2.434501
normalized oxygen units:	6.270814	3.091749	2.013636	1.074911	0.034765	0.002007	-0.00092	-0.00074	0.002164	0.011611		
atom units:	3.135407	2.061166	2.013636	1.074911	0.034765	0.001338	-0.00092	-0.00147	0.004328	0.005805		

II.5. Feldspar

Mineral formula:	**A1**		**T2**		**Si2**		**Normalize to Oxygen #**
Feldspar	Na2O	0.016357	Al2O3	1.007882	SiO2	2	8
$A_1T_2Si_2O_8$	K2O	1.011141	FeO	0.002475			
	CaO	-0.00511	SiO2	0.989227			
Sum	**A**	**1.022391**	**B**	**1.999584**	**SiO**	**2**	

DataSet/Point	**SiO2**	**Al2O3**	**CaO**	**FeO**	**MnO**	**Cr2O3**	**MgO**	**Na2O**	**K2O**	**TiO2**	**H2O**	**Total**
107 / 1 .	64.0275	18.3173	-0.1021	0.0634	-0.0101	0.0035	0.0007	0.1807	16.977	-0.0176	99.4402	feldspar
GFW (atomic weight)	60.0843	101.9613	56.0774	71.8444	70.93745	151.9904	40.3044	61.97894	94.196	79.8658	18.01528	
mole units (apfu):	1.065628	0.17965	-0.00182	0.000882	-0.00014	2.3E-05	1.74E-05	0.002916	0.180231	-0.00022		
oxygen units:	2.131256	0.538949	-0.00182	0.000882	-0.00014	6.91E-05	1.74E-05	0.002916	0.180231	-0.00044		2.851916
normalized oxygen units:	5.978454	1.511822	-0.00511	0.002475	-0.0004	0.000194	4.87E-05	0.008178	0.505571	-0.00124		
atom units:	2.989227	1.007882	-0.00511	0.002475	-0.0004	0.000129	4.87E-05	0.016357	1.011141	-0.00062		

II.6. Garnet

Mineral formula:	**X3**		**Y2**		**Z3**		**Normalize to Oxygen #**
Garnet	MgO	0.145518	TiO2	0.004236	SiO2	2.970174	12
$X_3Y_2Z_3O_{12}$	FeO	1.802847	Al2O3	1.976919	Al2O3	0	
	CaO	0.504987	Cr2O3	0.001808	FeO		
	MnO	0.61383	FeO	0.017036	TiO2		
Sum	**X**	**3.067182**	**Y**	**2**	**Z**	**2.970174**	

DataSet/Point	**SiO2**	**Al2O3**	**CaO**	**FeO**	**MnO**	**Cr2O3**	**MgO**	**Na2O**	**K2O**	**TiO2**	**H2O**	**Total**
84 / 1 .	36.2368	20.4645	5.7501	26.5487	8.8416	0.0186	1.1909	-0.0041	0.0019	0.0687		99.1178
GFW (atomic weight)	60.0843	101.9613	56.0774	71.8444	70.93745	151.9904	40.3044	61.97894	94.196	79.8658	18.01528	
mole units (apfu):	0.603099	0.200709	0.102539	0.369531	0.124639	0.000122	0.029548	-6.6E-05	2.02E-05	0.00086		
oxygen units:	1.206199	0.602126	0.102539	0.369531	0.124639	0.000367	0.029548	-6.6E-05	2.02E-05	0.00172		2.436622
normalized oxygen units:	5.940348	2.965379	0.504987	1.819883	0.61383	0.001808	0.145518	-0.00033	9.93E-05	0.008473		
atom units:	2.970174	1.976919	0.504987	1.819883	0.61383	0.001205	0.145518	-0.00065	0.000199	0.004236		

Bibliography

ANDERSEN, T. B. 1998a. Extensional tectonics in the Caledonides of southern Norway, an overview. *Tectonophysics,* 285**,** 333-351.

ANDERSEN, T. B. 1998b. Extensional tectonics in the Caledonides of southern Norway, an overview. *Tectonophysics,* 285**,** 333-351.

ANDERSEN, T. B., CORFU, F., LABROUSSE, L. & OSMUNDSEN, P.-T. 2012. Evidence for hyperextension along the pre-Caledonian margin of Baltica. *Journal of the Geological Society,* 169**,** 601-612.

ANDERSEN, T. B. & JAMTVEIT, B. 1990. Uplift of deep crust during orogenic extensional collapse: a model based on field studies in the Sogn-Sunnfjord region of western Norway. *Tectonics,* 9**,** 1097-1111.

ANDERSEN, T. B., JAMTVEIT, B., DEWEY, J. F. & SWENSSON, E. 1991. Subduction and eduction of continental crust: major mechanisms during continent‐continent collision and orogenic extensional collapse, a model based on the south Norwegian Caledonides. *Terra Nova,* 3**,** 303-310.

ANDERSEN, T. B., SKJERLIE, K. P. & FURNES, H. 1990. The Sunnfjord Melande, evidence of Silurian ophiolite accretion in the west Norwegian Caledonides. *Journal of the Geological Society, London,* 147**,** 59-68.

ANDERSON, E. M. 1951. *The dynamics of faulting and dyke formation with applications to Britain*, Hafner Pub. Co.

AUGLAND, L. E., ANDRESEN, A., GASSER, D. & STELTENPOHL, M. G. 2014. Early Ordovician to Silurian evolution of exotic terranes in the Scandinavian Caledonides of the Ofoten–Troms area – terrane characterization and correlation based on new U–Pb zircon ages and Lu–Hf isotopic data. *Geological Society, London, Special Publications,* 390**,** 655-678.

BAIRD, G. B., FIGG, S. A. & CHAMBERLAIN, K. R. 2014. Intrusive age and geochemistry of the Kebne Dyke Complex in the Seve Nappe Complex, Kebnekaise Massif, arctic Sweden Caledonides. *GFF,* 136**,** 556-570.

BARKER, A. J. 1998. *Introduction to Metamorphic Textures and Microstructures,* Cheltenham, Stanley Thornes (Publishers) Ltd.

BARNES, C. G., FROST, C. D., YOSHINOBU, A. S., MCARTHUR, K., BARNES, M. A., ALLEN, C. M., NORDGULEN, Ø. & PRESTVIK, T. 2007. Timing of sedimentation, metamorphism, and plutonism in the Helgeland Nappe Complex, north-central Norwegian Caledonides. *Geosphere,* 3**,** 683-703.

BEINLICH, A., AUSTRHEIM, H., GLODNY, J., ERAMBERT, M. & ANDERSEN, T. B. 2010. CO2 sequestration and extreme Mg depletion in serpentinized peridotite clasts from the Devonian Solund basin, SW-Norway. *Geochimica et Cosmochimica Acta,* 74**,** 6935-6964.

BELTRANDO, M., MANATSCHAL, G., MOHN, G., DAL PIAZ, G. V., VITALE BROVARONE, A. & MASINI, E. 2014. Recognizing remnants of magma-poor rifted margins in high-pressure orogenic belts: The alpine case study. *Earth Science Reviews,* 131**,** 88-115.

BERNOULLI, D. & WEISSERT , H. 1985. Sedimentary fabrics in Alpine ophicalcites, South Pennine Arosa zone, Switzerland. *Geology,* 13**,** 755-758.

BEYER, E. E., BRUECKNER, H. K., GRIFFIN, W. L. & O'REILLY, S. Y. 2012. Laurentian Provenance of Archean Mantle Fragments in the Proterozoic Baltic Crust of the Norwegian Caledonides. *Journal of Petrology,* 53**,** 1357-1383.

BINGEN, B., DEMAIFFE, D. & VAN BREEMEN, O. 1998. The 616 Ma Old Egersund Basaltic Dike Swarm, SW Norway, and Late Neoproterozoic Opening of the Iapetus Ocean. *The Journal of Geology,* 106**,** 565-574.

BJERKGÅRD, T. & BJØRLYKKE, A. 1994. Geology of the Folldal area, southern Trondheim region Caledonides, Norway. *Norges geologiske undersøkelse Bulletin,* 426**,** 53-75.

BØE, R., STURT, B. A. & RAMSAY, D. M. 1993. The conglomerates of the Sel Group, Otta-Vågå area, Central Norway: an example of a terrrane-linking succession. *Norges geologiske undersøkelse, Bulletin,* 425**,** 1-23.

BOILLOT, G., GRIMAUD, S., MAUFFRET, A. & MOUGENOT, D. 1980. Ocean-continent boundary off the Iberian margin: A serpentinite diapir west of the Galicia Bank. *Earth and Planetary Science Letters,* 48**,** 23-34.

BOILLOT, G., RECQ, M., WINTERER, E. L., MEYER, A. W., APPLEGATE, J., BALTUCK, M., BERGEN, J. A., COMAS, M. C., DAVIES, T. A., DUNHAM, K., EVANS, C. A., GIRARDEAU, J., GOLDBERG, G., HAGGERTY, J., JANSA, L. F., JOHNSON, J. A., KASAHARA, J., LOREAU, J. P., LUNA-SIERRA, E., MOULLADE, M., OGG, J., SARTI, M., THUROW, J. & WILLIAMSON, M. 1987. Tectonic denudation of the upper mantle along passive margins: a model based on drilling results (ODP leg 103, western Galicia margin, Spain). *Tectonophysics,* 132**,** 335-342.

BRUTON, D. L. & HARPER, D. A. 1981. Brachiopods and trilobites of the early Ordovician serpentine Otta Conglomerate, south central Norway. *Norsk Geologisk Tidsskrift,* 61**,** 153-181.

CAWOOD, P. A., MCCAUSLAND, P. J. & DUNNING, G. R. 2001. Opening Iapetus: Constraints from the Laurentian margin in Newfoundland. *Geological Society of America Bulletin,* 113**,** 443-453.

CHEW, D. M. & VAN STAAL, C. R. 2014. The ocean - continent transition zones along the Appalachian - Caledonian margin of Laurentia: examples of large-scale hyperextension during the opening of the Iapetus ocean. *Geoscience Canada,* 41**,** 165-185.

CHOUKRANE, P. & MATTAUER, M. 1978. Tectonique des plaques et Pyrénées: Sur le fonctionnement de la faille transformante nord-Pyrénéenne; comparaisons avec les modèles actuels. *Bulletin de la société géologique de France,* 20**,** 689-700.

CLAESSON, S. & RODDICK, J. C. 1983. 40Ar/39Ar data on the age and metamorphism of the Ottfjället dolerites, Särv Nappe, Swedish Caledonides. *Lithos,* 16**,** 61-73.

CLERC, C., BOULVAIS, P., LAGABRIELLE, Y. & DE SAINT BLANQUAT, M. 2014. Ophicalcites from the northern Pyrenean belt: a field, petrographic and stable isotope study. *International Journal of Each Science,* 103**,** 141-163.

CLERC, C. & LAGABRIELLE, Y. 2014. Thermal control on the modes of crustal thinning leading to mantle exhumation: Insights from the Cretaceous Pyrenean hot paleomargins. *Tectonics,* 33**,** 2013TC003471.

CLERC, C., LAHFID, A., MONIÉ, P., LAGABRIELLE, Y., CHOPIN, C., POUJOL, M., BOULVAIS, P., RINGENBAC, J. C., MASINI, E. & DE ST BLANQUAT, M. 2015. High-temperature metamorphism during extreme thinning of the continental crust: a reappraisal of the north Pyrenean paleo-passive margin. *Solid Earth Discuss.,* 7**,** 797-857.

COCHRAN, J. R. & KARNER, G. D. 2007. Constraints on the deformation and rupturing of continental lithosphere of the Red Sea; the transition from rifting to drifting. *Geological Society, London, Special Publications,* 282**,** 265-289.

COCKS, L. R. M. & FORTEY, R. A. 1982. Faunal evidence for oceanic separations in the Palaeozoic of Britain. *Journal of The Geological Society,* 139**,** 465-478.

COCKS, L. R. M. & TORSVIK, T. H. 2002. Earth geography from 500 to 400 million years ago: a faunal and palaeomagnetic review. *Journal of the Geological Society,* 159**,** 631-644.

COFFIN, M. F. & ELDHOLM, O. 1992. Volcanism and continental break-up: a global compilation of large igneous provinces. *Geological Society, London, Special Publications,* 68**,** 17-30.

COFFIN, M. F. & ELDHOLM, O. 1994. Large igneous provinces: crustal structure, dimensions, and external consequences. *Reviews of Geophysics,* 32**,** 1-36.

COLLETTINI, C. & SIBSON, R. H. 2001. Normal faults, normal friction? *Geology,* 29**,** 927-930.

CONTRUCCI, I., MATIAS, L., MOULIN, M., GELI, L., KLINGELHOFER, F., NOUZE, H., ASLANIAN, D., OLIVET, J. L., REHAULT, J. P. & SIBUET, J. C. 2004. Deep structure of the West African continental margin (Congo, Zaïre, Angola), between 5°S and 8°S, from reflection/refraction seismics and gravity data. *Geophysical Journal International,* 158**,** 529-553.

CORFU, F., ANDERSEN, T. B. & GASSER, D. 2014a. The Scandinavian Caledonides: main features, conceptual advances and critical questions. *Geological Society, London, Special Publications,* 390**,** 9-43.

CORFU, F., AUSTRHEIM, H. & GANZHOM, A.-C. 2014b. Localized granulite and eclogite facies metamorphism at Flatraket and Kråkeneset, Western Gneiss Region: U-Pb data and tectonic implications. *Geological Society, London, Special Publications,* 390**,** 425-442.

CORFU, F., GERBER, M., ANDERSEN, T. B., TORSVIK, T. H. & ASHWAL, L. D. 2011. Age and significance of Grenvillian and Silurian orogenic events in the Finnmark Caledonides, northern Norway. *Canadian Journal of Earth Sciences,* 48**,** 419-440.

CORFU, F., ROBERTS, R. J., TORSVIK, T. H., ASHWAL, L. D. & RAMSAY, D. M. 2007. Peri-Gondwanan elements in the Caledonian Nappes of Finnmark, Northern Norway: Implications for the paleogeographic framework of the Scandinavian Caledonides. *American Journal of Science,* 307**,** 434-458.

CORFU, F., TORSVIK, T. H., ANDERSEN, T. B., ASHWAL, L. D., RAMSAY, D. M. & ROBERTS, R. J. 2006. Early Silurian mafic–ultramafic and granitic plutonism in contemporaneous flysch, Magerøy, northern Norway: U–Pb ages and regional significance. *Journal of the Geological Society, London,* 163**,** 291-301.

CORNEN, G., BESLIER, M. O. & GIRARDEAU, J. 1996. Petrology of the mafic rocks cored in the Iberia Abyssal Plain. *In:* WHITMARSH, R. B., SAWYER, D. S., KLAUS, A. & MASSON, D. G. (eds.) *Proceedings of the Ocean Drilling Program, Scientific, Results, 149.* Texas: Ocean Drilling Program, College Station.

D'ACREMONT, E., LEROY, S., MAIA, M., PATRIAT, P., BESLIER, M. O., BELLAHSEN, N., FOURNIER, M. & GENTE, P. 2006. Structure and evolution of the eastern Gulf of Aden; insights from magnetic and gravity dat. *Geophysical Journal International,* 165**,** 786-803.

DE KAENEL, E. & BERGEN, J. A. 1996. Mesozoic Calcareous Nanofossil Biostratigraphy from Sites 897, 899, and 901, Iberia Abyssal Plain: New Biostratigraphic Evidence. *In:* WHITMARSH, R. B., SAWYER, D. S., KLAUS, A. & MASSON, D. G. (eds.) *Proceedings of the Ocean Drilling Progam, Scientific Results, 149.* Texas: Ocean Drilling Program, College Station.

DICKIN, A. P. 2005. *Radiogenic Isotope Geology,* Cambridge, University Press.

DILEK, Y. & FURNES, H. 2011. Ophiolite genesis and global tectonics: geochemical and tectonic fingerprinting of ancient oceanic lithosphere. *Geological Society of America***,** 387-411.

DIREEN, N. G., BORISSOVA, I., STAGG, H. M. J., COLWELL, J. B. & SYMONDS, P. A. 2007. Nature of the continent-ocean transition zone along the southern Australian continental margin; a comparison of the Naturaliste Plateau, SW Australia, and the central Great Australian Bight sectors. *Geological Society, London, Special Publications,* 282**,** 239-263.

DUNNING, G. R. & PEDERSEN, R. B. 1988. U/Pb ages of ophiolites and arc related plutons of the Norwegian Caledonides: implications for the development of Iapetus. *Contributions to Mineralogy and Petrology,* 98**,** 13-23.

FÆRSETH, R. B., THON, A., LARSEN, S. G., SIVERTSEN, A. & ELVESTAD, L. 1977. geology of the lower Palaeozoic rocks in the Samnanger–Osterøy, area, major Bergen Arc, western Norway. *Bulletin Norges geologiske undersøkelse,* 334**,** 19-58.

FLINN, D. 1962. ON FOLDING DURING THREE-DIMENSIONAL PROGRESSIVE DEFORMATION. *Quarterly Journal of the Geological Society,* 118**,** 385-428.

FOSSEN, H. 2010. Extensional tectonics in the North Atlantic Caledonides: a regional view. *Geological Society, London, Special Publications,* 335**,** 767-793.

FRANKE, D., BARCKHAUSEN, U., BARISTEAS, N., ENGELS, M., LADAGE, S., LUTZ, R., MONTANO, J., PELLEJERA, N., RAMOS, E. G. & SCHNABEL, M. 2011. The continent-ocean transition at the southeastern margin of the South China Sea. *Marine and Petroleum Geology,* 28**,** 1187-1204.

GEE, D. G. 1975. A tectonic model for the central part of the Scandinavian Caledonindes. *American Journal of Science,* 275**,** 468-515.

GEE, D. G., JANÁK, M., MAJKA, J., ROBINSON, P. & VAN ROERMUND, H. 2013. Subduction along and within the Baltoscandian margin during closing of the Iapetus Ocean and Baltica-Laurentia collision. *Lithosphere,* 5**,** 169-178.

GEE, D. G., KUMPULAINEN, R., ROBERTS, D., STEPHENS, M. B., THON, A. & ZACHRISSON, E. 1985. Scandinavian Caledonides, Tectonostratigraphic map, scale 1:2 000 000. *In:* GEE, D. G. & STURT, B. A. (eds.) *The Caledonide Orogen – Scandinavia and Related Areas.* Chichester: Wiler.

HACKER, B. R., ANDERSEN, T. B., JOHNSTON, S., KYLANDER-CLARK, A., PETERMAN, E., WALSH, E. & YOUNG, D. 2010. High-temperature deformation during continental margin subduction and exhumation: the ultrahigh-pressure Western Gneiss Region of Norway. *Tectonophysics,* 480**,** 1479-171.

HACKER, B. R., ANDERSEN, T. B., ROOT, D. B., MEHL, L., MATTINSON, J. M. & WOODEN, J. L. 2003. Exhumation of high-pressure rocks beneath the Solund Basin, Western Gneiss Region of Norway. *Journal of Metamorphic Geology,* 21**,** 613-629.

HARLOV, D. E. & AUSTRHEIM, H. 2012. *Metasomatism and the chemical transformation of rock: The role of fluids in terrestrial and extraterrestrial processes*, Springer Science & Business Media.

HARPER, D. A. T., BRUTON, D. L. & RASMUSSEN, C. M. Ø. 2008. The Otta brachiopod and trilobite fauna: palaeogeography of Early Palaeozoic terranes and biotas across Baltoscandia. *Fossils and Strata,* 54**,** 31-40.

HARTZ, E. H. & TORSVIK, T. H. 2002. Baltica upside down: A new plate tectonic model for Rodinia and the Iapetus Ocean. *Geology,* 30**,** 255-258.

HELDAL, T. & JANSEN, O. J. 2000. *Steinbyen Bergen: Fortellingen om Brostein, Bygg og Brudd.,* Trondheim, NGU.

HENDERSON, I., HELDAL, T., FURUHAUG, L. & LYNUM, R. 2002. Undersøkelse av serpentinkonglomerat på Reiggehaugen, Vågå. Trondheim: Norges geologiske undersøkelse.

INGDAHL, S. E. 1985. Stratigraphy, structural geology and metamorphism in the Os area, Major Bergen arc. Cand. scient. (Master) thesis, University of Bergen.

KAMO, S. L., GOWER, C. F. & KROGH, T. E. 1989. Birthdate for the Iapetus Ocean? A precise U-Pb zircon and baddeleyite age for the Long Range dikes, southeast Labrador. *Geology,* 17**,** 602-605.

KIRKLAND, C. L., DALY, J. S., CHEW, D. M. & PAGE, L. M. 2008. The Finnmarkian Orogeny revisited: An isotopic investigation in eastern Finnmark, Arctic Norway. *Tectonophysics,* 460**,** 458-177.

KIRKLAND, C. L., DALY, J. S. & WHITEHOUSE, M. J. 2007. Provenance and Terrane Evolution of the Kalak Nappe Complex, Norwegian Caledonides: Implications for Neoproterozoic Paleogeography and Tectonics. *The Journal of Geology,* 115**,** 21-41.

KOLDERUP, C. F. & KOLDERUP, N. H. 1940. Geology of the Bergen Arc System. *Bergens Museums Skrifter,* 20.

KOSTENKO, O., JAMTVEIT, B., AUSTRHEIM, H., POLLOK, K. & PUTNIS, C. 2002. The mechanism of fluid infiltration in peridotites at Almklovdalen, western Norway. *Geofluids,* 2**,** 203-215.

KROGH, T. E. 1982. Improved accuracy of U–Pb zircon dating by selection of more concordant fractions using a high-gradient magnetic separation technique. *Geochimica et Cosmochimica Acta,* 46**,** 631-635.

KUHN, A., GLODNY, J., AUSTRHEIM, H. & RÅHEIM, A. 2002. The Caledonian tectono-metamorphic evolution of the Lindås Nappe: Constraints from U-Pb, Sm-Nd and Rb-Sr ages of granitoid dykes. *Norsk Geologisk Tidsskrift,* 82**,** 45-57.

LABROUSSE, L., HETÉNYI, G., RAIMBOURG, H., JOLIVET, L. & ANDERSEN, T. B. 2010. Initiation of crustal-scale thrusts triggered by metamorphic reactions at depth: Insights from a comparison between the Himalayas and Scandinavian Caledonides. *Tectonics,* 29**,** TC5002.

LAGABRIELLE, Y. & BODINIER, J.-L. 2008. Submarine reworking of exhumed subcontinental mantle rocks: field evidence from the Lherz peridotites, French Pyrenees. *Terra Nova,* 20**,** 11-21.

LAGABRIELLE, Y. & CANNAT, M. 1990. Alpine Jurassic ophiolites resemble the modern central Atlantic basement. *Geology,* 18**,** 319-322.

LAGABRIELLE, Y., LABAUME, P. & DE SAINT BKANQUAT, M. 2010. Mantle exhumation, crustal denudation, and gravity tectonics during Cretaceous rifting in the Pyrenean realm (SW Europe): insights from the geological setting of the Iherzolite bodies. *Tectonics,* 29**,** TC4012.

LAGABRIELLE, Y., VITALE BROVARONE, A. & ILDEFONSE, B. 2015. Fossil oceanic core complexes recognized in the blueschist metaophiolites of Western Alps and Corsica. *Earth-Science Reviews,* 141**,** 1-26.

LE PICHON, X., BONNIN, J. & SIBUET, J. C. 1970. La faille nord-Pyrénéenne: faille transformante liée à l'ouverture du Golfe de Gascogne. *Comptes Rendus de l'Académie des Sciences,* D 271**,** 1941-1944.

LEMOINE, M. 1980. Serpentinites, gabbros and ophicalcites in the Piemont-Ligurian domain of the Western Alps: possible indicators of oceanic fracture zones and of associated serpentinite protrusions in the Jurassic-Cretaceous Tethys. *Archives des Sciences (Genève),* 33**,** 103-115.

LEMOINE , M., TRICART , P. & BOILLOT , G. 1987. Ultramafic and gabbroic ocean floor of the Ligurian Tethys (Alps, Corsica, Apennines): in search of a genetic model. *Geology,* 15**,** 622-625.

LUNDIN, E. R. & DORÉ, A. G. 2011. Hyperextension, serpentinization, and weakening: A new paradigm for rifted margin compressional deformation. *Geology,* 390**,** 347-350.

LUNDMARK, A. M. & CORFU, F. 2007. Age and origin of the A ° rdal dike complex, SW Norway: False isochrons, incomplete mixing, and the origin of Caledonian granites in basement nappes. *Tectonics,* 26**,** TC2007.

LUNDMARK, A. M., CORFU, F., SPURGIN, S. & SELBEKK, R. S. 2007. Proterozoic evolution and provenance of the high-grade Jotun Nappe complex, SW Norway: U-Pb geochronology. *Precambrian Research,* 159**,** 133-154.

MANATSCHAL, G. 2004. New models for evolution of magma-poor rifted margins based on a review of data and concepts from West Iberia and the Alps. *International Journal of Earth Sciences,* 93**,** 432-466.

MANATSCHAL, G., ENGSTROM, A., DESMURS, L., SCHALTEGGER, U., COSCA, M., MUNTENER, O. & BERNOULLI, D. 2006. What is the tectono-metamorphic evolution of continental break-up: the example of the Tasna ocean–continent transition. *Journal of Structural Geology,* 28**,** 1849-1869.

MANATSCHAL, G., FROITZHEIM, N., RUBENACH, M. & TURRIN, B. D. 2001. The role of detachment faulting in the formation of an ocean-continent transition; insights from the Iberia abyssal plain. *Geological Society, London, Special Publications,* 184**,** 405-428.

MANATSCHAL, G. & MÜNTENER, O. 2009. A type sequence across an ancient magma-poor ocean–continent transition: the example of the western Alpine Tethys ophiolites. *Tectonophysics,* 473**,** 4-19.

MCARTHUR, K. L., FROST, C. D., BARNES, C. G., PRESTVIK, T. & NORDGULEN, Ø. 2014. Tectonic reconstruction and sediment provenance of a far-travelled oceanic nappe, Helgeland NappeComplex, west-central Norway. *Geological Society, London, Special Publications,* 390**,** 583-602.

MEERT, J. G., TORSVIK, T. H., EIDE, E. A. & DAHLGREN, S. 1998. Tectonic Significance of the Fen Province, S. Norway: Constraints from Geochronology and Paleomagnetism. *The Journal of Geology,* 106**,** 553-564.

MEERT, J. G., WALDERHAUG, H. J., TORSVIK, T. H. & HENDRIKS, B. W. H. 2007. Age and paleomagnetic signature of the Alnø carbonatite complex (NE Sweden): Additional controversy for the Neoproterozoic paleoposition of Baltica. *Precambrian Research,* 154**,** 159-174.

MOHN, G., MANATSCHAL, G., MUNTENER, O., VELTRANDO, M. & MASINI, E. 2010. Unravelling the interaction between tectonic and sedimentary processes during lithospheric thinning in the Alpine Tethys margins. *International Journal of Earth Sciences,* 99**,** 75-101.

MONIGLE, P. W., NABELEK, J., BRAUNMILLER, J. & CARPENTER, N. S. 2012. Evidence for low-angle normal faulting in the Pumqu-Xianza Rift, Tibet. *Geophysical Journal International,* 190**,** 1335-1340.

MOULIN, M., ASLANIAN, D., OLIVET, J. L., CONTRUCCI, I., MATIAS, L., GELI, L., KLINGELHOEFER, F., NOUZE, H., REHAULT, J. P. & UNTERNEHR, P. 2005. Geological constraints on the evolution of the Angolan margin based on reflection and refraction seismic data (ZaiAngo Project).",. *Geophysical Journal International,* 162**,** 739-810.

MÜNTENER, O. & MANATSCHAL, G. 2006. High degrees of melt extraction recorded by spinel harzburgite of the Newfoundland margin: The role of inheritance and consequences for the evolution of the southern North Atlantic. *Earth and Planetary Science Letters,* 252**,** 437-452.

MÜNTENER, O., MANATSCHAL, G., DESMURS, L. & PETTKE, T. 2009. Plagioclase Peridotites in Ocean–Continent Transitions: Refertilized Mantle Domains Generated by Melt Stagnation in the Shallow Mantle Lithosphere. *Journal of Petrology,* 51**,** 225-294.

MÜNTENER, O., PETTKE, T., DESMURS, L., MEIER, M. & SCHALTEGGER, U. 2004. Refertilization of mantle peridotite in embryonic ocean basins: trace element and Nd isotopic evidence and implications for crust–mantle relationships. *Earth and Planetary Science Letters,* 22**,** 293-308.

NICHOLS, G. 1999. *Sedimentology & Stratigraphy,* Oxford, Blackwell Publishing.

NYSTUEN, J. P., ANDRESEN, A., KUMPULAINEN, R. A. & SIEDLECKA, A. 2008. Neoproterozoic basin evolution in Fennoscandia, East Greenland and Svalbard. *Episodes,* 31**,** 35-43.

O'REILLY, B. M., HAUSER, F., JACOB, A. W. & SHANNON, P. M. 1996. The lithosphere below the Rockall Trough; wide-angle seismic evidence for extensive serpentinisation. *Tectonophysics,* 255**,** 1-23.

OFTEDAHL, C. 1969. Caledonian pyroclastic (?) serpentine in central Norway. *Geological Society of America, Memoir,* 115**,** 305-315.

OSMUNDSEN, P. T. & EBBING, J. 2008. Styles of extension offshore mid-Norway and implications for mechanisms of crustal thinning at passive margins. *Tectonics,* 27**,** TC6016.

PAULSSON, O. & ANDREASSON, P.-G. 2002. Attempted break-up of Rodinia at 850 Ma: geochronological evidence from the Seve–Kalak Superterrane, Scandinavian Caledonides. *Journal of the Geological Society,* 159**,** 751-761.

PÉREZ-GUSSINYÉ, M. 2013. A tectonic model for hyperextension at magma-poor rifted margins: an example from the West Iberia-Newfoundland conjugate margins. *Geological Society, London, Special Publications,* 369**,** 403-427.

PÉREZ-GUSSINYÉ, M., RANERO, C. R., RESTON, T. J. & SAWYER, D. 2003. Structure and extensional mechanisms of the Galicia interior basin, west Iberia margin. *Journal of Geophysical Research: Solid Earth,* 108.

PÉREZ-GUSSINYÉ, M. & RESTON, T. 2001. Rheological evolution during extension at nonvolcanic rifted margins: Onset of serpentinization and development of detachments leading to continental breakup. *Journal of Geophysical REsearch,* 106**,** 3961-3975.

PERON-PINVIDIC, G., GERNIGON, L., GAINA, C. & BALL, P. 2012a. Insights from the Jan Mayen system in the Norwegian–Greenland sea—I. Mapping of a microcontinent. *Geophysical Journal International,* 191**,** 385-412.

PERON-PINVIDIC, G., GERNIGON, L., GAINA, C. & BALL, P. 2012b. Insights from the Jan Mayen system in the Norwegian–Greenland Sea—II. Architecture of a microcontinent. *Geophysical Journal International,* 191**,** 413-435.

PÉRON-PINVIDIC, G. & MANATSCHAL, G. 2009. The final rifting evolution at deep magma-poor passive margins from Iberia-Newfoundland: a new point of view. *International Journal of Earth Sciences,* 98**,** 1581-1597.

PÉRON-PINVIDIC, G., MANATSCHAL, G., MINSHULL, T. A. & SAWYER, D. S. 2007. Tectonosedimentary evolution of the deep Iberia-Newfoundland margins; evidence for a complex breakup history. *Tectonics,* 26**,** TC2011.

PFIFFNER, O. A., LEHNER, P., HEITZMANN, P., MUELLER, S. & STECK, A. 1997. *Deep Structure of the Swiss Alps - Results from the National Research Program 20 (NRP 20),* Basel, Birkhäuser Basel.

PICAZO, S., CANNAT, M., DELACOUR, A., ESCARTIN, J., ROUMEJON, S. & SILANTYEV, S. 2012. Deformation associated with the denudation of mantle-derived rocks at the Mid-Atlantic

Ridge 13°–15°N: The role of magmatic injections and hydrothermal alteration. *Geochemistry, Geophysics, Geosystems,* 13**,** 3306-3313.
PINHEIRO, L. M., WILSON , R. C., PENA DOS REIS, R., WHITMARSH , R. B. & RIBEIRO, A. 1996. the western Iberia margin: a geophysical and geological overview. *In:* WHITMARSH , R. B., SAWYER , D. S., KLAUS , A. & MASSON , D. G. (eds.) *PROCEEDINGS-OCEAN DRILLING PROGRAM, SCIENTIFIC RESULTS, 149.* College Station, Texas: Ocean Drilling Program.
POUCHOU, J. & PICHOIR, F. 1991. Quantitative Analysis of Homogeneous or Stratified Microvolumes Applying the Model "PAP". *In:* HEINRICH, K. F. J. & NEWBURY, D. E. (eds.) *Electron Probe Quantitation.* Springer US.
QVALE, H. 1978. Geologisk undersølelse av et kaledonsk serpentinittfelt ved Balderheim, Hordaland. Cand. Real (Master) thesis, University of Oslo.
QVALE, H. & STIGH, J. 1985. Ultramafic rocks in the Scandinavian Caledonides. *In:* GEE, D. G. & STURT, B. A. (eds.) *The Caledonide Orogen - Scandinavia and Related Areas.* Chichester: Wiley.
RESTON, T. J. 2005. Polyphase faulting during the development of the west Galicia rifted margin. *Earth and Planetary Science Letters,* 237**,** 561-576.
ROBERTS, D. & GEE, D. G. 1985. An introduction to the structure of the Scandinavian Caledonides. *In:* GEE, D. G. & STURT, B. A. (eds.) *The Caledonide Orogen – Scandinavia and Related Areas.* Chichester: Wiley.
ROBERTS, D., MELEZHIK, V. A. & HELDAN, T. 2002. Carbonate formations and early NW-directed thrusting in the highest allochthons of the Norwegian Caledonides: evidence of a Laurentian ancestry. *Journal of the Geology Society, London,* 159**,** 117-120.
ROBERTS, R. J., TORSVIK, T. H., ANDERSEN, T. B. & REHNSTRÖM, E. F. 2003. The Early Carboniferous Magerøy Dykes, Northern Norway: Palaeomagnetism and Palaeogeography. *Geological Magazine,* 140**,** 443-451.
ROOT, D. & CORFU, F. 2012. U–Pb geochronology of two discrete Ordovician high-pressure metamorphic events in the Seve Nappe Complex, Scandinavian Caledonides. *Contributions to Mineralogy and Petrology,* 163**,** 769-788.
SKELTON , A. D. & VALLEY, J. W. 2000. he relative timing of serpentinization and mantle exhumation at the ocean-continent transition, Iberia: constraints from oxygen isotopes. *Earth and Planetary Science Letters,* 178**,** 327-338.
SPOONER, E. T. C. & FYFE, W. S. 1973. Sub-sea-floor metamorphism, heat and mass transfer. *Contributions to Mineralogy and Petrology,* 42**,** 287-304.
STOREMYR, P. & HELDAL, T. 2002. Soapstone Production through Norwegian History: Geology, Properties, Quarrying and Use. *In:* HERRMANN, J., HERZ, N. & NEWMAN, R. (eds.) *ASMOSIA 5, Interdisciplinary Studies on Ancient Stone – Proceedings of the Fifth International Conference of the Association for the Study of Marble and Other Stones in Antiquity, Museum of Fine Arts, Boston, June 11-15, 1998.* London: Archetype Publications.
STØRMER, L. 1967. Some aspects of the Caledonian geosyncline and foreland west of the Baltic Shield. *Quarterly Journal of the Geological Society,* 123**,** 183-214.
STRAND, T. 1951. The Sel and Vågå map areas, geology and petrology of the a part of the Caledonides of Central Southern Norway. *Norges geologiske undersøkelse,* 17.
STRAND, T. 1970. On the mode of formation of the Otta serpentine conglomerate. *Norwegian Journal of Geology,* 50**,** 393-395.
STURT, B. A. & RAMSAY, D. M. 1999. Early Ordovician terrane-linkages between oceanic and continental terranes in the central Scandinavian Caledonides. *Terra Nova,* 11**,** 79-85.
STURT, B. A., RAMSAY, D. M. & NEUMAN, R. B. 1991. The Otta Conglomerate, the Vågåmo Ophiolite - further indications of early Ordovician Orogenesis in the Scandinavian Caledonides. *Norsk Geologisk Tidsskrift,* 71**,** 107-115.
SVENNINGSEN, O. 2001. Onset of seafloor spreading in the Iapetus Ocean at 608Ma: precise age of the Sarek Dyke Swarm, northern Swedish Caledonides. *American Journal of Science,* 110**,** 241-254.

THON, A. 1985. The Gullfjellet ophiolite complex and the structural evolution of the major Bergen arc, west Norwegian Caledonides. *The Caledonide Orogen: Scandinavia and related areas*, 671-677.

TORSVIK, T. H. 2003. The Rodinia Jigsaw Puzzle. *Science,* 300**,** 1379-1381.

TORSVIK, T. H. & COCKS, L. R. 2005. Norway in space and time: a centennial cavalcade. *Norwegian Journal of Geology,* 85**,** 73-86.

TORSVIK, T. H., RYAN, P. D., TRENCH, A. & HARPER, D. A. T. 1991. Cambrian-Ordovician paleogeography of Baltica. *Geology,* 19**,** 7-10.

TORSVIK, T. H., SMETHURST, M. A., MEERT, J. G., VAN DER VOO, R., MCKERROW, W. S., BRASIER, M. D., STURT, B. A. & WALDERHAUG, H. J. 1996. Continental break-up and collision in the Neoproterozoic and Palaeozoic — A tale of Baltica and Laurentia. *Earth-Science Reviews,* 40**,** 229-258.

UNTERNEHR, P., PÉRON-PINVIDIC, G., MANATSCHAL, G. & SUTRA, E. 2010. Hyper-extended crust in the South Atlantic: in search of a model. *Petroleum Geoscience,* 16**,** 207-215.

VAN STAAL, C., DEWEY, J., MAC NIOCAILL, C. & MCKERROW, W. 1998. The Cambrian-Silurian tectonic evolution of the northern Appalachians and British Caledonides: history of a complex, west and southwest Pacific-type segment of Iapetus. *Geological Society, London, Special Publications,* 143**,** 197-242.

VAN STAAL, C. R., CHEW, D. M., ZAGOREVSKI, A., MCNICOLL, V., HIBBARD, J., SKULSKI, T., CASTONGUAY, S., ESCAYOLA, M. P. & SYLVESTER, P. J. 2013. Evidence of Late Ediacaran Hyperextension of the Laurentian Iapetan Margin in the Birchy Complex, Baie Verte Peninsula, Northwest Newfoundland: Implications for the Opening of Iapetus, Formation of Peri-Laurentian Microcontinents and Taconic - Grampian Or. *Geoscience Canada,* 40**,** 94-107.

VAUCHEZ, A., CLERC, C., BESTANI, L., LAGABRIELLE, Y., CHAUVET, A., LAHFID, A. & MAINPRICE, D. 2013. Preorogenic exhumation of the North Pyrenean Agly massif (Eastern Pyrenees-France). *Tectonics,* 32**,** 95-106.

WERNICKE, B. 1985. Uniform-sense normal simple shear of the continental lithosphere. *Canadian Journal of Earth Sciences,* 22**,** 108-125.

WERNICKE, B. & BURCHFIEL, B. C. 1982. Modes of extensional tectonics. *Journal of Structural Geology,* 4**,** 105-115.

WHITMARSH, R. B., BESLIER, M. O., WALLACE, P. J. & AL., E. 1998. Proceedings of the Ocean Drilling Program, Initial Reports, 173. Texas: Ocean Drilling Program.

WHITMARSH, R. B. & MILES, P. R. 1995. Models of the development of the West Iberia rifted continental margin at 40° 30′ N deduced from surface and deep-tow magnetic anomalies. *Journal of Geophysical Research: Solid Earth,* 100**,** 3789-3806.